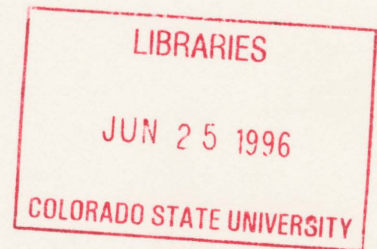


**SURFACE PRESSURE TRANSIENTS IN  
MESOSCALE CONVECTIVE SYSTEMS**

by  
Jason C. Knievel



Research supported by the National Science Foundation under grant ATM-9313716

**Colorado  
State  
University**

**DEPARTMENT OF  
ATMOSPHERIC SCIENCE**

PAPER NO. 605

# SURFACE PRESSURE TRANSIENTS IN MESOSCALE CONVECTIVE SYSTEMS

Jason C. Knievel

Department of Atmospheric Science  
Colorado State University  
Fort Collins, Colorado 80523-1371

Spring 1996

Atmospheric Science Paper No. 605



018401 3960413

QC  
852  
.Clp  
No. 605  
ATMDS

## ABSTRACT

### SURFACE PRESSURE TRANSIENTS IN MESOSCALE CONVECTIVE SYSTEMS

For decades meteorologists have observed that mesoscale convective systems (MCSs) increase surface pressure beneath and immediately behind their leading cumulonimbi (the mesohigh) and reduce surface pressure at the rear edge of their anvils (the wake low). By enhancing coarse surface pressure observations of 12 PRE-STORM MCSs, I exposed transitory highs and lows living within mesohighs and wake lows. I propose that these transients are the more elemental MCS surface pressure perturbations; *mesohighs and wake lows are merely temporal and spatial envelopes of transients*. Moreover, existing theories of mesohigh and wake low origins readily apply to the ephemeral transients.

A quasi-Lagrangian analysis of 92 transients produced five primary results. First, as the MCSs matured, the difference between each complex's transitory highs' mean pressure and transitory lows' mean pressure increased in 78% of the conclusive cases. Second, there is no clear evidence that transitory highs consistently strengthened before their partner transitory lows. Third, transient paths reflect MCSs' occasional symmetric-to-asymmetric metamorphoses. Fourth, composites of the time-evolution of the numbers and apparent sizes of transients partially support theories of MCS upscale evolution. Fifth, composite transient numbers and apparent sizes vary almost identically with time in a pattern that closely resembles the fluctuation of stratiform and convective volumetric rain rates of MCSs studied by McAnelly and Cotton (1992).

Jason C. Knievel  
Department of Atmospheric Science  
Colorado State University  
Fort Collins, Colorado 80523-1371  
Spring 1996

## ACKNOWLEDGEMENTS

Science is collaborative. Each step in research extends the endless miles trod by others. I founded this thesis on the studies of many scientists, most notably Scot Loehrer. He supplied me with data and programs and never tired of my e-mail inquiries.

Paul Ciesielski, Patrick Haertel, Xin Lin, and Rick Taft rescued me from countless computing emergencies. Patrick also sacrificed his time to help manage my data and organize my words. Jason Nachamkin fueled my imagination with insightful comments and marked research paths hidden to me. Other helpers include Jim Bresch, Steve Finley, Bill Gallus, Ken Hart, Eric Hilgendorf, and Michael Mutmansky, my fly-fishing partner.

Gail Cordova keeps Richard Johnson's research group running smoothly. Jane Wilkins, Judy Gueswel, and many others manage affairs at the departmental level and improve the quality of academic life for all Atmospheric Science graduate students.

During their highly successful experimental course on writing in the sciences, Gerald Callahan and David Mogen proved to me there are still an invaluable handful of researchers at major universities who inspire students through well-written and well-spoken ideas.

The same Dr. Callahan kindly agreed to serve on my committee despite the late request. From Atmospheric Science, my other two committee members were Thomas McKee and Richard Johnson, my advisor.

I owe the most to Dr. Johnson. He patiently left me to my own devices when I needed independence and devotedly attended to me when I needed guidance. He is a good scientist and a good teacher, but what's more, he is a good man.

The National Science Foundation supported my research under grant ATM-9313716.

*Thank you all. Thank you Lord.*

DEDICATION

To Mom, Dad, and Ann.

*I love you.*

## CONTENTS

<b>1 Introduction</b>	<b>1</b>
1.1 Mesoscale Convective Systems . . . . .	1
1.2 A New Look at Familiar Subjects . . . . .	2
<b>2 Review of MCS Pressure Perturbation Research</b>	<b>5</b>
2.1 Mesohighs . . . . .	6
2.1.1 Hydrostatic Contribution to Mesohighs . . . . .	7
2.1.2 Dynamic Contribution to Mesohighs . . . . .	8
2.2 Wake Lows . . . . .	10
2.3 Summary of Literature Review . . . . .	13
<b>3 Data and Methods of Analysis</b>	<b>15</b>
3.1 The 12 Subject MCSs . . . . .	15
3.2 Observations . . . . .	17
3.2.1 Station Pressure . . . . .	18
3.2.2 Equivalent Potential Temperature . . . . .	19
3.2.3 Radar Composites . . . . .	19
3.3 Data Processing . . . . .	19
3.3.1 Creating Space from Time . . . . .	19
3.3.2 Objective Analysis . . . . .	21
3.4 NCAR Graphics Plots . . . . .	24
3.4.1 Contour Maps . . . . .	24
3.4.2 Movies . . . . .	24
3.5 Analysis Legitimacy . . . . .	25
<b>4 Transients and Their Possible Origins</b>	<b>31</b>
4.1 Problems with Current Mental Models . . . . .	31
4.2 Movie Evidence of Transients . . . . .	33
4.3 The Origin of Transitory Highs . . . . .	33
4.4 The Origin of Transitory Lows . . . . .	34
4.4.1 Variations in Rain and Snow Rates . . . . .	36
4.4.2 Speed Variations in Rear-To-Front Flow . . . . .	37
4.4.3 Humidity Variations in Rear-To-Front Flow . . . . .	38
<b>5 The PRE-STORM Transients</b>	<b>41</b>
5.1 Criteria for Transient Selection . . . . .	41
5.1.1 Final Instrument Error Removal . . . . .	41
5.1.2 NCAR Graphics Red Herrings . . . . .	42
5.1.3 The Problem of Inoperative Stations . . . . .	43

5.1.4	Radar Verification . . . . .	43
5.2	Roster of Transients . . . . .	44
5.3	Lifetimes . . . . .	54
5.4	Displacements . . . . .	55
5.5	Quasi-Lagrangian Traces . . . . .	55
5.5.1	7 May . . . . .	56
5.5.2	13 May (N) . . . . .	57
5.5.3	13 May (S) . . . . .	58
5.5.4	27 May . . . . .	59
5.5.5	28 May . . . . .	60
5.5.6	3 June . . . . .	61
5.5.7	3–4 June . . . . .	61
5.5.8	4 June . . . . .	62
5.5.9	11 June . . . . .	63
5.5.10	15 June . . . . .	64
5.5.11	24 June . . . . .	65
5.5.12	26–27 June . . . . .	66
5.6	Summary of Quasi-Lagrangian Traces . . . . .	67
<b>6</b>	<b>Transient Paths and MCS Symmetry</b>	<b>71</b>
6.1	Observations and Modeling of Horizontal MCS Structure . . . . .	71
6.2	Transient Paths . . . . .	90
6.2.1	Intra-Family Paths . . . . .	90
6.2.2	Inter-Family Paths . . . . .	92
<b>7</b>	<b>The Question of Upscale Evolution</b>	<b>97</b>
7.1	Existing Theories and Evidence . . . . .	97
7.2	Evolution of the Number of Transients . . . . .	98
7.2.1	Creating the Figure . . . . .	98
7.2.2	Interpreting the Figure . . . . .	102
7.3	Evolution of the Sizes of Transients . . . . .	104
7.3.1	Creating the Figure . . . . .	105
7.3.2	Interpreting the Figure . . . . .	106
7.4	Comparison with Volumetric Rain Rate . . . . .	109
<b>8</b>	<b>Concluding Remarks</b>	<b>111</b>
8.1	Summary . . . . .	111
8.2	Final Thoughts . . . . .	113
8.3	Future Research . . . . .	114
	<b>REFERENCES</b>	<b>117</b>
<b>A</b>	<b>Mesoscale Size Classifications</b>	<b>133</b>

## LIST OF FIGURES

2.1	Schema of a Midlatitude MCS . . . . .	6
2.2	Schema of an Asymmetric Midlatitude MCS . . . . .	7
3.1	PRE-STORM Surface Observing Array . . . . .	17
3.2	Time-to-Space Conversion Example . . . . .	21
3.3	Data Distribution After Time-Space Enhancement . . . . .	22
3.4	Combined Barnes Absolute Pressure Departure . . . . .	24
3.5	Test Pressure Field for Analysis Verification . . . . .	25
3.6	Verification Pressure Field . . . . .	26
4.1	Station Pressure and $\theta_e$ for 0310 UTC 11 June 1985 . . . . .	32
4.2	Schema of MCS Stratiform Region . . . . .	35
5.1	Station Pressure and $\theta_e$ for 0410 UTC 15 June 1985. . . . .	42
5.2	Average MCS Transient Lifetime vs. Leading-Line Speed . . . . .	43
5.3	Total Transitory High Lifetimes . . . . .	50
5.4	Total Transitory Low Lifetimes . . . . .	50
5.5	Fully-Sampled Transitory High Lifetimes . . . . .	51
5.6	Fully-Sampled Transitory Low Lifetimes . . . . .	51
5.7	Total Transitory High Displacements . . . . .	52
5.8	Total Transitory Low Displacements . . . . .	52
5.9	Fully-Sampled Transitory High Displacements . . . . .	53
5.10	Fully-Sampled Transitory Low Displacements . . . . .	53
5.11	Central Pressure of the 7 May Transients . . . . .	57
5.12	Central Pressure of the 13 May (N) Transients . . . . .	58
5.13	Central Pressure of the 13 May (S) Transients . . . . .	59
5.14	Central Pressure of the 27 May Transients . . . . .	60
5.15	Central Pressure of the 28 May Transients . . . . .	61
5.16	Central Pressure of the 3 June Transients . . . . .	62
5.17	Central Pressure of the 3-4 June Transients . . . . .	63
5.18	Central Pressure of the 4 June Transients . . . . .	64
5.19	Central Pressure of the 10-11 June Transients . . . . .	65
5.20	Central Pressure of the 15 June Transients . . . . .	66
5.21	Central Pressure of the 24 June Transients . . . . .	67
5.22	Central Pressure of the 26-27 June Transients . . . . .	68
6.1	Schemata of a Symmetric and an Asymmetric MCS . . . . .	72
6.2	Schema of Parallel and Skew Path Types . . . . .	73
6.3	Transient Paths for 7 May . . . . .	74
6.4	Transient Paths for 13 May (N) . . . . .	75

6.5	Transient Paths for 13 May (S) . . . . .	76
6.6	Transient Paths for 27 May . . . . .	77
6.7	Transient Paths for 28 May . . . . .	78
6.8	Transient Paths for 3 June . . . . .	79
6.9	Transient Paths for 3–4 June . . . . .	80
6.10	Transient Paths for 4 June . . . . .	81
6.11	Transient Paths for 10–11 June . . . . .	82
6.12	Transient Paths for 15 June . . . . .	84
6.13	Transient Paths for 24 June . . . . .	86
6.14	Transient Paths for 26–27 June . . . . .	87
6.15	Skew Paths to Asymmetry on 28 May 1985 . . . . .	92
6.16	Parallel Paths to Asymmetry on 4 June 1985 . . . . .	94
7.1	Composite Number of Transients vs. Time . . . . .	99
7.2	0423 UTC 11 June 1985: Surface Transitory Lows and Radar Composite . . . .	100
7.3	1400 UTC 28 May 1985: Surface Transitory Lows and Radar Composite . . . .	101
7.4	0935 UTC 4 June 1985: Surface Transitory Lows and Radar Composite . . . .	102
7.5	0723 UTC 11 June 1985: Surface Transitory Lows and Radar Composite . . . .	103
7.6	Composite Perimeter of Transients vs. Time . . . . .	105
7.7	Perimeter of the Transitory High and Transitory Low Envelopes at 0940 UTC 4 June 1985 . . . . .	107
7.8	Composite MCC Stratiform and Convective Volumetric Rain Rates . . . . .	110

LIST OF TABLES

3.1	PRE-STORM MCSs . . . . .	15
3.2	STA Station Pressure . . . . .	20
3.3	Comprehensive Case References . . . . .	27
3.4	References By Case: May . . . . .	28
3.5	References By Case: June . . . . .	29
5.1	7 May Pressure Transients . . . . .	45
5.2	13 May (N) Pressure Transients . . . . .	45
5.3	13 May (S) Pressure Transients . . . . .	45
5.4	27 May Pressure Transients . . . . .	46
5.5	28 May Pressure Transients . . . . .	46
5.6	3 June Pressure Transients . . . . .	46
5.7	3-4 June Pressure Transients . . . . .	47
5.8	4 June Pressure Transients . . . . .	47
5.9	10-11 June Pressure Transients . . . . .	48
5.10	15 June Pressure Transients . . . . .	48
5.11	24 June Pressure Transients . . . . .	49
5.12	26-27 June Pressure Transients . . . . .	49

*For the man sound in body and serene of mind there is no such thing as bad weather; every sky has its beauty, and storms which whip the blood do but make it pulse more vigorously.*

—George Gissing,  
The Private Papers of Henry Ryecroft

*In science there is no authority other than observation and experiment illuminated by reason.*

—Craig F. Bohren,  
Clouds in a Glass of Beer: Simple  
Experiments in Atmospheric Physics

*I love our American language as if it were my own child . . . I wince with pain when I see or hear a good old word being broken on the wheel of ill usages. It's as if my own child were having a finger snapped.*

—Earl Ubell,  
Harper Dictionary of Contemporary Usage

## Chapter 1

### INTRODUCTION

*The pressure variations accompanying a thunderstorm have been familiar to meteorologists since the time when barographs were first constructed.*

—Joseph Levine,  
“The Effect of Vertical Accelerations  
of Pressure During Thunderstorms”

If Joseph Levine is correct, the history of observations of storm-induced atmospheric pressure fluctuations must be rich indeed, for barographs date back to the late 17th Century (Middleton 1964). In this thesis I address the transitory surface pressure perturbations generated by some of the largest, most potent warm-season storms the American Great Plains can muster: Mesoscale Convective Systems (MCSs).

#### 1.1 Mesoscale Convective Systems

MCSs are large conglomerates of convective towers and stratiform anvils that live longer and circulate over a wider domain than their member cumulonimbi. They generate vast cloud shields that extend tens to hundreds of thousands of square kilometers, endure for tens of hours, and often move faster than  $10 \text{ m s}^{-1}$ , traveling hundreds of kilometers before dissipating. MCSs may be sorted into categories that include tropical storms, mesoscale convective complexes (MCCs), squall lines, and convective clusters, which are unorganized MCSs. Why cumulonimbi sometimes organize into MCSs rather than remain independent is a perplexing and only partially-understood topic unto itself. Vertical wind shear, convective available potential energy (CAPE), and triggers' linearity are three important factors (Bluestein and Jain 1985; Rotunno et al. 1988; Scott 1994). Having said that, I leave the issue to others.

The immensity of organized MCSs insures their longevity. Lone thunderheads are at the mercy of synoptic shear and dry-air intrusions that rip at updrafts and downdrafts and sap latent energy, but organized MCSs modify their immediate environments and buffer themselves from synoptic disruption (Newton 1950). They harness energy from latent heating more efficiently than small-scale convection in which most energy rapidly disperses from the convection site as gravity waves (Schubert et al. 1980). MCSs also rejuvenate themselves as their cool, dense outflows surge into the base of the convectively unstable lower troposphere and spawn new energetic cells that replace dying towers.

MCSs are common to much of the world, but spring and summer weather between the Rocky Mountains and the Mississippi Valley particularly favors the complexes. Deep Gulf moisture rides warm southerly surface wind, supplying abundant sensible and latent energy in the lower troposphere. Overhead, cool air flows from the Pacific Ocean and Canada. Often lower-tropospheric convergence along a cold front or dryline forces air to ascend into this unstable stratification, triggering vigorous convection. Other times, storms over the Rockies generate a pool of cold air at the surface that is captured by synoptic westerlies and conveyed to the Plains where it initiates convection. Even the absence of a strong surface trigger may be overcome if an arriving middle- or upper-tropospheric disturbance is sufficiently potent.

Since the 1940s, meteorologists have observed that organized MCSs (I now drop “organized,” but that is implied henceforth) are usually accompanied by some or all of three types of surface pressure perturbations: a pre-squall low, a mesohigh, and a wake low. This thesis concerns the latter two, or, more properly, what *composes* the latter two. I term the sub-elements within the mesohigh and wake low “transients” or “transitory highs and lows” for reasons that will become clear in upcoming pages.

## 1.2 A New Look at Familiar Subjects

Most MCS researchers document pressure changes at fixed observation points beneath a traveling and evolving complex, which is not very insightful if one wishes to thoroughly track the strength and motion of transitory highs and lows from birth to death. Instead I

employed a quasi-Lagrangian trace of 12 Great Plains MCSs. This allows me to address four specific central issues, the first two of which most researchers have overlooked: (1) the temporal evolution of the strengths of transitory highs and lows; (2) transient paths as MCSs evolve from infancy to maturity, which sometimes entail a metamorphosis from horizontal symmetry to horizontal asymmetry; (3) changes in circulation scales as MCSs mature; and (4) associations among transient numbers, transient sizes, and MCS rain rates. There is a less tangible but more profound fifth issue, too, and it is this: *Perhaps meteorologists' current mental models of mesohighs and wake lows have been distorted by coarse observations that fail to capture transients' true smallness and brevity.*

## Chapter 2

### REVIEW OF MCS PRESSURE PERTURBATION RESEARCH

*To look at his picture as a whole, a painter requires distance; and to judge the total scientific achievement of any age, the standpoint of a succeeding age is desirable.*

—John Tyndall,  
Fragments of Science, Vol. II

Figure 2.1 is a plan-view schema of a midlatitude MCS and its three characteristic meso- $\beta$ -scale (see Appendix A) surface pressure perturbations: the pre-squall low, mesohigh, and wake low. A convective line of cumulonimbi leads the complex. Forward of this line is the pre-squall low, and co-located or just behind the line is the mesohigh. A band of minimal precipitation called the transition zone separates the thundershowers of the convective line and the often steady but not necessarily hard rain of the stratiform region (Ligda 1956; Sommeria and Testud 1984; Chong et al. 1987; Smull and Houze 1987b; Johnson and Hamilton 1988; Zhang and Gao 1989; Biggerstaff and Houze 1991a). The wake low is centered at the back edge of the stratiform anvil.

This arrangement represents the idealized MCS, but most observed complexes deviate from this archetype. Often the most vigorous cumulonimbi favor the southern part of the convective line (Newton and Frankhauser 1964; Skamarock et al. 1994; Scott and Rutledge 1995), resulting in a sickle- or comma-like pattern (Figure 2.2). Not all MCSs contain a distinct transition zone and stratiform region. When the mean vertical wind shear vector parallels the convective line instead of crossing it front-to-rear (FTR), little or no anvil and stratiform rain develops (Heymsfield and Schotz 1985). Very strong upper-tropospheric rear-to-front (RTF) winds may spread the stratiform anvil ahead of the leading cumulonimbi instead of behind them (Newton 1966; Houze and Rappaport 1984; Roux 1988). When stratiform regions trail their parent storms, often the anvil and the precipitation falling from

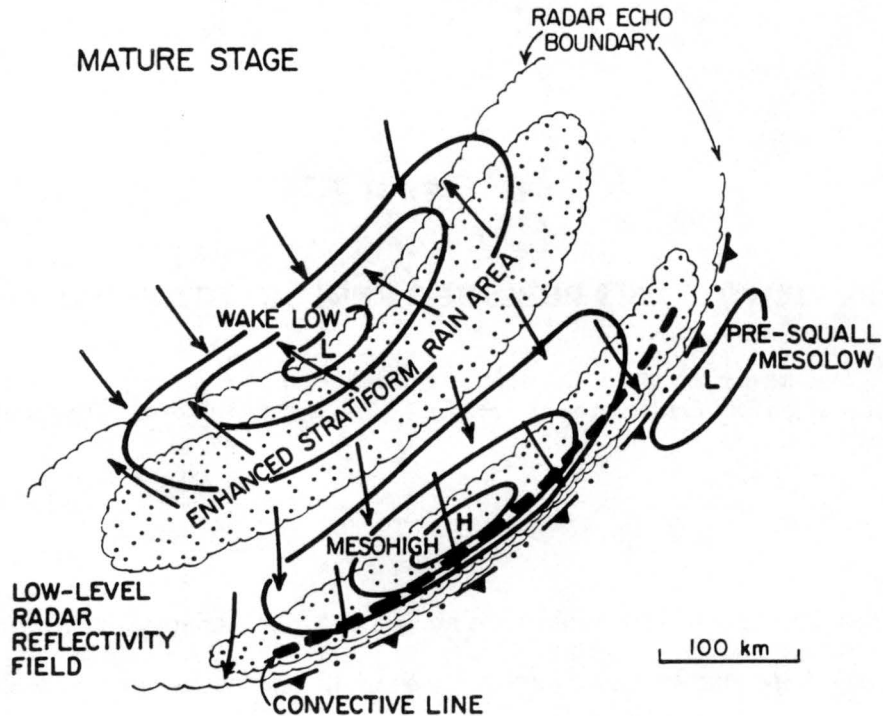


Figure 2.1: Schema of a Midlatitude MCS. A mesohigh is centered beneath the leading convective line and a wake low is centered at the rear edge of the stratiform rain. The two post-squall perturbations contain centered unique extrema and are roughly  $100 \times 300$  km (from Johnson and Hamilton 1988).

it will be more intense, or will be spread over a broader area, either northwest or southwest of an eastbound complex (Newton 1950; Pedgley 1962; Schmidt and Cotton 1985; Ogura and Liou 1980; Srivastava et al. 1986; Houze et al. 1990; Loehrer 1992; Skamarock et al. 1994). I explain these deviations from the idealized MCS layout in much greater detail in Chapter 6.

## 2.1 Mesohighs

Of the three surface pressure features, the mesohigh has the longest, richest history in meteorological literature. Pressure increases at a point on the ground *dynamically* as thunderstorms drive downdrafts against the ground, and it increases *hydrostatically* as the integrated mass above that point increases. Early storm observers seized the second explanation for mesohighs, the hydrostatic contribution, more quickly—probably because the

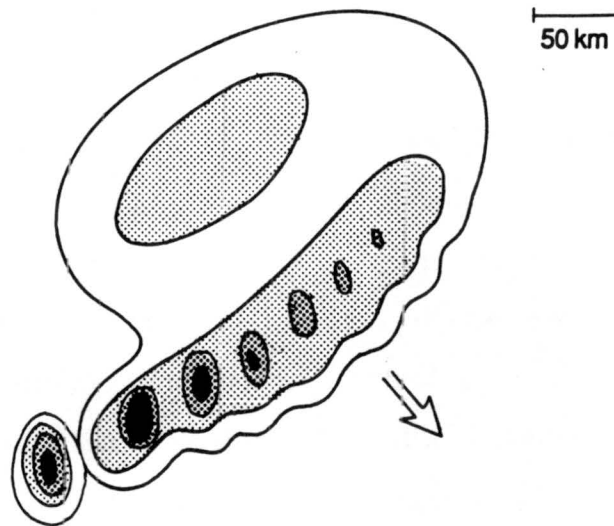


Figure 2.2: Schema of an Asymmetric Midlatitude MCS. Increasingly dark grays represent increasing radar reflectivity. Stratiform rain is located on the left, rear part of the MCS (relative to the motion of the complex) and the most intense cumulonimbi are located to the right (from Houze et al. 1990).

refreshing cool outflows from a thunderstorm is one of its most immediately tangible, and measurable, traits.

### 2.1.1 Hydrostatic Contribution to Mesohighs

In the Thunderstorm chapter of his detailed 1929 treatise *Physics of the Air*, Humphreys established what, for the following seven decades, would be the most prevalent theory of why MCS convective precipitation produces mesohighs. To increase mass in a fixed-height column of the atmosphere, some part of that column must become more dense; in other words, if we ignore changes in humidity, it must simply become colder. First, Humphreys offered that thunderstorms might produce their well-known cold surface outflow when: (1) potentially cold air descends; (2) cold raindrops conductively chill the surrounding air; or (3) raindrops evaporate. He then qualitatively illustrated why the first two candidates were unlikely. Only evaporation remained. In the 1930s Suckstorff studied many cases of pressure rises and falls during the passage of thunderstorms. He dubbed the initial rise the *Gewitternase* (“thunderstorm nose”) (Bleeker and Andre 1950) and in 1935 published a paper agreeing with Humphreys that evaporating raindrops from cumulonimbi

chill the air enough to generate mesohighs hydrostatically (although this was before use of “mesohigh”).

Similar to Suckstorff (1935) and later Sawyer (1946) and Byers and Braham (1949), Fujita (1955) theorized that mesohighs are formed when “high momentum air aloft is cooled and brought down by the downdraft, and spreads out over the ground forming a large thunderstorm high.” Four years later, Fujita (1959) partially quantified existing theories when he established that, given a cloud base, one may directly calculate the mass of a storm’s rain-chilled air from its rainfall. In 1969, Atlas et al. calculated some simple microphysical comparisons of the latent heat of fusion and the latent heat of vaporization. They concluded that Fujita’s (1959) evaporation told only part of the mesohigh-cooling story: melting can produce almost as much chilled storm air as evaporation.

Shaw and Dines (1904) were some of the earliest to propose, in print, a second way in which pressure beneath storms may hydrostatically rise. They asserted that raindrops within storms add enough mass to vertical columns of the atmosphere to raise pressure independent of latent cooling. Almost a century has passed since then, but comparatively few observational studies have addressed the question of water loading. In one of those few, Sanders and Emanuel (1977) quantitatively evaluated the liquid water suspended below 450 mb in an Oklahoma thunderstorm and concluded that “liquid water aloft must be taken into account in the hydrostatic computation of the pressure field.” Modeling by Nicholls et al. (1988) suggested that in some MCSs water-loading pressure contributions approach 2 mb.

Raindrops contribute significantly to mesohighs in a third way as well. As they fall to earth, they drag with them the surrounding air, generating downdrafts (Byers and Braham 1949; Das 1964). These downdrafts drive the *dynamic* pressure rises discussed in the next section.

### *2.1.2 Dynamic Contribution to Mesohighs*

One of the first to suggest that thunderstorm updrafts and downdrafts also alter pressure dynamically was the latent-cooling advocate Suckstorff (1939) (Bleeker and Andre

1950). In the 1940s meteorologists attempted to quantify Suckstorff's theory by manipulating the vertical equation of motion, but they included few other factors (Bleeker and Andre 1950). The simplicity of these pioneers' work and their varied unique assumptions yielded individualized results, so they criticized one another's differences and came to no published consensus. One such meteorologist, Levine (1942), studied the apparent symmetry of mesohighs' signatures on many barograph traces (Shaw and Dines 1904) and inferred that some highs must be the handiwork of vertical accelerations because, according to him, cooling-generated highs would exhibit a more gradual asymmetric pressure moderation as the leading edge of cool outflow departed, not a pressure drop that mirrored the initial rise. He calculated that vertical accelerations dynamically increase surface pressure by an amount comparable to the hydrostatic rise.

Buell (1943a,b) modified Levine's work to account for the decelerations that a rapidly ascending cumulonimbus plume undergoes above its level of neutral buoyancy—Levine had ignored these. Buell's equations yielded a pressure rise *for both updrafts and downdrafts*. Mal and Rao (1945) applauded Buell's modification, but pointed out that in his calculations Buell ignored a term of first-order importance for mature cumulonimbi. When they included the term, Mal and Rao discovered that vertical accelerations produce pressure *falls*, not rises, *for both updrafts and downdrafts*.

In 1947 Schaffer approached the puzzle of dynamic pressure perturbations by dividing an updraft into "stream-tubes" (idealized filaments of homogeneous fluid), but he assumed steady vertical motion, so his peers questioned his conclusions that both drafts force highs (Bleeker and Andre 1950). The applicability of his work is doubtful anyway, for Schaffer addressed barograph ridges that were superposed on larger, deeper troughs, so he really only attempted to explain how vertical cumulonimbus accelerations can mitigate perturbed lows, not generate true mesohighs (see Schaffer's Figure 4).

In 1962 Pedgley surveyed the contradictory work of the previous decade and wrote simply, "It seems the net effect of buoyancy is to produce little or no effect on the surface pressure." He offered this not out of diplomacy or sloth but because a few years earlier Malkus and Scorer (1955) had concluded that environmental drag in cumulus towers was

sufficient to balance buoyancy so that “cloudy air does not accelerate but maintains a constant vertical speed (Pedgley 1962).”

In fact MCS convective downdrafts *do* significantly contribute to mesohighs when they strike the ground and decelerate. Using Foster’s (1958) conclusion that downdrafts’ kinetic energy is a function of the distance a draft travels and of its temperature when it reaches the ground, Fujita (1963) calculated that the impact of downdrafts on the ground does, in some cases, increase surface pressure by values comparable to those from integrated mass changes. However, the amount of pressure change, and in some cases even the *sign* of the change, may depend highly on a sensor’s proximity to the center of the downdraft (Wakimoto 1982; Fujita 1985).

## 2.2 Wake Lows

Wake lows have proven more troublesome than mesohighs. Barographs did feel the lows and register them in distinct V- and U-shaped troughs comparable to the inked ridges signed by the mesohighs (Brunk 1949, 1953; Williams 1953; Pedgley 1962), but few pages were devoted to wake lows, possibly because (1) what produced them was not readily apparent in surface observations; (2) they appeared in barograph traces less often than mesohighs (Pedgley 1962); or (3) they did not connote the violence and destruction that often accompanied MCS cumulonimbi with their attendant mesohighs. Addressing this third point, Williams (1954) rationalized, “[Wake lows] do not generally coincide with severe weather or even ‘bad’ weather. For this reason there appears to be little justification for even noticing them.” Indeed, the scarce early work on wake lows that *was* published apparently was motivated by a misguided and not universally-held presumption that the lows spawned tornadoes (Brunk 1948; Williams 1953).

Early speculation on what produces wake lows—Fujita’s (1955), for example—was flawed. At the time Fujita thought wake lows were generated when the dense surging storm outflow “acts as a solid body” and moves forward relative to the immediate environment, reducing pressure in its wake. He added that if the winds proximate to the pressure surge line move relatively *forward* then the wake depression will form *ahead of the thunderstorm*.

Perhaps this was an early nod to the pre-squall low, but that is unclear, if not actually doubtful. Even if that were the case, the mechanism is still wrong (Hoxit et al. 1976). Fujita's hypothesis was accepted for a time, in part because it explained why the strongest wake lows often accompany the strongest mesohighs (Pedgley 1962).

Because wake lows travel behind the towering cumulonimbi of the convective line, Brunk (1953) speculated that thunderhead tops might excite gravity waves along the tropopause when they strike it, and that wake lows are a surface response to the waves. But most gravity wave energy disperses much too quickly to explain the sustained wake lows (Schubert et al. 1980), and gravity waves would create a more expansive ring of low pressure around the main convection. Even in the 1940s and 1950s, meteorologists knew that wake lows are localized (Pedgley 1962).

Some of the first writers to broach the currently-accepted kinematic and latent energy explanations of wake lows did so unwittingly. One such scientist, Krumm (1954), had read the contemporary (and, it turns out, generally accurate) theories that convective downdrafts owe much of their strength to raindrops that drag air groundward as they fall (Byers and Braham 1949). Krumm noticed his local Montana storms frequently delivered gusty, chilled downdrafts even when the rain that supposedly energized the drafts fell in only sporadic drops, or not at all. He reasoned that evaporative cooling must sometimes be potent enough to drive downdrafts from lofty cloud bases even when raindrops do not accompany the descending air columns to the ground (Braham 1952; Pedgley 1962).

In his seminal 1963 paper, Williams synthesized the thinking of Krumm and his peers, and constructed the framework of present wake low understanding. On the night of 3–4 May 1961 a group of thunderstorms traversed the National Severe Storms Project Beta Network in southern Oklahoma. Pressure dropped in the immediate wake of the storms, and the dense surface array with its supplemental radar and soundings provided Williams with the revealing data he needed to formulate his theory. He found (1) middle-tropospheric air subsided behind the thunderstorms, which (2) hydrostatically reduced surface pressure and (3) introduced warm, dry air into the lower troposphere.

In the years that followed, abundant studies confirmed one or more of Williams wake observations (Brown 1963; Rhiel 1968; Zipser 1969, 1977; Ogura and Liou 1980; Gamache and Houze 1982; Leary and Rappaport 1987). Zipser (1969) used the conserved atmospheric variable equivalent potential temperature,  $\theta_e$ , to trace the origin of the lower-tropospheric wakes of tropical squall lines and discovered that the boundary layer air that lay in the aftermath of ocean storms—boundary layer air fundamentally similar to Williams' 1961 wake—bore the low- $\theta_e$  signature of the middle troposphere. (See Section 3.2.2 for an explanation of  $\theta_e$ .) Subsequent studies of both tropical (Houze 1977; Johnson and Nicholls 1983) and midlatitude MCSs (Johnson et al. 1989) produced storm wake soundings that displayed the same distinct drying and warming characteristic of redistributed middle-tropospheric air.

Meteorologists of recent decades have built on long-established concepts of kinematics and latent energy exchanges to theorize *why* mesoscale downdrafts in MCSs descend and generate wake lows. Johnson and Hamilton's (1988) exhaustive analysis of the intense 10–11 June PRE-STORM squall line exposed a link among descending RTF flow, precipitation rates along the rear of the stratiform region, and wake lows. Biggerstaff and Houze (1991) examined the same MCS and concurred with the 1988 study, stressing even more greatly the link between stratiform precipitation and the RTF mesoscale downdraft.

Many observational studies (Leary and Bals 1989; Johnson et al. 1989; Brandes 1990; Stumpf et al. 1991) and numerically simulated MCSs (Zhang and Gao 1989; Gallus and Johnson 1995a; Yang and Houze 1995b) have corroborated this link and have answered some of the questions about the interactions among the precipitation, RTF flow, and mesoscale downdraft that Johnson and Hamilton (1988) found so crucial to the production of wake lows. The RTF flow appears to be a combination of (1) baroclinically-induced synoptic westerlies that descend into the MCS, possibly accelerating during descent, and (2) intra-storm RTF flow that is accelerated, even *created* by, horizontal pressure gradients within MCSs (LeMone 1983; LeMone et al. 1984; Smull and Houze 1987b; Rotunno et al. 1988; Zhang and Gao 1989; Schmidt and Cotton 1990; Gallus and Johnson 1992). Latent cooling under the rear edge of the anvil increases the density of the RTF flow, drawing it downward from the middle-troposphere (Zhang and Gao 1989), and this is how low- $\theta_e$  air observed

by Williams (1963) and others leaves the middle troposphere for the boundary layer in the wake of MCSs. Such latent cooling is not only evaporative, it is also produced by melting and sublimating snow (Atlas et al. 1969; Zhang and Gao 1989; Yang and Houze 1995b; Gallus and Johnson 1995a).

For a wake low to form, the mesoscale downdraft must descend adiabatically until it is warmer than the environment at the same altitude (Humphreys 1929; Krumm 1954; Fujita 1963), so it is crucial that hydrometeors do not accompany and latently cool the mesoscale downdraft during its entire descent to the surface. Once the downdraft adiabatically warms the lower troposphere and, by depressing the top surface of the boundary layer cold dome, reduces the depth of storm-chilled air generated by the convective line (Stumpf et al. 1991), the atmosphere's columnar mass is reduced and a wake low forms.

### **2.3 Summary of Literature Review**

Today meteorologists generally agree that mesohighs are produced by cool, saturated downdrafts that raise pressure hydrostatically (the coolness); dynamically (downdrafts striking the ground), and through water loading (the added mass of the rain and ice within downdrafts). Mostly it is the coolness.

Concerning wake lows, compelling evidence suggests rain and snow latently cool RTF flow and render it more dense than its immediate surroundings (negatively buoyant); the newly-created mesoscale downdraft accelerates, and once its accompanying precipitation is weakened or gone, the draft's adiabatic warming prevails; inertia conveys downdraft air to the ground even though it eventually becomes warmer and less dense than the adjacent atmosphere (positively buoyant) and begins decelerating; the resultant pocket of warm surface air reduces the integrated atmospheric mass over the ground.

## Chapter 3

### DATA AND METHODS OF ANALYSIS

*Don't tell me of facts; I never believe facts ...*

—Sydney Smith,  
Lady Holland's Memoir

I founded this research on observations from the Oklahoma-Kansas Preliminary Regional Experiment for STORM-Central (PRE-STORM) conducted during May and June 1985. The data are more than a decade old, but no experiment since PRE-STORM has so successfully captured the signal of MCS transitory pressure perturbations.

#### 3.1 The 12 Subject MCSs

Table 3.1: PRE-STORM MCSs

Date	Observation Interval (UTC)	Synoptics	Velocity (m/s)	Type
7 May	0600/07 to 1250/07	J SF	19.2 from 287°	4
13 May (N)	1225/13 to 1945/13	J CF	20.0 from 213°	5
13 May (S)	1505/13 to 1845/13	J CF	16.2 from 275°	2
27 May	0510/27 to 0830/27	J T DL OB	17.5 from 280°	3
28 May	0900/28 to 1520/28	SF	18.3 from 300°	3
3 June	1510/03 to 1845/03	SF	18.5 from 260°	1
3–4 June	2120/03 to 0230/04	SF	18.6 from 250°	4
4 June	0735/04 to 1225/04	J SF	19.0 from 246°	1
10–11 June	2235/10 to 0750/11	CF T OB	15.6 from 308°	2
15 June	0150/15 to 0950/15	J CF	12.1 from 338°	5
24 June	0045/24 to 0820/24	J SF DL OB	10.0 from 350°	2
26–27 June	2005/26 to 0615/27	J CF	08.6 from 316°	5

Table 3.1 is a cursory description of the MCSs that produced the transients I analyzed. The first column contains the dates of the MCSs. Two MCSs crossed the PRE-STORM

array on 13 May; I indicate the northern of the two with an N and the southern with an S. The second column contains the interval during which the PRE-STORM array observed the transients. For column three, Synoptics, J means a southerly 850-mb jet was present; complexes in the vicinity of a stationary front have an SF; complexes that were dynamically forced by an approaching cold front are labeled CF; those near a surface trough have a T; those forced by a dryline have a DL; and in two cases an outflow boundary from existing convection contributed to MCSs' triggering, so I label them OB. Column four lists the velocities (in degrees from north) of the leading edges of the MCS convective lines (Loehrer 1992). The last column characterizes the shape and evolution of each MCS (Loehrer 1992). Type 1 storms grew from disorganization into asymmetric complexes with small convective lines in the south and stratiform rain in the north. Blanchard (1990) called these systems "chaotic," but Doswell (1991) took issue with the name, arguing it implies a dynamic character that Blanchard did not intend. Type 1 MCSs are loosely comparable to Bluestein and Jain's (1985) "broken area" storms (Loehrer 1995). Type 2 complexes were at first linear, then their northern stratiform areas gradually developed. These are some of Blanchard's (1990) "linear" and Houze et al.'s (1990) "symmetric" MCSs. Fresh convection in Type 3 complexes back-built as their southwestern gust fronts converged with the ambient flow. Stratiform characteristics formed in the north where convection was older. Bluestein and Jain (1985) use a similar classification when examining squall line formations. The last of the eventually-asymmetric MCSs are Type 4. In these, east-west and northeast-southwest convective lines intersected, enhanced stratiform rain developed northwest of the apex, then the east-west line died. Blanchard's hotly-contested name for these storms is "occluded," but likely a "superposition of two preferred convective modes" produced only the coincidental appearance of an occlusion (Smull and Augustine 1993). The remaining MCSs did not turn asymmetric within the PRE-STORM array; they are Type 5. Italicized numbers mark MCSs that spent a significant early part of their lives symmetric in the classical sense of Houze et al. (1990), then became asymmetric. More thorough descriptions of each MCS are available from many sources; I list some of them at the end of the chapter in Tables 3.3–3.5.

### 3.2 Observations

PRE-STORM in situ instruments included 42 National Center for Atmospheric Research (NCAR) second generation Portable Automated Mesonet (PAM II) stations and 42 National Severe Storms Laboratory (NSSL) Surface Automated Mesonet (SAM) stations. Scientists deployed them in a quasi-regular grid with roughly 50 km between sites (Figure 3.1). Each station measured dry- and wet-bulb temperatures, station pressure, 5-min averages of wind speed and direction, peak wind over those 5 min, and accumulated rainfall.

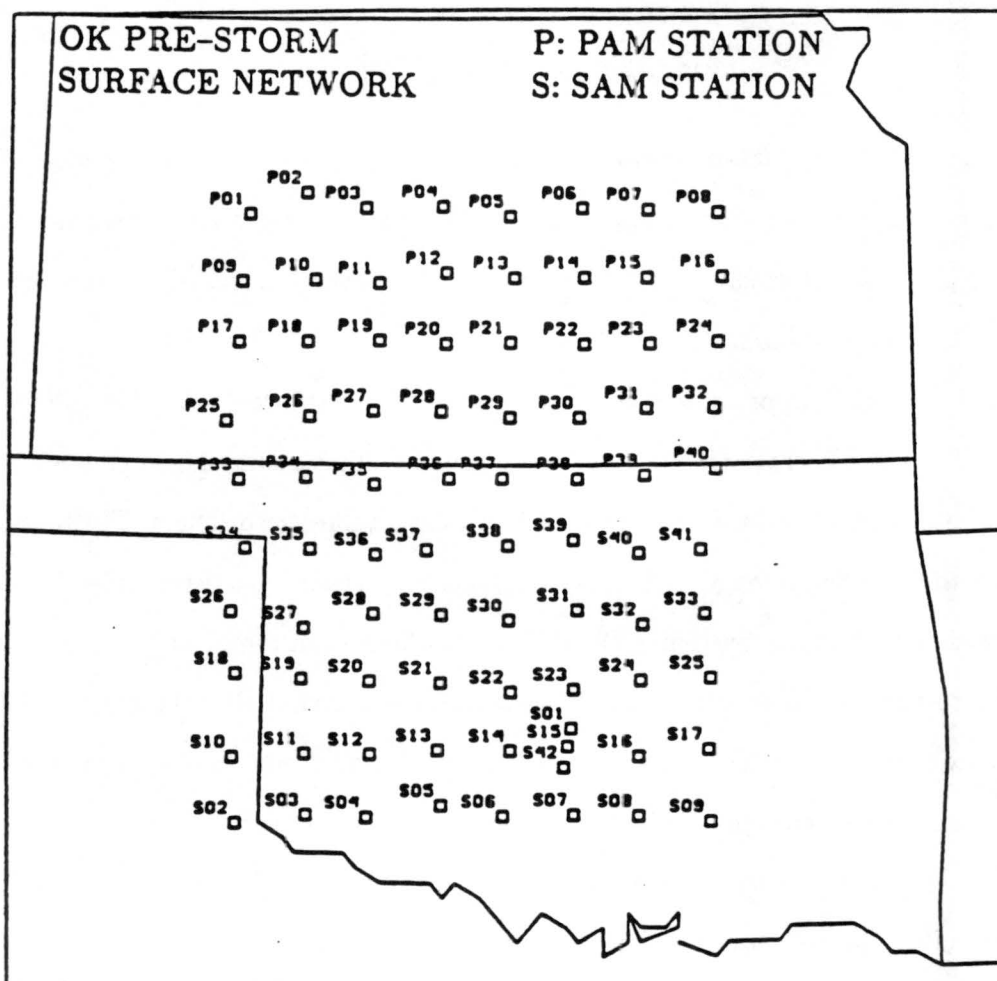


Figure 3.1: PRE-STORM Surface Observing Array. 42 PAM II and 42 SAM stations were located roughly 50 km from one another over parts of Kansas, Oklahoma, and Texas. Stations measured surface conditions every 5 min.

### 3.2.1 Station Pressure

I manipulated the station pressure data in three ways. PAM II and SAM site elevations ranged from 207 m to 823 m, which produced site-to-site station pressure variations that overwhelmed pressure gradients generated by the MCSs. So first I negated the influence of station elevation by normalizing the station pressures to 480 m (the average PRE-STORM station elevation) following the example of Loehrer (1992). I assumed the virtual temperature at each station represented the virtual temperature of a column of the atmosphere extending from a station's elevation either up or down to 480 m. This assumption allowed me to translate an observed station pressure to a 480-m station pressure by

$$P_{480} = P_s \exp \left[ \frac{g(z_s - 480)}{R_d \bar{T}_v} \right]$$

where  $P_{480}$  is the desired 480-m adjusted station pressure,  $P_s$  is the observed station pressure,  $g$  is gravity's acceleration of  $9.8 \text{ m s}^{-2}$ ,  $z_s$  is the station elevation in meters,  $R_d$  is the dry-air gas constant of  $287 \text{ J kg}^{-1} \text{ K}^{-1}$ , and  $\bar{T}_v$  is the mean virtual temperature of the previously-mentioned column.

Second, I filtered out pressure oscillations produced by the diurnal solar tide (Chapman and Lindzen 1970). Loehrer (1992) published a table of adjustments that originated with Stumpf (1988); I merely added or subtracted that table's values accordingly. The tides did not distort the apparent strength or longevity of transient pressure gradients—they forced a maximum change of only a few tenths of a millibar per hour—but the 12 MCSs in my study lived for 3 to 10 h within the PRE-STORM array, so the tides did alter the pressure fields the complexes produced during their observed lives. (I call them *observed* lives because many of the systems were born or died in obscurity outside the array.)

Third, I removed systematic station-specific errors by using the corrections provided by Loehrer (1992) in Appendix A of his thesis. Loehrer determined his corrections based on altitude-adjusted station pressures from nearby National Weather Service (NWS) surface synoptic stations according to the method described by Fujita (1963) and Johnson and Toth (1986). The biases were sufficiently consistent to require only one set of adjustments per MCS passage—a single correction set was valid for the entire 10–11 June event, for

instance—but most MCSs required a unique correction because station inaccuracies changed almost daily.

### 3.2.2 Equivalent Potential Temperature

In addition to station pressure, I contoured equivalent potential temperature,  $\theta_e$ , where

$$\theta_e = \theta \exp\left(\frac{Lw_s}{c_p T}\right).$$

Here  $\theta$  is dry air's potential temperature at 1000 mb,  $L$  is water's 0° latent heat of vaporization of  $2.5 \times 10^6$  J kg<sup>-1</sup>,  $w_s$  is the saturation mixing ratio with respect to water,  $c_p$  is dry air's isobaric specific heat of 1004 J kg<sup>-1</sup> K<sup>-1</sup>, and  $T$  is temperature in K. Because  $\theta_e$  is conserved for all non-precipitating, non-radiative atmospheric processes, it is a useful tracer. I referred to  $\theta_e$  when qualitatively locating outflow boundaries.

### 3.2.3 Radar Composites

I used plots of 0.5° Plan Position Indicator (PPI) reflectivity scans composited from NWS WSR-57s located at Amarillo, TX; Oklahoma City and Norman, OK; Wichita and Garden City, KS; and Monett, MO. The NWS second generation Radar Data Processor (RADAP-II) digitized most of the data. The exceptions were at Wichita, where researchers used the Hurricane Research Division NOAA/ERL/AOML digitizer, and in one case at Norman, where they used the NOAA/ERL/NSSL digitizer. All scans were resolved to at least 2° radially, with gates every 2 km. Although I have reproduced only one radar plot in this thesis, they were invaluable references, as I explain later.

## 3.3 Data Processing

### 3.3.1 Creating Space from Time

I did not judge the 50-km PRE-STORM station spacing sufficient to fully capture transitory MCS pressure perturbations. However, the temporally dense observations allowed me to enhance data from the sparse stations by using the technique Fujita (1955) and Pedgley (1962) employed.

First, I assumed none of the 12 MCSs evolved internally during any single 0.5 h as they moved across the PRE-STORM array. In other words, at any specific time an MCS presumably had the same structure as it did 15 min earlier, and 15 min later it still had that structure, even though the MCS's location changed. This allowed me to take an observed pressure at some time,  $t$ , relocate it 15 min upstream, then assign that pressure to that upstream location at time  $t - 15$ . Downstream adjustments followed similarly. Imagine that a station called STA observed the pressures in Table 3.2 before and after noon UTC on some day in question: Converting time to space produces data positioned as in Figure

Table 3.2: STA Station Pressure

UTC Time	Pressure (mb)
1145	952.4
1150	952.4
1155	952.6
1200	952.8
1205	952.9
1210	953.1
1215	953.2

3.2. The data fall along a line defined by the direction of MCS motion, and the represented space between data along this line is the distance the MCS moved in 5 min.

Fujita (1955) quantified this method for a continuous data set. Observing stations on the ground appear to move beneath an MCS with a velocity  $-V$ . If we choose some property of the complex and dub it property  $A$ , then the local temporal change of that property is  $\partial A/\partial t$  and the advection of that property by the mean MCS motion is  $-V \cdot \nabla A$  where  $\nabla A$  is the horizontal gradient of property  $A$  and may be written  $i\partial A/\partial x + j\partial A/\partial y$ . So the total change in  $A$  at a surface observing station apparently moving beneath an MCS is

$$\frac{DA}{Dt} = \frac{\partial A}{\partial t} + (-V \cdot \nabla A).$$

Assuming 30 min of steady state is equivalent to assuming  $\partial A/\partial t$  is negligibly small over that 0.5 h. This simplifies the total change in property  $A$  to

$$\frac{DA}{Dt} = (-V \cdot \nabla A).$$

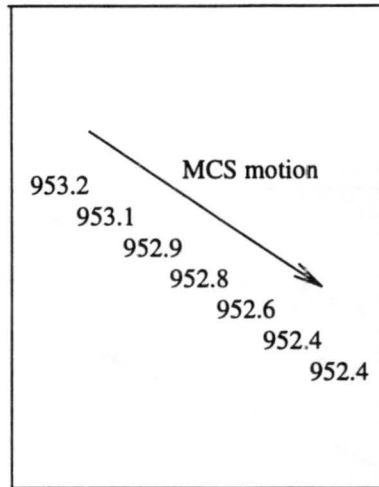


Figure 3.2: Time-to-Space Conversion Example. Seven observations at a single point at different times are translated to observations at seven different points at a single time. See the text for an explanation.

With this equation we can translate changes in property  $A$  over time (the left term) to changes in property  $A$  over space (the right part of the right term). In the specific application for my discrete data set,  $A$  is an observed station pressure, so the units are

$$\left(\frac{mb}{s}\right) = \left(\frac{m}{s}\right) \left(\frac{mb}{m}\right).$$

### 3.3.2 Objective Analysis

I objectively analyzed these enhanced data using the iterative weighted-average interpolation scheme developed by Barnes (1964). The scheme assigns to a grid datum a value based on surrounding raw data that fall within a radius of influence (ROI). The contributions of these surrounding data are weighted according to their proximity to the grid datum, and the weighting function is

$$\eta = \exp\left(\frac{-r^2 E}{R^2}\right)$$

where  $r$  is the distance between the grid datum being calculated and each contributing raw datum, and  $R$  is the ROI.  $E$  describes how many e-folds in weighting occur for raw data one ROI away from a grid datum. In other words, setting  $E$  to 4, as I did, ensures that raw data exactly at the ROI (where  $r = R$ ) will be weighted by  $e^{-4}$ , or 0.018. Compare this to the 0.999 weighting of raw data only 1 km from the grid datum (where  $r = 1$ ). The

sharp decrease of weight with distance insulates the highly localized gradients inherent in convective and mesoscale phenomena from smoothing by more broad-scale gradients.

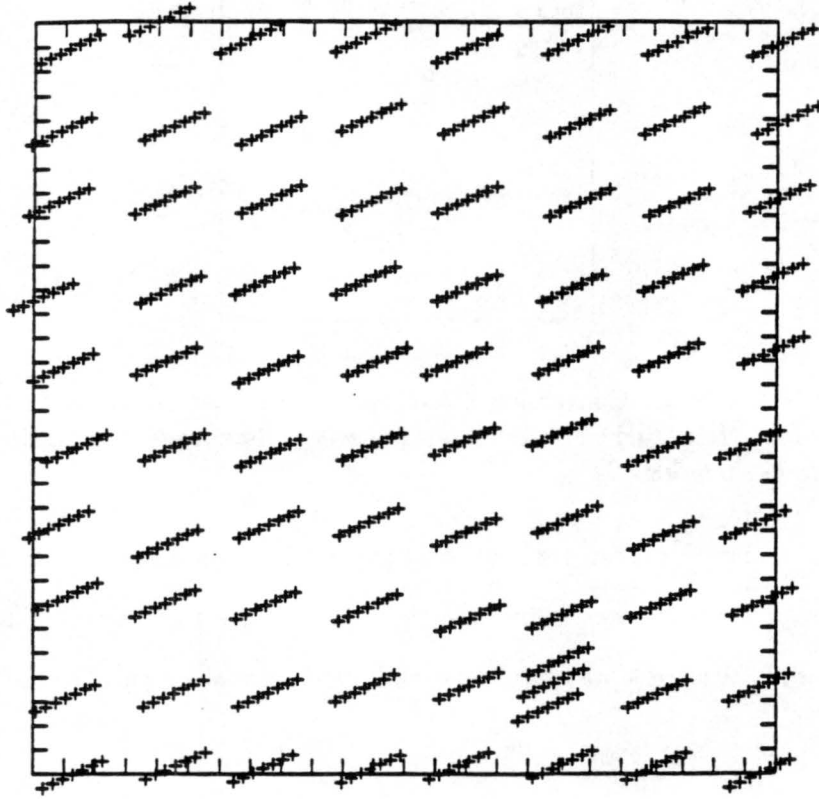


Figure 3.3: Data Distribution After Time-Space Enhancement. Data are arranged in clumps of seven. Each clump is separated by roughly 50 km.

The time-space translation produced data distributed in clumps (Figure 3.3). Data within clumps are separated by just a few kilometers, but the clumps themselves are spaced nearly 50 km apart. Finding a meaningful mean distance between data—normally the first step in determining a suitable ROI—is nearly impossible, so I ignored the enhanced density within the clumps and tested an ROI of 50 km. Results were good, except missing data were occasionally arranged so no reliable raw values fell within a certain grid datum's ROI. Subsequent isoplething treated the void as a 0.0-mb datum and assigned a black-hole-esque closed low to the position. To combat this I slowly increased the ROI and examined the results. At 55 km the voids vanished, so I decided to produce all my plots with a 55-km ROI. But even that generous value occasionally fostered unrealistic isobar gradients if multiple

stations around a grid datum were missing in an imbalanced pattern. Rather than increase the ROI even more, which would have smoothed the field unnecessarily for the denser areas of data, I coded a variable ROI. When a minimum number of reliable data (which I set to seven) were not included in the calculation of a grid datum, the routine temporarily tripled the ROI, then reset it to 55 km for the next datum.

Each iteration of a Barnes objective analysis produces a gridded data field that is *decreasingly* smoothed from the original field. So why not run the routine many times to presumably produce results closer to reality in all its magnificent disorder? Each run after the first amplifies small inherent errors in the original data (Barnes 1964). After a few iterations, these errors grow faster than the desired signals, so two to four iterations is usually the best compromise between fields drowning in noise and fields smoothed featureless.

I am primarily interested in gradients between, and the central pressure of, transitory highs and lows. In order to quantify how well the gridded data retain these original qualities, I recorded the maximum and minimum pressures that appear in the ungridded (pre-Barnes scheme) data and compared them to the two extrema produced after each iteration of the Barnes scheme. The calculation is

$$CAD = |B_{max} - O_{max}| + |B_{min} - O_{min}|$$

where  $CAD$  is the combined absolute departure,  $B_{max}$  is the highest pressure produced by the Barnes objective analysis,  $O_{max}$  is the highest pressure observed by the PRE-STORM array,  $B_{min}$  is the Barnes minimum, and  $O_{min}$  is the observed minimum. Figure 3.4 documents the results. Combined absolute departures decreased rapidly from iterations zero through two, then dropped slightly from iterations three through five. Based on Barnes' findings and the negligible improvements in combined absolute departure produced by later iterations, I chose to iterate my data three times. Interestingly, three iterations produced the most consistently aesthetic plots.

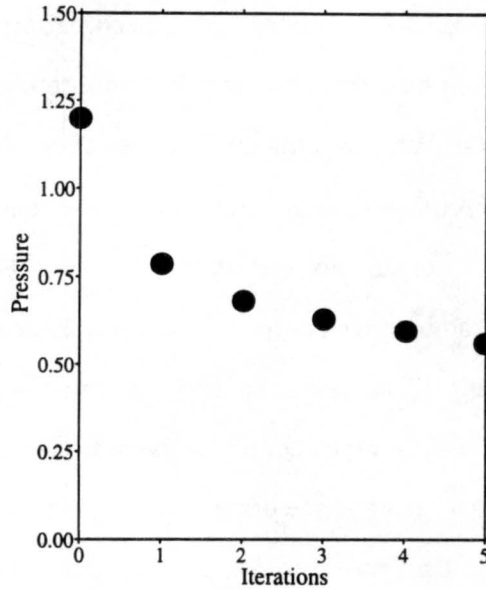


Figure 3.4: Combined Barnes Absolute Pressure Departure. Each iteration of the Barnes objective analysis produced extrema values closer to the values observed by the PRE-STORM array. By iteration three, improvements were negligible.

### 3.4 NCAR Graphics Plots

#### 3.4.1 Contour Maps

The Barnes objective analysis merely produces a regularly-spaced array of numbers. To contour the array I employed NCAR Graphics 3.2, which uses cubic splines under tension to draw its isolines, so this step necessarily smoothed the fields one additional time. Station pressure is isoplethed in solid lines at half-millibar intervals,  $\theta_e$  in dashed lines at intervals of one K.

#### 3.4.2 Movies

Once I had generated hundreds of individual plots spanning the lives of the 12 MCSs, I animated them with the NCAR Graphics 3.2 X-Window Interactive Image Display Tool (IDT). The contour plots are the frames of the animation sequences, or movies—one for each MCS. Isobars are colored according to pre-event mean pressure. Lines of increasingly lower pressure appear as deeper and deeper reds, high pressure appears similarly in blue, and the isobar nearest the pre-event mean station pressure is off-white. Isolines of equi-

valent potential temperature are dashed and colored a background yellow-green. They are references only, intended to give the viewer a qualitative idea of the thermal character of the lowest level of the troposphere. IDT displays five movie frames per second, so monitoring individual isoline labels as they dance about the screen is unrealistic; the color promotes quick assessment of the overall pressure field evolution (see accompanying video tape).

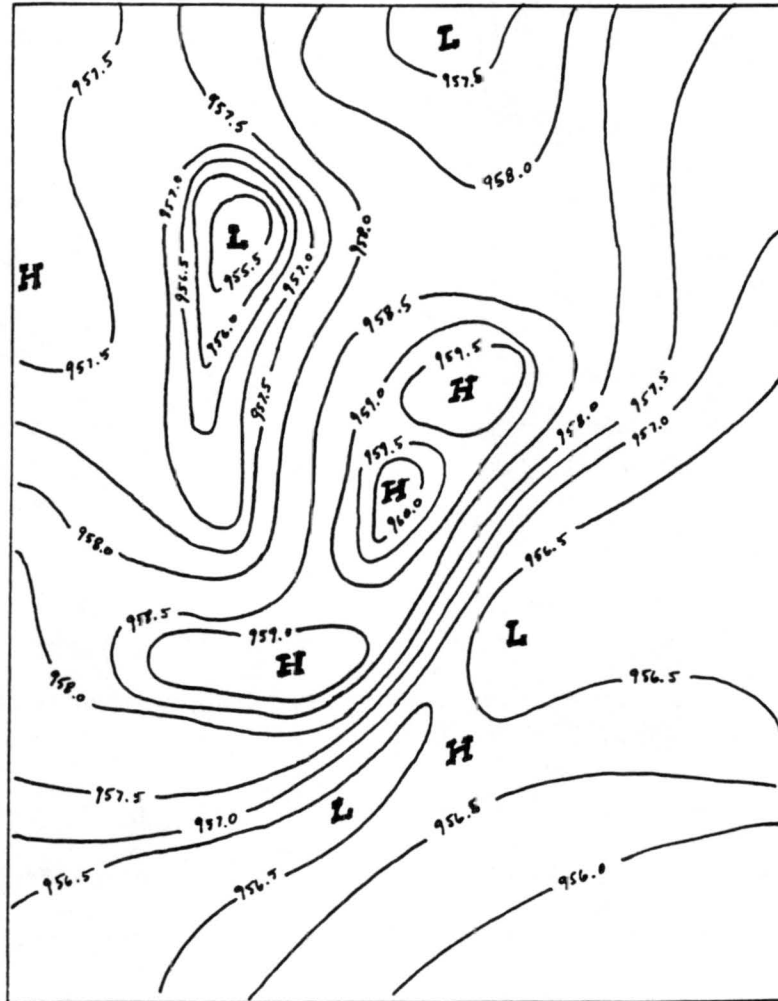


Figure 3.5: Test Pressure Field for Analysis Verification. I submitted this synthetic field to three data-processing steps. The resultant field is shown in Figure 3.6.

### 3.5 Analysis Legitimacy

Without accurate station pressure analyses almost nothing that follows would merit attention. My list of transients and my evaluation of their properties are based entirely on

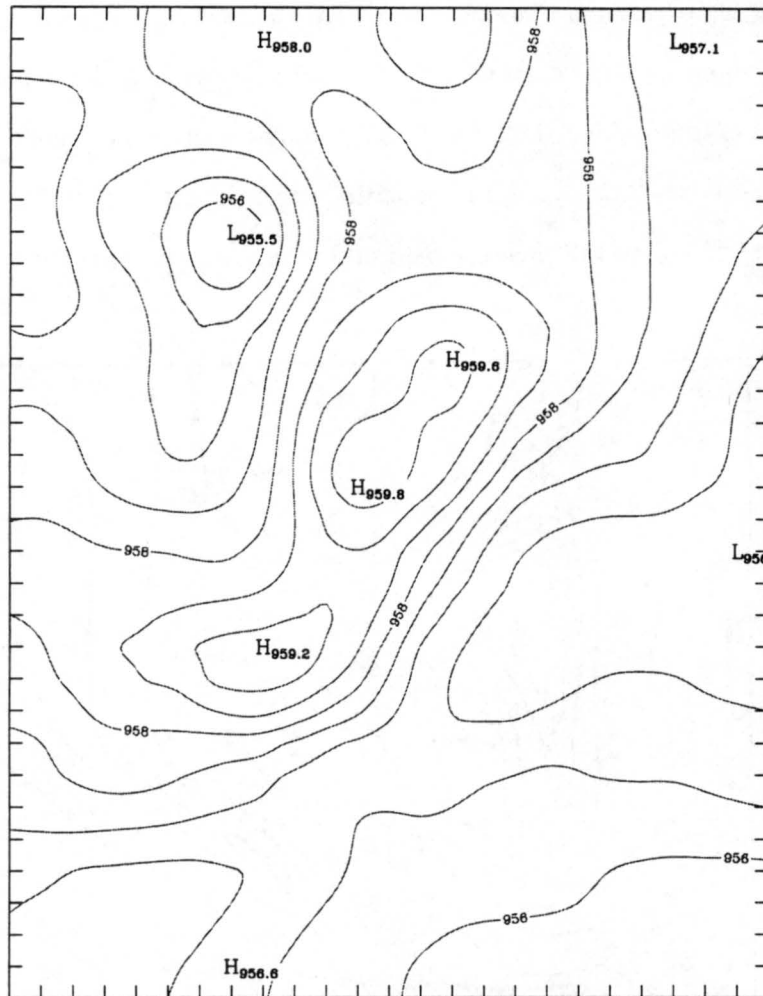


Figure 3.6: Verification Pressure Field. My three-step data processing transformed Figure 3.5 into this generated field. The plots is fundamentally the same as the original pressure field.

the features that appear in the NCAR Graphics plots. Those final plots (and the movies of the plots) synthesize the three stages I mentioned above: (1) sensing by the PRE-STORM PAM II and SAM stations, (2) objective analysis by the Barnes scheme, and (3) isoplething by NCAR Graphics 3.2.

Although I addressed step (1) contaminations by removing systematic and severe errors from the PAM II and SAM data, how reliably do the second and third steps treat the data? I constructed an artificial but representative MCS pressure field (Figure 3.5), then mimicked an MCS's trek across the Great Plains by sliding the drawn field across a map of the PRE-STORM array with a scale velocity of  $16 \text{ m s}^{-1}$  from  $315^\circ$ . For seven times ( $t - 15$

through  $t + 15$  at 5-min intervals) I recorded the station pressure that each of the 84 stations would have observed had the event been real (and the instruments flawless). I passed the resultant data through the objective analysis and the NCAR Graphics isoplething, and produced Figure 3.6.

The input and output fields resemble one another quite closely. Both contain four transients—three highs and one low. Additionally, the analysis resolved the two lobes of pre-squall low pressure and the local low in the northern part of the array. The true magnitudes of the local extrema did not completely survive the process—the lows are not low enough and the highs are not high enough—but the differences are only a few tenths of a millibar. Most importantly, *the analysis did not introduce any false transients or conceal any real ones.*

In my simulation I did not omit groups of observations in an attempt to simulate missing data, but the test plot is still valid. The objective analysis treats data voids by smoothing with either the original 55-km ROI or with the temporary 165-km ROI. Voids can only increase field smoothness, so missing data cannot introduce false transients. Certainly vast areas of missing data may harbor undetected legitimate transients, but the blame for that falls upon the PRE-STORM array, not on subsequent analyses.

Table 3.3: Comprehensive Case References

Date	References
Survey of Most or All 12 Cases	Cunning (1986) Blanchard (1990) Loehrer (1992) Augustine and Howard (1988)

Table 3.4: References By Case: May

Date	References
7 May	Fortune (1989) Brandes (1990) Brandes and Ziegler (1992)
13 May (N)	none
13 May (S)	none
27 May	Carbone et al. (1990) Crook et al. (1990)
28 May	Smull and Houze (1987b) Houze et al. (1989) Scott and Rutledge (1995)

Table 3.5: References By Case: June

Date	References
3 June	Fortune (1989) Green (1989) Stumpf and Johnson (1989) Holle et al. (1990, 1994) Fortune et al. (1992) McAnelly and Cotton (1992) Nachamkin (1992)
3-4 June	Stumpf (1988) Fortune (1989) Green (1989) Leary and Bals (1989) Meitín and Watson (1989) Smull and Augustine (1989) Holle et al. (1990, 1994) Leary and Bals (1990) Smull et al. (1991) Stumpf et al. (1991) Fortune et al. (1992) Smull and Augustine (1993) Hane and Jorgensen (1995)
4 June	Fortune (1989) Green (1989) Holle et al. (1990, 1994) Fortune et al. (1992) McAnelly and Cotton (1992) Trier and Parsons (1993)
10-11 June	Smull and Houze (1987b) Johnson and Hamilton (1988) Rutledge et al. (1988) Houze et al. (1989) Meitín and Watson (1989) Zhang and Gao (1989) Zhang et al. (1989) Gao et al. (1990) Biggerstaff and Houze (1991a,b) Vescio and Johnson (1992) Gallus and Johnson (1995a,b) Yang and Houze (1995b) Braun and Houze (1995)
15 June	Johnson and Miner (1994)
24 June	Johnson et al. (1989) Stensrud and Maddox (1991) Stensrud et al. (1991) Johnson and Bartels (1992) Bernstein and Johnson (1994)
26-27 June	Stumpf and Gallus (1989) Bélair and Zhang (1996)

## Chapter 4

### TRANSIENTS AND THEIR POSSIBLE ORIGINS

*We look around and perceive that . . . every object is related to every other object . . . not only spatially but temporally . . . As a fact of pure experience, there is no space without time, no time without space; they are interpenetrating.*

—D. T. Suzuki,  
B. L. Suzuki's Mahayana Buddhism

Before continuing, I must explain what I mean by the term surface pressure transient. Consider them the building blocks, the generation sites, of mesohighs and wake lows. *Transients are elements of mesohighs and wake lows*, for close study of the 12 subject MCSs indicates the latter two are really just spatial *and temporal* envelopes of smaller, more brief perturbations. Mesohighs and wake lows are products of the short-term memory of the lower half of the troposphere, for when the kinematics and latent energy exchanges that generate the transients are shut off, the perturbed mass fields do not melt away immediately into the ambient pressure field. They linger. Mesohighs and wake lows are blends of extant transients and the vestiges of recently-faded transients that are being slowly assimilated by the synoptic atmosphere.

#### 4.1 Problems with Current Mental Models

You will notice two points if you scrutinize both older and recent mesohigh and wake low schemata. First, there are very few of them—at least very few *different* ones. Authors frequently reproduce conceptual figures others have developed, so one depiction appears again and again. Second, you will notice that the few unique schemata that do exist often, although not exclusively, depict highly elongated mesohighs and wake lows with major axes perpendicular to storm motion. In one popular recent schema (Figure 2.1), Johnson and Hamilton (1988) depicted eccentricities (ratios of minor to major axes) exceeding 1:3,

where the minor axes of both features are roughly 100 km. Other researchers have portrayed mesohighs and wake lows in a roughly similar way (Fujita 1955; Pedgley 1962; Vescio and Johnson 1992).

In actual analyses, instantaneous footprints of mesohighs and wake lows almost invariably are more circular. When the footprint of a broad mesohigh or wake low is greatly elongated and parallel to the convective line, usually a few embedded adjacent quasi-circular highs or lows create the eccentric perturbation envelope (Figure 4.1).

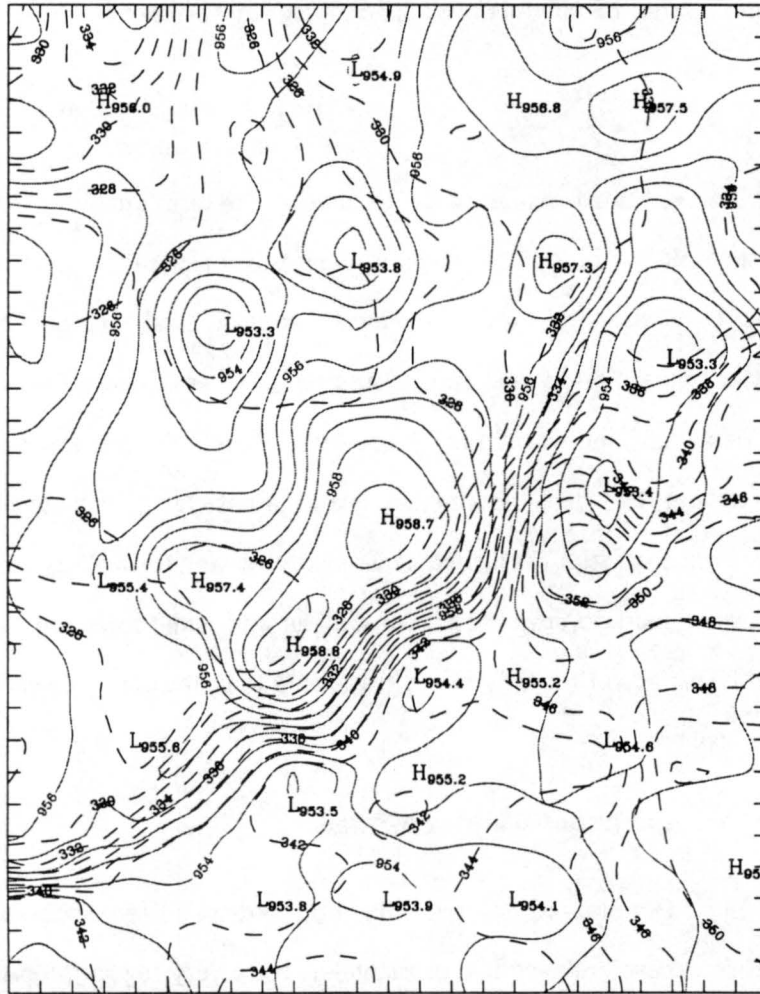


Figure 4.1: Station Pressure and  $\theta_e$  for 0310 UTC 11 June 1985. The NE-SW gradient maximum marks the southwestward-moving squall line. Post-squall pressure perturbations are quasi-circular, not elongated as they are often portrayed in schemata.

The distinction is important. When scientists search for the origins of mesohighs and wake lows, and when they search for better ways to model them, they focus their efforts

on processes that perturb the pressure over some area a few millibars for a few hours. The explanation of how a  $50 \times 80$  km area is perturbed for 2 h may not be identical to the explanation of how a  $100 \times 300$  km area is perturbed for 6 h. Moreover, the latter may not even exist unto itself; it may be the collective disguise worn by a small band of transients.

#### 4.2 Movie Evidence of Transients

Highly-resolved NCAR Graphics movies provided the first evidence that considering mesohighs and wake lows separate from transients may be inaccurate. The mesohighs and wake lows appear to comprise quasi-circular transients that grow quickly, move about, then disappear, only to be replaced by one or two more transients. Such successions maintain the migrating eccentric footprint. Without temporally fine data, an observer might miss these successions altogether. In 5 or 10 min one transient dies, and in nearly the same spot another appears, looking very much the same as the first. Data resolved to 0.5 h would hide the phenomenon, and an observer would conclude the original was still present. One must peruse the 5-min movies to truly appreciate the elegant and fluid, yet mercurial surface MCS environment. (View these movies on the Colorado State University Atmospheric Science computer named Tornado or on the accompanying video tape.)

Do these newly recognized transitory pressure perturbations force us to disregard existing mesohigh or wake low origin theories (see Chapter 2) and search elsewhere for explanations of MCS surface pressure fields? No. A meso- $\beta$ -scale feature may have a quasi-circular instead of highly eccentric footprint, but it is still a meso- $\beta$ -scale feature, subject to meso- $\beta$ -scale thermodynamics and kinematics.

#### 4.3 The Origin of Transitory Highs

Squall lines are not uniformly strong along their length. Member cumulonimbi are usually arranged shoulder-to-shoulder (Rotunno et al. 1988), but at any one time some cumulonimbi are old and some are young; some are weak, others are strong (Fovell and Ogura 1988; Houze et al. 1990). Although their outflows mix, the towers and the convective downdrafts within these towers are separate (Redelsperger and Lafore 1988). Downdraft

accelerations and water loading from rain and hail shafts raise surface pressure unequally along the line. But this does not wholly explain pronounced pressure variations within meso-highs because: (1) pressure changes induced by downdraft momentum and water loading are usually not large enough to account for the entire perturbation high pressure (Bleeker and Andre 1950; Nicholls et al. 1988); and (2) transitory highs' scale is meso- $\beta$ , but the instantaneous footprints of the downdraft and rainshaft are convective.

A 1959 paper by Fujita may explain how convective cells within an MCS can generate thermodynamic forcing that is sufficiently strong and sufficiently expansive to produce transitory highs. Fujita found that a cumulonimbus' evaporatively-chilled outflow mass is directly correlated with its rainfall, even though the cold pool spreads well beyond the horizontal extent of the main rain shaft (Byers and Braham 1947; Bleeker and Andre 1950). In a sense, a meso- $\gamma$ -scale event provokes a meso- $\beta$ -scale change in boundary layer thermal properties. The increase in integrated atmospheric mass under these cold pools is often sufficient to collectively create a mesohigh (Nicholls et al. 1988). Cumulonimbus rainfalls vary within a squall line so cold pool masses vary.

Cold pools are not born of only chilling liquid drops, however, for above the evaporating rain lies snow that sublimates and evaporates and also cools the air. Atlas et al. 1969 calculated that melting snow may chill downdrafts nearly as much (80%) as evaporating rain. Of course it makes no sense to regard pockets of heavy snow and pockets of heavy rain as two different cold pool mechanisms: the former transform into the latter. Regardless of what lowers their temperature, mixing and energy fluxes at the edges of neighboring cold pools is insufficient to instantaneously homogenize the entire post-squall boundary layer. Consequently, high pressure strength varies within the overall mesohigh envelope (Williams 1953; Pedgley 1962). These areas of localized higher pressure are high pressure transients.

#### 4.4 The Origin of Transitory Lows

If we superficially examine infrared or coarse radar images of MCS stratiform regions, they appear to be nearly horizontally homogeneous—at least much more homogeneous than the convective line. And in their schemata scientists often draw anvils as single canopies

that overlie broad two-dimensional conveyor-belt flows (Figure 4.2). This makes explaining transitory lows difficult, for we expect a homogeneous stratiform region to produce one large homogeneous wake low. Real stratiform regions must harbor vital smaller pockets of varied thermodynamics that produce more than one low under or at the rear of the anvil. Some moisture, temperature, or flow property must vary on the scale of the small transitory lows illustrated in my movies.

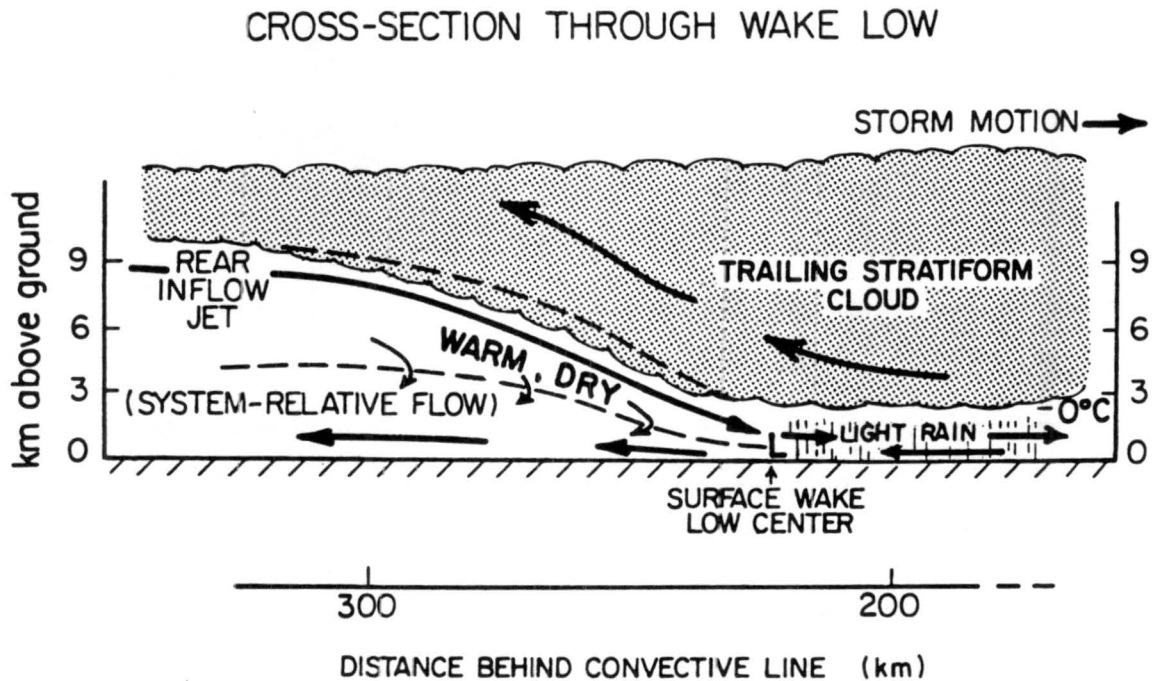


Figure 4.2: Schema of MCS Stratiform Region. Anvils are usually portrayed as homogeneous umbrellas over smooth two-dimensional conveyor-belt flows (from Johnson and Hamilton 1988).

I remain loyal to current hypotheses of wake low formation (see Chapter 2) so transitory lows must exist within wake low envelopes because of meso- $\beta$ -scale inhomogeneities in the rate of latent cooling of the inflow under the anvil. “Evaporation is the most important latent cooling process determining the structure and strength of the descending rear inflow and the mesoscale downdraft” according to Yang and Houze (1995b). True or not, we cannot ignore sublimation. When Braun and Houze (1995) ignored sublimation in their nonhydrostatic model, their simulated 10–11 June squall line lacked a strong core rear inflow and was a

mere shadow of its real self. And Atlas et al. (1969) demonstrated the important air-chilling role of melting snow. Three factors primarily control evaporation, sublimation, and melting in the RTF flow: (1) rain and snow rates; (2) the speed of RTF flow; and (3) the humidity of RTF flow. Inhomogeneities in one or more of these three may be the origins of transitory lows.

#### 4.4.1 *Variations in Rain and Snow Rates*

Biggerstaff and Houze (1991a) found that meso- $\beta$ -scale pockets of high rain rates develop in the stratiform region immediately rearward of the most vigorous cells in a convective line. Gallus and Johnson (1995b) agreed. During the 10–11 June MCS, reflectivities within such pockets exceeded those of the lightest stratiform precipitation by up to 20 dBZ. Biggerstaff and Houze noted that “[t]he mesoscale downdraft was most pronounced in the area associated with the strongest precipitation and was, on average, virtually nonexistent in the weak stratiform precipitation regions.” Rutledge et al. (1988) bypassed the bland and cautious “associated with” and wrote that maxima in sublimative and evaporative cooling actually “drive” the mesoscale downdraft.

A multiple Doppler study of a May 1977 squall line over Oklahoma revealed a similar embedded 50-km pocket of 25-dBZ stratiform rain (Kessinger et al. 1987). The young squall line’s stratiform rain was undeveloped, and the RTF flow was weak, so their interactive role in altering the surface pressure is in doubt; Kessinger et al. did not bother to include analyses of the surface pressure in the rear part of the squall line. Still, this is more evidence for meso- $\beta$ -scale variations in the stratiform rain intensity.

Generally, immediately above shafts of heavy rain lie shafts of heavy snow, so high rain rates and high snow rates may be effectively grouped in the same category. In one specific study of the distribution of snow mixing ratios within an anvil, Braun and Houze (1995) simulated the 10–11 June MCS with the nonhydrostatic model MM5. Meso- $\beta$ -scale maxima of snow mixing ratios formed and shortly thereafter invigorated, through sublimative cooling, the proximate part of the modeled RTF flow.

Even if RTF inflow is initially homogeneous along the length of a squall line, such pockets of heavier rain or snow will cool bands of flow and force them to descend more quickly than portions of the flow that encounter only light rain (Gallus and Johnson 1995a; Braun and Houze 1995). The high downward momentum of the inflow bands may enable them to descend well past their level of neutral buoyancy where their relatively low density would reduce the integrated mass beneath the downdrafts so the pressure under them would fall (Stumpf et al. 1991).

In his 1995 paper, Gallus proposed that it is not the precipitation rate, but the *change* in the precipitation rate that fosters the strongest wake lows. He used a two-dimensional cloud model that contained a domain that fully encompassed the back edge of a stratiform region, and initiated an exclusively snow-based microphysical field. Then he made adjustments until the model produced radar reflectivities similar to those observed. Gallus found that although invariant snow rates produced heavy rain at the surface and induced strong subsidence, latent cooling almost negated subsidence warming so no realistically strong wake lows developed. Decreasing the snow rate within the anvil lessened the latent cooling and the warmer, less dense downdraft generated stronger, more realistic wake lows. This implies that horizontal variations in *the change of* precipitation rates may be as successful at generating individual transitory lows within a wake low envelope as horizontal variations in the rates themselves.

#### 4.4.2 *Speed Variations in Rear-To-Front Flow*

Most studies of RTF flow are two-dimensional. They depict flow as a vast conveyor belt that extends hundreds of kilometers along the back of the squall line and descends uniformly beneath the melting layer. Often one cannot tell whether the uniformity is real or the product of modelers' or observers' treatments.

Some studies do deviate from the conveyor-belt representation, though. Biggerstaff and Houze (1991a) found that flow just below the melting layer in the 10–11 June MCS varied by 2–5 m s<sup>-1</sup> along the length of the stratiform region. But the fastest RTF flow was not directly upwind of the deepest surface lows, so in their case the connection between

RTF flow speeds, latent energy exchanges, and surface pressure is seemingly buried in microphysical complexity.

On 28–29 June 1989 a squall line traversed the North Dakota Thunderstorm Project. Klimowski (1994) used five dual-Doppler analyses to monitor the development and character of the line's RTF flow. He found that the RTF flow harbored speed inhomogeneities on two scales. First, flow was broadly strongest behind the northern, most mature part of the line, underneath the most well developed segment of the anvil. Second, and most importantly, local meso- $\beta$ -scale maxima appeared. Horizontal windspeeds within these maxima were occasionally more than  $5 \text{ m s}^{-1}$  greater than RTF flow speeds only 20 km away at the same elevation.

#### 4.4.3 Humidity Variations in Rear-To-Front Flow

Any meso- $\beta$ -scale regions of localized dry RTF flow may produce heightened evaporative cooling. Greater cooling produces greater descent and greater downward momentum that overcomes a mesoscale downdraft's positive buoyancy (Yang and Houze 1995b).

Johnson and Hamilton (1988) discovered such regions in the RTF flow of the highly-scrutinized 10–11 June MCS. Their depictions are composite cross-sections developed from rawinsonde data recorded during 3 h of the MCS's maturity. Relative humidity at a fixed altitude and distance behind the convective line varied by as much as 30% over 100–200 km. During those 3 h, two strong wake lows existed, separated by a weak depression. Upwind of both wake lows, RTF flow was relatively strong and dry, but inflow was almost nonexistent in the middle of the stratiform region (measured in distance from both ends), just to the rear of the weak depression. The flow present there was strongest on the convective-line side of the surface depression and had a composite relative humidity surpassing 80% in places. The data imply that weak RTF flow and reduced evaporation in the middle of the line hindered the surface depression from deepening to the levels of the lows on the line's ends, where RTF flow was initially drier.

It appears current theories on mesohigh and wake low origins are readily applicable to post-squall MCS pressure transients. Indeed, they may apply more seamlessly to transients than to the larger perturbations because repeatedly observed and modeled temporal and spatial variations in the phenomena that perturb surface pressure beneath MCSs are at odds with current mental models of large, persistent, homogeneous mesohighs and wake lows. I have suggested why 92 transients appeared beneath 12 PRE-STORM MCSs; the following chapters explain what happened to the 92 after they formed.

## Chapter 5

### THE PRE-STORM TRANSIENTS

*What we have not named or beheld as a symbol escapes our notice.*

—W. H. Auden,  
“I Am Not a Camera”

My 12 PRE-STORM MCSs produced 92 transients: 53 highs and 39 lows. I excluded pre-squall pressure perturbations, but included all other meso- $\beta$ -scale highs and lows that met specific criteria. The sizes, lifetimes, and displacements of the chosen 92 appear in Tables 5.1–5.12.

#### 5.1 Criteria for Transient Selection

Figure 5.1 is a representative pressure/ $\theta_e$  plot. No fewer than 23 local extrema appear on the page, but not all of them represent real mesoscale extrema, and not all of the real extrema were born of the MCS that crossed the Great Plains on 15 June. I established specific tests to segregate the real from the non-real for 15 June and its 11 counterparts.

##### 5.1.1 Final Instrument Error Removal

To isolate and disregard the lingering false signals that eluded my front-end quality control (see Chapter 3), I scrutinized the 12 movies over and over, fast and slow, forward and backward. False signals produced by instrument errors stood fixed at station sites the way boulders stand immovable in a rushing trout stream. Their signature is unmistakable. I ignored these and all signals produced by a lone PAM II or SAM station and not corroborated by neighboring stations.

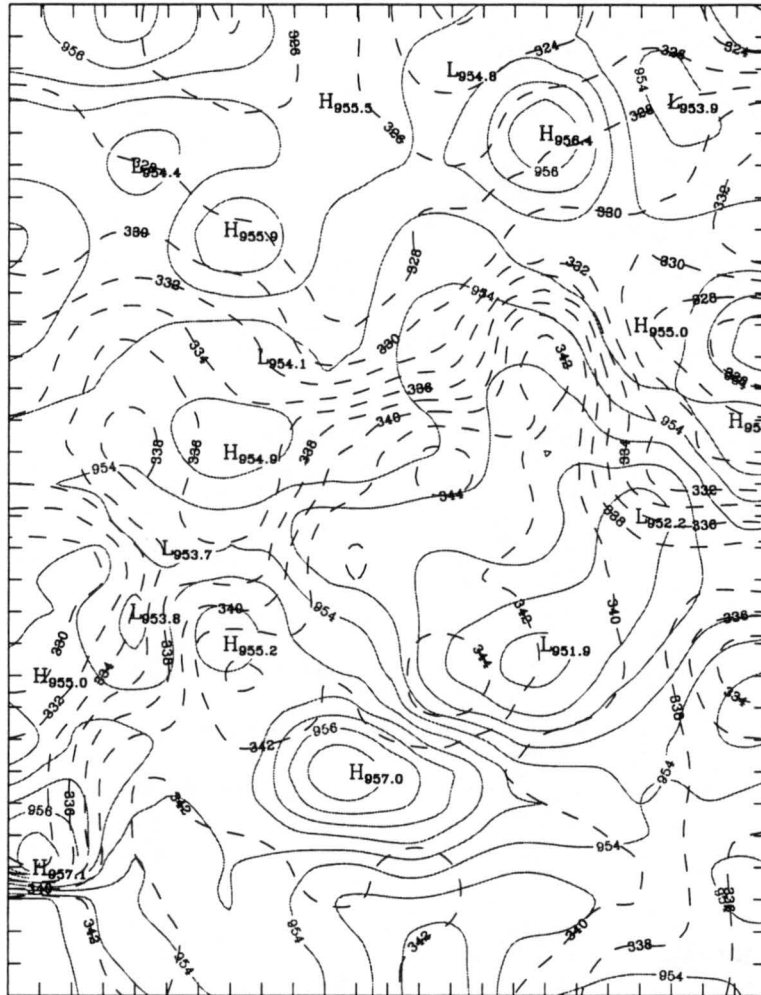


Figure 5.1: Station Pressure (solid in mbs) and  $\theta_e$  (dashed in K) for 0410 UTC 15 June 1985. On a single image such as this, data errors appear similar to real perturbations, and without referring to composite radar reflectivities it is impossible to determine which perturbations are associated with MCS precipitation regions and which are not.

### 5.1.2 NCAR Graphics Red Herrings

Theoretically, the time-space conversion described in Chapter 3 forces transients to live on the plots at least 0.5 h. A single observation is translated across a 30-min band, so all perturbations, real or false, should last that long. Some did not. The fault lies with the NCAR Graphics isoplething routine. While applying isobars, the routine occasionally drew kinks and labeled local extrema that were products of noise in the data or vagaries within the NCAR Graphics code, not products of stormy early summer weather over the Great Plains. The kinks and extrema appear on the plots for 5 or 10 min, then vanish. In

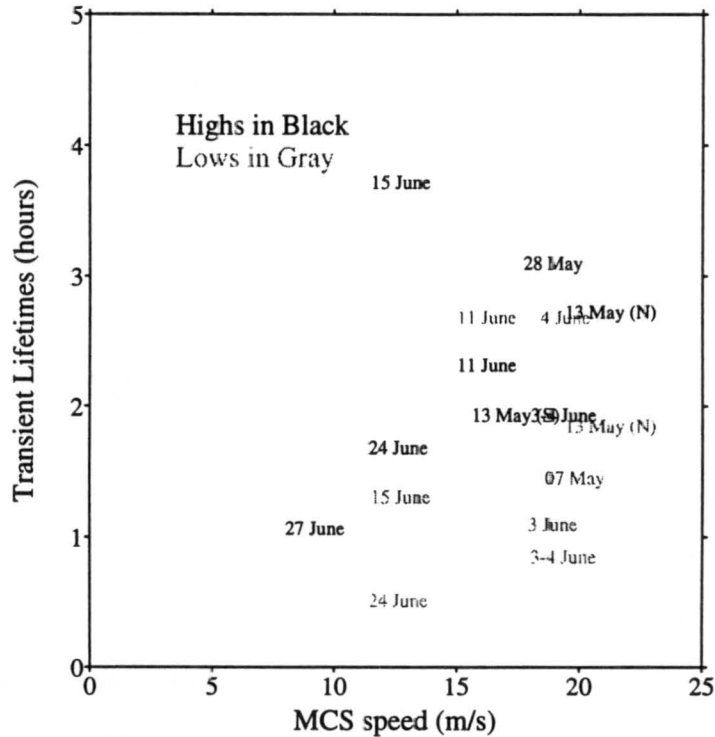


Figure 5.2: Average MCS Transient Lifetime vs. Leading-Line Speed. The fastest MCSs produced the most long-lived transitory highs and lows. Data are for fully-sampled transients only.

the end, I included transients younger than 0.5 h only if their observed lives were cut short as they ventured beyond sight of the PRE-STORM array.

### 5.1.3 The Problem of Inoperative Stations

Transients that crossed the domain of inoperative stations disappeared for a time, then reemerged as reliable stations detected them farther downstream. Each reemerging transient might have been easily mistaken for a second, separate creature. I compensated for the blind spots in the array by exhaustively studying the lows and highs as they approached these voids and by projecting their paths across the voids until the transients reemerged. Ultimately, the technique is subjective.

### 5.1.4 Radar Verification

Just because a perturbation appears to be a legitimate transitory high or low does not mean that it is directly associated with an MCS. Referring to composite radar plots (see

Chapter 3), I included in my survey highs only under or near convection and post-squall lows only under or near any part of the reflectivity field, convective or stratiform.

## 5.2 Roster of Transients

The transients lived in families whose members I judged to be physically linked (1) if they were proximate and separated by extremely high pressure gradients; (2) when a tandem of high and low transients moved similarly and remained close to each other during their lives; or (3) when a single transient divided into two or more. Usually the distinction between families was obvious; occasionally it was ambiguous, but book-keeping demanded a decision even if it was arbitrary.

The first letter of a transient's name signifies its pressure perturbation: names of highs begin with an H, lows with an L. The second letter is a transient's family name. The third character, a number, gives a name its unambiguity. I assigned those numbers sequentially from 1 through 9. A family usually (but not always) contains both transitory highs and transitory lows. For instance HA2 and LA1 belong to the same family because they are presumably physically linked. Notice that the third character, the number, does not imply a special sub-family association among transients with like numbers. HB2 and LB2 belong to the same family, but that is the extent of the link. The lifetimes of the two may not even coincide. Also keep in mind that by separating transients into families I have not implied that members of different families are physically isolated from each other, merely that links across families are distinctly less apparent than links within families. In the end, the family groupings are only secondarily important. They aided book-keeping and are the simplest way to keep readers and me from mistakenly associating transients that were hundreds of kilometers or a few hours apart.

Tables 5.1–5.12 list the transients and some of their characteristics. Lifetimes are the differences between the times the transients were first and last observed. Displacements are the net distances the transients traveled (*not* the total distances traveled). Transients that began or ended outside the array have an "N" in the Coverage column. Their lifetimes and displacements are only partially known, but I have listed values for them anyway.

Table 5.1: 7 May Pressure Transients

Name	Lifetime (min)	Displacement (km)	Coverage
HA1	250	255	N
HB1	220	255	N
HB2	250	345	N
HB3	115	168	N
Avg.	209	256	—
LA1	190	171	Y
LB1	295	338	N
LB2	045	045	Y
LB3	075	087	Y
LB4	035	030	Y
LB5	030	064	N
Avg.	112	123	—

Table 5.2: 13 May (N) Pressure Transients

Name	Lifetime (min)	Displacement (km)	Coverage
HA1	250	308	Y
HB1	080	096	N
HB2	125	195	N
HC1	075	087	Y
HC2	075	075	N
Avg.	121	152	—
LB1	180	234	Y
LB2	035	047	Y
LB3	115	138	Y
Avg.	110	140	—

Table 5.3: 13 May (S) Pressure Transients

Name	Lifetime (min)	Displacement (km)	Coverage
HA1	115	105	Y
HB1	150	128	N
Avg.	133	117	—
LB1	170	090	N
LB2	080	120	N
Avg.	125	105	—

Table 5.4: 27 May Pressure Transients

Name	Lifetime (min)	Displacement (km)	Coverage
HA1	160	210	N
HB1	085	121	Y
HC1	090	165	N
Avg.	112	165	—
LA1	070	045	N
Avg.	070	045	—

Table 5.5: 28 May Pressure Transients

Name	Lifetime (min)	Displacement (km)	Coverage
HA1	185	204	Y
HB1	165	090	N
HC1	160	202	N
Avg.	170	165	—
LB1	295	270	N
LC1	125	136	N
Avg.	210	203	—

Table 5.6: 3 June Pressure Transients

Name	Lifetime (min)	Displacement (km)	Coverage
HA1	125	204	N
HB1	170	188	N
Avg.	148	196	—
LB1	030	034	Y
LB2	100	075	Y
Avg.	065	055	—

Table 5.7: 3-4 June Pressure Transients

Name	Lifetime (min)	Displacement (km)	Coverage
HA1	050	045	N
HA2	115	134	Y
HB1	140	171	N
HC1	060	076	N
HD1	185	235	N
Avg.	110	132	—
LA1	050	047	Y
LB1	170	162	N
Avg.	110	105	—

Table 5.8: 4 June Pressure Transients

Name	Lifetime (min)	Displacement (km)	Coverage
HA1	140	225	N
HB1	135	170	N
HC1	075	127	N
Avg.	117	174	—
LA1	100	085	N
LB1	090	121	N
LB2	160	150	Y
Avg.	117	119	—

Table 5.9: 10–11 June Pressure Transients

Name	Lifetime (min)	Displacement (km)	Coverage
HA1	125	121	Y
HB1	215	267	Y
HB2	245	229	Y
HC1	045	034	N
HC2	030	042	Y
HD1	070	105	N
HE1	075	081	Y
Avg.	115	126	—
LA1	060	054	N
LB1	155	162	N
LB2	160	129	Y
LB3	090	120	N
LC1	105	128	N
LE1	195	129	N
LE2	065	054	N
LE3	140	138	N
LE4	025	045	N
Avg.	111	107	—

Table 5.10: 15 June Pressure Transients

Name	Lifetime (min)	Displacement (km)	Coverage
HA1	255	151	Y
HB1	180	121	Y
HC1	015	015	N
HD1	230	247	Y
HE1	115	127	N
HF1	035	054	N
Avg.	138	119	—
LD1	130	091	N
LF1	090	095	N
LF2	140	081	N
LG1	090	034	Y
LG2	065	030	Y
Avg.	103	066	—

Table 5.11: 24 June Pressure Transients

Name	Lifetime (min)	Displacement (km)	Coverage
HA1	145	047	N
HA2	175	109	Y
HB1	110	076	N
HB2	215	108	N
HC1	030	015	N
HC2	080	034	Y
HC3	045	021	Y
Avg.	114	059	—
LA1	260	000	N
LA2	030	015	Y
Avg.	145	008	—

Table 5.12: 26–27 June Pressure Transients

Name	Lifetime (min)	Displacement (km)	Coverage
HA1	060	064	Y
HB1	040	030	Y
HC1	115	067	Y
HD1	075	045	Y
HE1	040	015	Y
HF1	045	042	Y
Avg.	063	044	—
LG1	175	181	N
LH1	100	096	N
Avg.	138	139	—

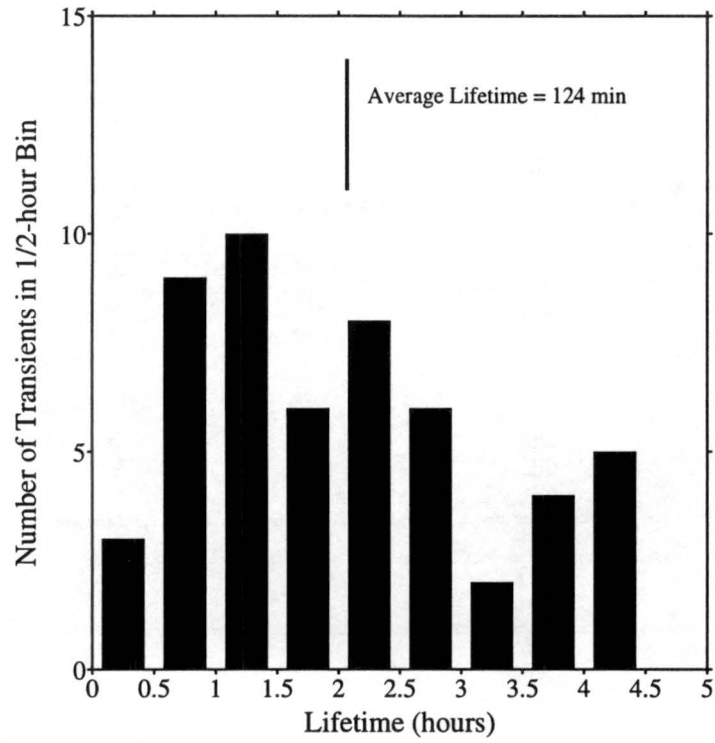


Figure 5.3: Total Transitory High Lifetimes

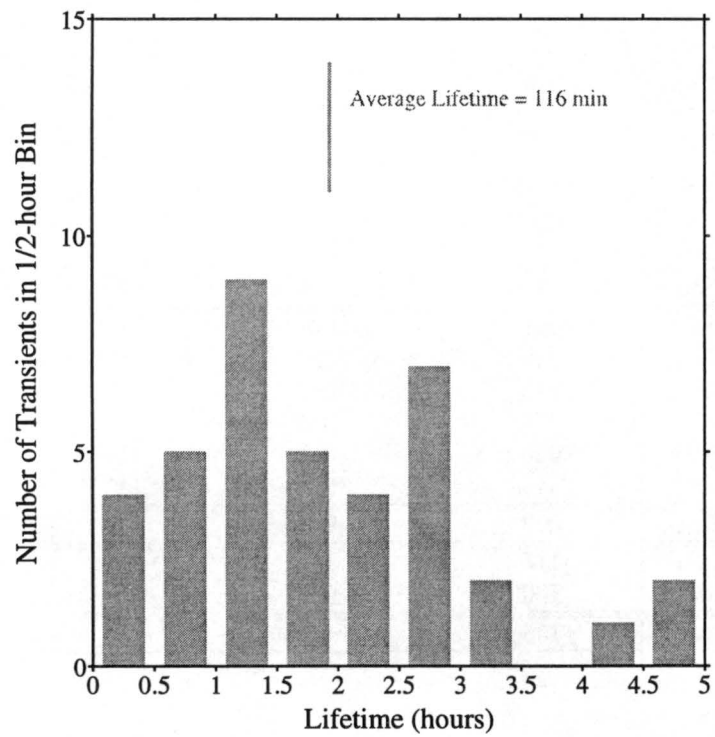


Figure 5.4: Total Transitory Low Lifetimes

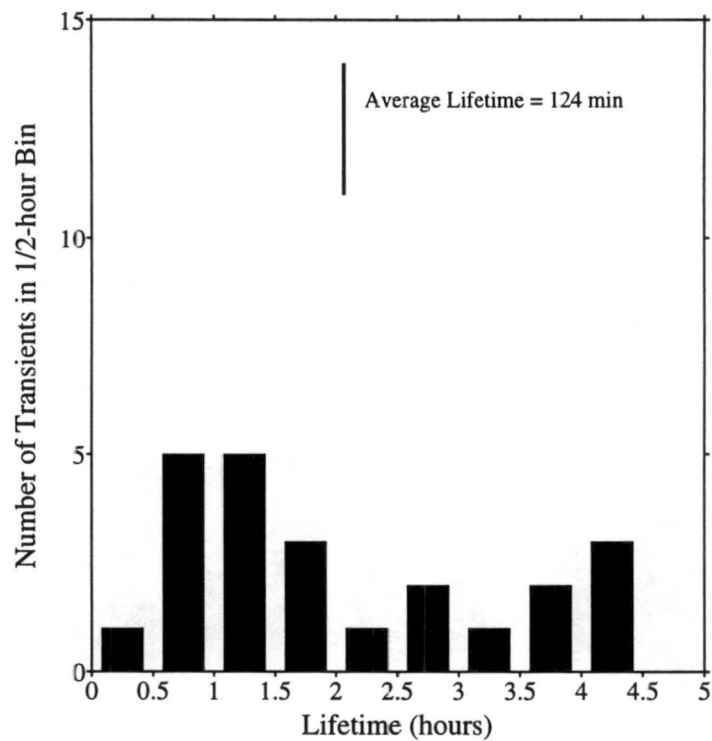


Figure 5.5: Fully-Sampled Transitory High Lifetimes

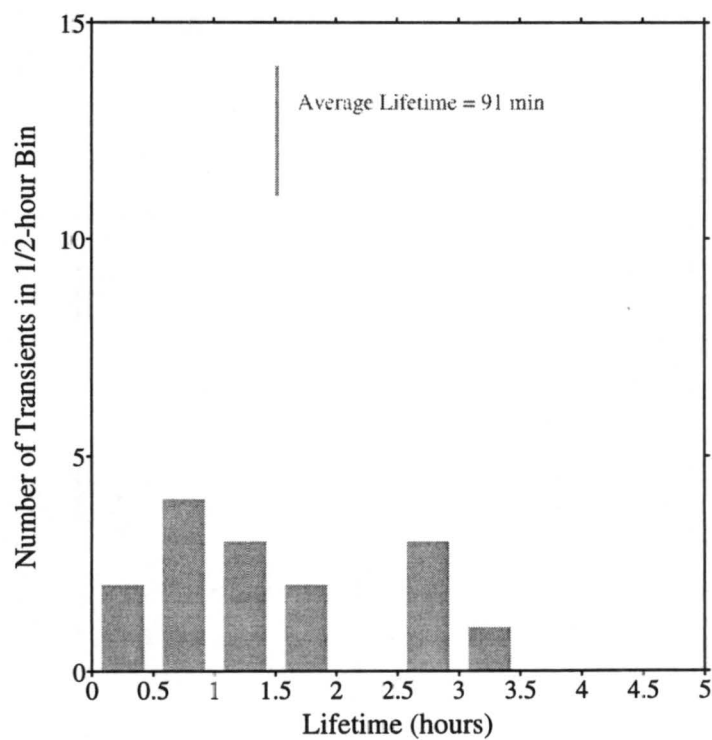


Figure 5.6: Fully-Sampled Transitory Low Lifetimes

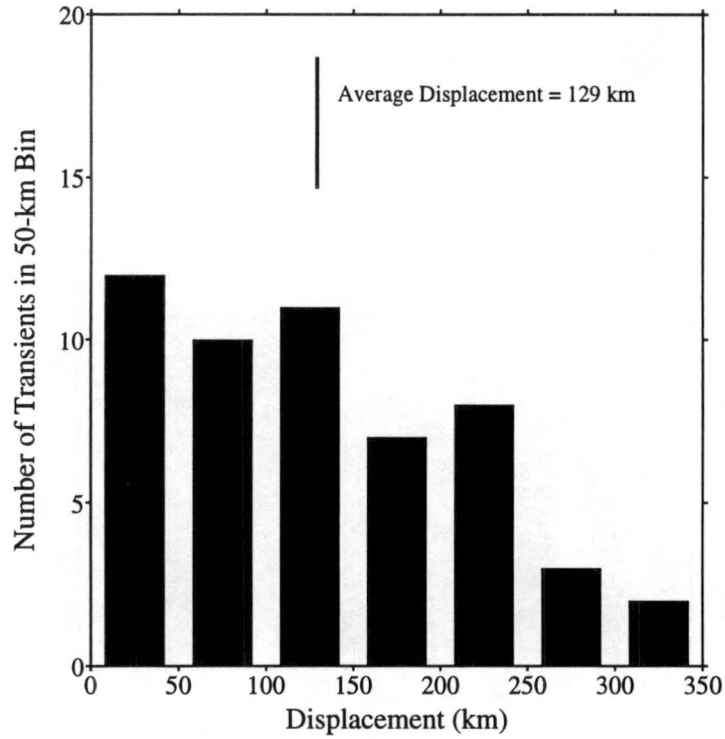


Figure 5.7: Total Transitory High Displacements

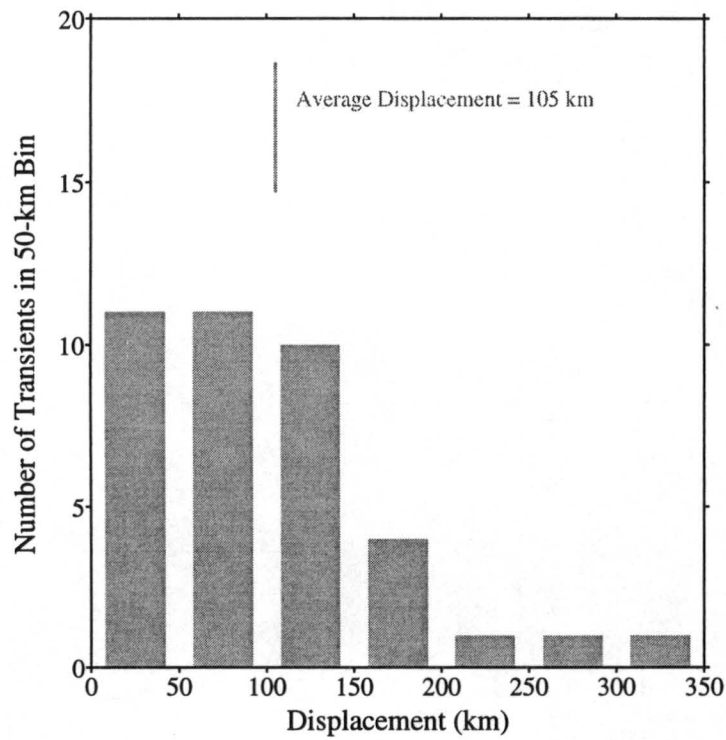


Figure 5.8: Total Transitory Low Displacements

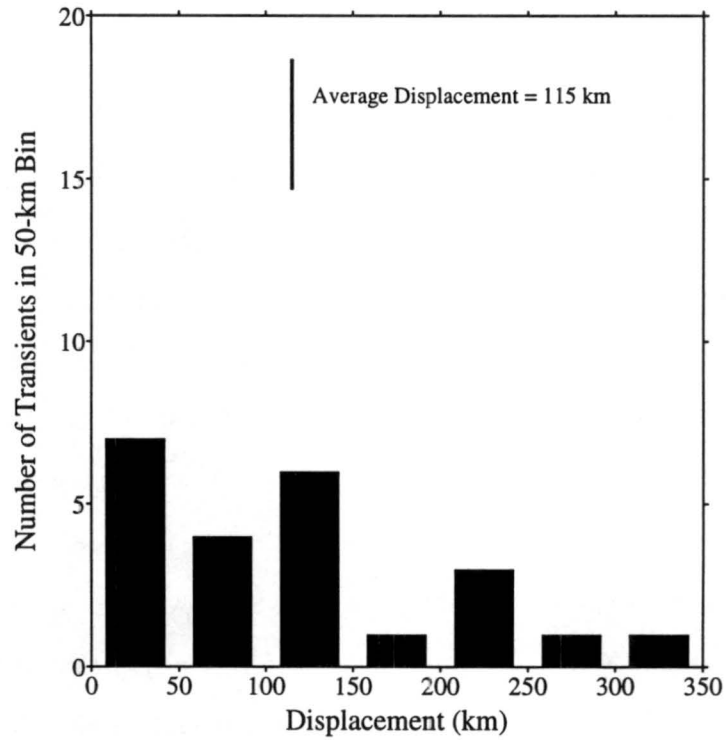


Figure 5.9: Fully-Sampled Transitory High Displacements

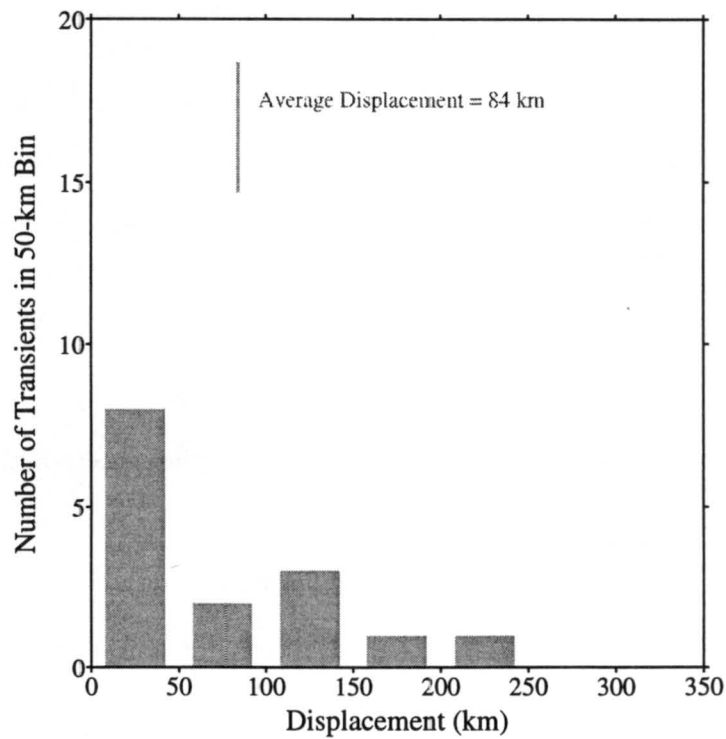


Figure 5.10: Fully-Sampled Transitory Low Displacements

### 5.3 Lifetimes

Only 38 of 92 (41%) transients spent their complete lives within the PRE-STORM array. These 38 do not represent the overall transient population because long-lived, well-traveled transients are more likely to escape detection than their shorter-lived, less mobile counterparts. There is no evidence that the slowest MCSs produced the most persistent transients, which would mitigate the imbalance somewhat (Figure 5.2). Indeed transitory high and low lifetimes are positively correlated with MCS speed, so the fastest MCSs actually contained the most persistent transients, which exacerbates the survey's bias.

Figures 5.3–5.6 are histograms of transient lifetimes. The first two depict all 92; I have limited the second two to transients the PRE-STORM array fully sampled from formation to dissipation. Neither lows nor highs have a clearly preferred longevity, and both populations have lifetimes that range from roughly a 0.5 h to almost 5 h. The average transitory high lifetime is 124 min and the average transitory low lifetime is 116 min. Most of the populations lived fewer than 3 h.

Excluding the partially-captured transitory lows markedly shifted that population to lower values, again because the brief transients were more likely to spend their comparatively short lives within the limited PRE-STORM instrument ranges. The population of highs also changes with the exclusion, but less drastically. Transitory highs with roughly 1-h lifetimes now lead the population, although comparatively many of the 3–4.5-h highs survived the cut. More than 0.5 h separates the average lifetimes of the transitory highs and lows. The difference implies that either the local thermodynamic perturbations responsible for forming lows did not persist for quite as long as those that produced highs, or, alternatively, that once the generating thermodynamics stopped, the atmosphere's mixing and fluxes more quickly rid itself of the lows' vestigial density gradients. Maybe both occurred.

Both Figures 5.5 and 5.6 are loosely bimodal. Transients with lifetimes less than 2 h account for at least half of each respective population, but both highs and lows have a secondary maximum at the long-lived end of their histograms, highs in the 3.5–4.5-h bins and lows in the 2.5–3.5-h bins. The instruments sampled only 23 highs and 15 lows,

which are small statistical populations, so assigning a physical explanation to the bimodal character of the plots would be presumptuous.

#### 5.4 Displacements

As in the previous section, the first two displacement histograms (Figures 5.7 and 5.8) survey all 92 transients, while only the fully-sampled transients compose the data for the second two (Figures 5.9 and 5.10). Transitory highs were not well-traveled. Most of them moved fewer than 150 km before dying. Incomplete sampling has not distorted the first histogram because when the population is limited to fully-captured highs, the reduced group retains the same character as the larger (compare Figures 5.7 and 5.9).

Well-traveled transitory lows were even more rare than well-traveled highs, which is consistent with their shorter average lifetime. Less than one sixth of the lows died more than 150 km from their origin.

Generally, highs' displacements were slightly greater than lows'. As an MCS stratiform region blossoms, the rear edge of the anvil must expand backward in a relative sense, so it moves forward more slowly than the squall line. (See Chapters 2 and 4 for a discussion of the association between the anvil and meso- $\beta$ -scale lows.) Convective cells predominately drive transitory highs, so they generally advance with the MCS leading edge, while mesoscale lows to the rear drag their feet (see Chapters 2 and 4).

#### 5.5 Quasi-Lagrangian Traces

Transients are fleet, ephemeral creatures. Only a quasi-Lagrangian analysis (Bluestein 1992; Fortune, personal communication) will expose their secrets. A ground-fixed reference frame provides temporally resolved data at a single point, but to understand the evolution of MCS surface pressure fields, meteorologists must monitor transients as they move with their parent complexes.

Figures 5.11–5.22 document the evolution of the central pressure of each of the 92 transients with the diurnal solar tidal effects removed (see Section 3.2.1). Each plot composes

two groups of traces oriented, in the most general sense, horizontally. Highs are in the upper group, lows in the lower.

The traces fluctuate on four scales. On the broadest scale, each plot exhibits some mean slope of all the lines—those of both highs and lows. This is some combination of the synoptic and meso- $\alpha$ -scale (or storm-scale) pressure tendency signatures. Even the shortest interval over which an MCS was observed—about 3 h—is long enough for synoptic pressure to have risen or fallen a few millibars. The MCS likely introduced into the troposphere a storm-scale integrated mass change as well, which is impossible to divorce from the synoptic change. I call the combined contributions of the two the large-scale signature or the large-scale forcing. On the second scale, the means of each group of high traces and each group of low traces show the general surface pressure forcing by the convective line and the stratiform region. Although the difference in the two means is not exactly the overall mesoscale pressure gradient induced by the MCS—for that we would also need the distances between perturbations—consider it a rough proxy for the gradient. The third scale is the families, which includes both highs and lows. They reveal any lag between the time of strongest highs and the time of strongest lows—or vice versa. On the finest scale are the individual transient traces.

Short vertical lines abut one or both ends of some traces. A vertical line at the start of a trace marks a developed transient's emergence into the array and a vertical line at the end of a trace marks a transient's disappearance as it travels beyond the edge of the array. Transients that spent their full lives within the array have traces not book-ended by vertical lines.

#### 5.5.1 7 May

The large-scale signal is faint (Figure 5.11). The surface front over the southern Great Plains on 7 May was weak and stationary in an environment of small synoptic surface pressure gradients. The transitory high and low traces are collectively divergent; the mean of the lows changes little over approximately 6 h, but the highs' mean increases slightly, predominantly due to Family B's strengthening high pressure envelope. Indeed, the collective

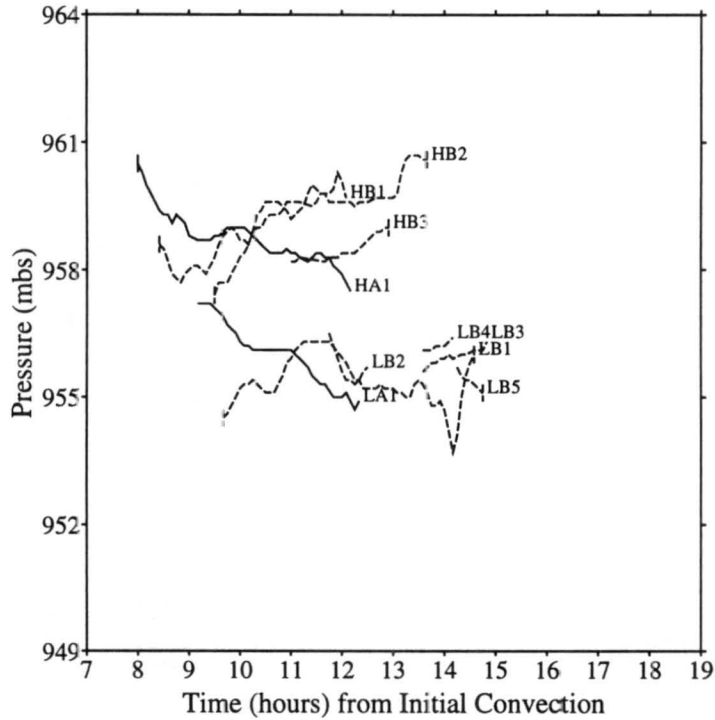


Figure 5.11: Central pressure of the 7 May transients.

rise in pressure of the three transitory highs in Family B is a marked change from the clear decrease in the pressure of both HA1 and LA1. HA1 was presumably weakening and dying when it entered the array, while the B highs spent only their early lives within the array and departed mature and strong.

Traces of HA1 and LB1 are nearly offset duplicates of each other, implying their kinematics or thermodynamics were closely linked. Such an *inter-family* signature is rare (see Section 5.2). The deepest pressure within the B lows lagged the strongest B highs, but we cannot be sure what happened to HB2 and HB3 as they traveled farther eastward. They may have strengthened, in which case the strong highs would have lagged the strong lows.

### 5.5.2 13 May (N)

Large-scale forcing on 13 May was also weak, although the surface synoptic pressure gradient was about twice that of 7 May. The high and low traces do not obviously diverge (Figure 5.12). However, if we had to declare the traces either convergent or divergent, we would probably choose the latter, mostly because of HA1's contribution.

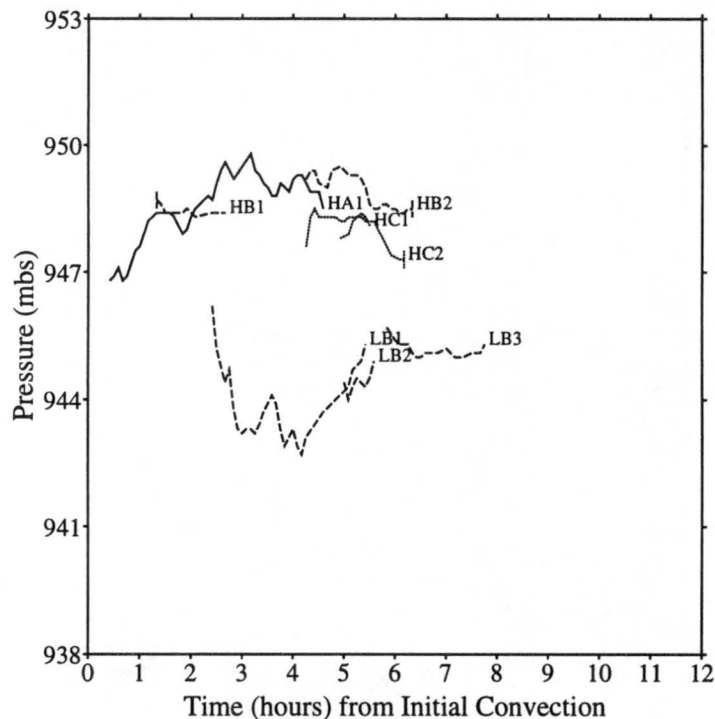


Figure 5.12: Central pressure of the 13 May (N) transients.

Only Family B contained lows, and no lag appears among the Bs. Oddly, the deepest low, LB2, lived most of its life apparently without a partner high. HB2 appeared just as LB2 began weakening. No C lows developed, but traces of the other 12 PRE-STORM MCSs' transients indicate it is not rare for a family to comprise just highs or just lows.

### 5.5.3 13 May (S)

If a large-scale signature exists in the second 13 May group, it had no time to show its face (Figure 5.13). The MCS lived only a short while in the array before exiting stage right and departing for places east. The traces are brief but obviously divergent, at least as far as the glimpses of HB1, LB1, and LB2 allow us to presume. It is possible that the pressure in HB1 plummeted and LB1 and LB2 filled somewhere in eastern Oklahoma. We cannot know.

The difference in pressure between the highs and lows is large, and a representative movie frame (not shown) indicates that only about 60 km separated the two sets of extrema; the resultant gradient was more than 2.5 mb in 10 km. I placed the two highs, HA1 and

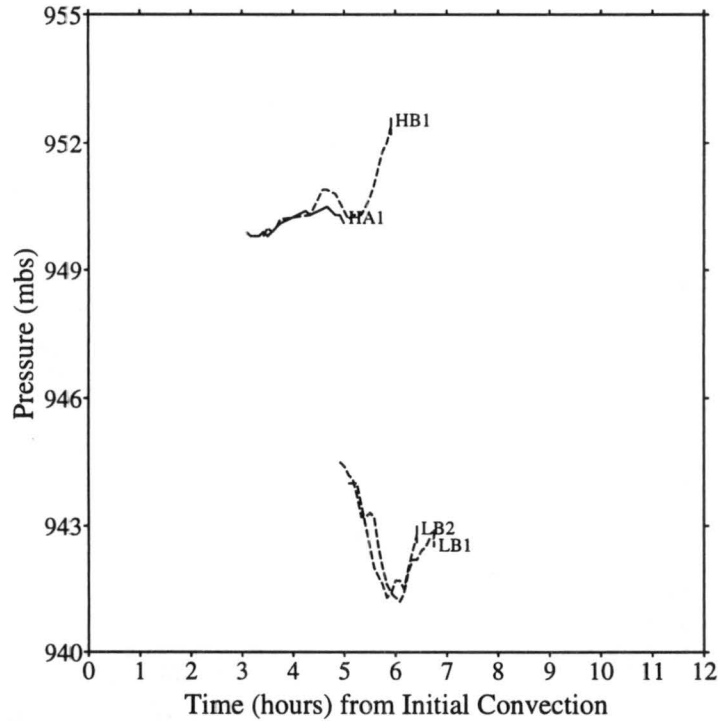


Figure 5.13: Central pressure of the 13 May (S) transients.

HB1, in two families, but pressure in the two evolved similarly. LB2 and LB1 played follow-the-leader as well. Such tandem traces are actually the exception rather than the rule. Extrema even within the same families of the other MCSs usually behaved uniquely.

#### 5.5.4 27 May

Like the second of the two MCSs two weeks earlier, the 27 May complex provided only a brief glimpse of the transients it produced (Figure 5.14). The high positive slopes of the traces of HA1, HC1, and LA1 display a strong rise in large-scale pressure. The traces may be divergent, but the evidence is inconclusive. LA1 departed the array too soon to reveal whether the array captured a representative period of its life, and HC1 was explosively strengthening when it disappeared.

The only lag in the traces—and it may be presumptuous to infer it given the transients' cameos—is between HA1 and LA1. The high gained strength as the low's strength ebbed, which is opposite the commonly-expected pattern wherein the maximum mesohigh envelope strength leads the maximum wake low envelope strength.

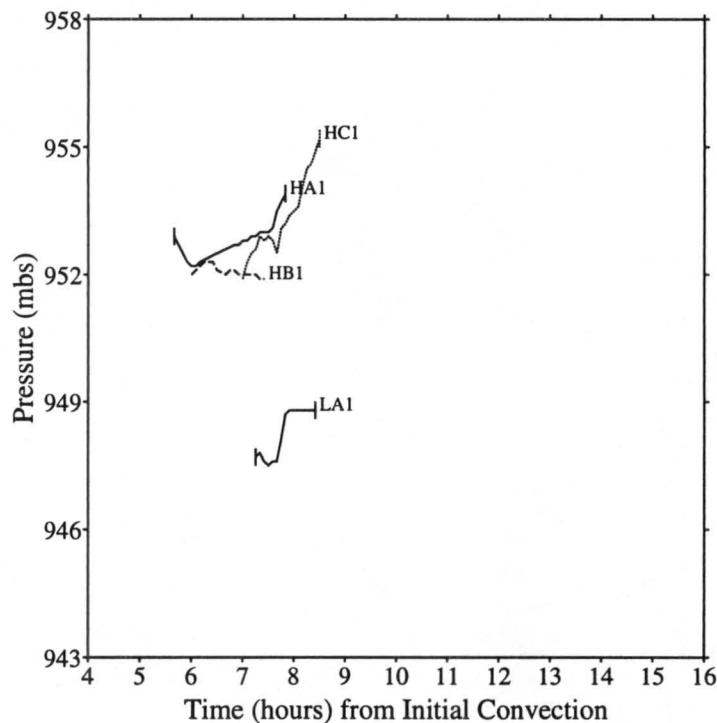


Figure 5.14: Central pressure of the 27 May transients.

### 5.5.5 28 May

For the first time—and, it turns out, the only time—the large-scale pressure markedly decreased during an event (Figure 5.15). Except for HC1, every transient died or departed the array with pressure lower than at the beginning of each one's observation period. Because of HC1's sharply-ascendent-then-moderately-descendent trace, the plot is slightly divergent; without HC1, that would not be the case. Even HC1 left the array almost as weak or weaker than at any other time during its observed life. In Family C, the transitory low formed only after the high's strength had climaxed and begun to fail. Recall that Family B of the 13 May (N) complex behaved similarly.

Note the two spikes in the overall trough of LB1's trace. Do not believe them. During its entire life, the transitory low hugged the northern edge of the PRE-STORM array, ducking in and out of view, and while north of the array's perimeter LB1's true strength was lost—those are the spikes. Missing stations fostered the same sawtooth pressure history when transients were lost in local data voids.

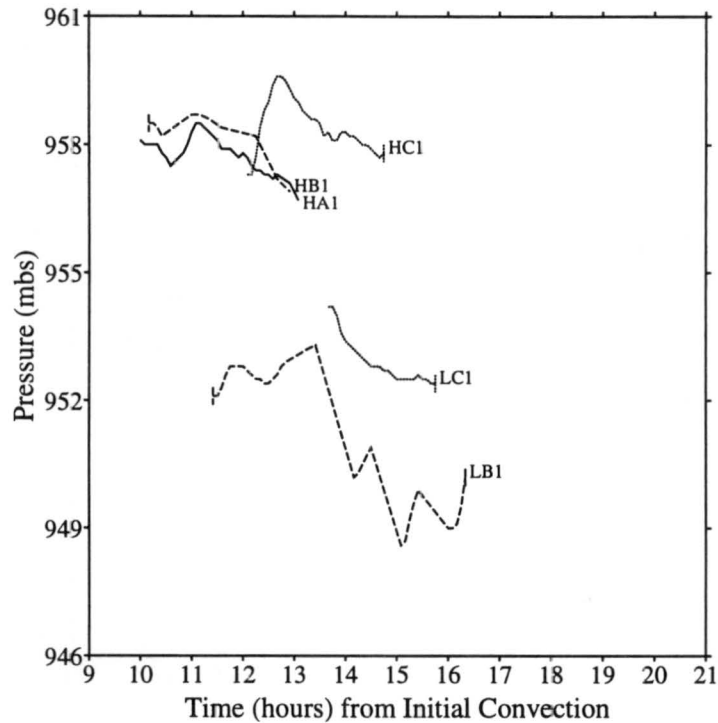


Figure 5.15: Central pressure of the 28 May transients.

#### 5.5.6 3 June

The 3 June traces are short (Figure 5.16), like those of 27 May and 13 May (S). No large-scale pressure tendency appears. Despite the traces' brevity, the collective values clearly diverge; this is the fourth MCS to display such a pattern.

HA1 apparently was not accompanied by a low. However, the high lived mostly in the northern part of the array, so possibly an A low existed in northern Kansas beyond the instruments' sight—possibly, but not probably, because radar composites do not show any large areas of stratiform rain north of the array around the time HA1 was detected. In Family B, the lows were very weak even though the single B high, HB1, was moderately strong and becoming more vigorous as it left the array. Note that LB1 and LB2 both died, they did not leave the array, so HB1 spent the last part of its observed life lowless.

#### 5.5.7 3–4 June

The traces for the 3–4 June MCS are so divergent they bury any large-scale pressure signature (Figure 5.17). Even removing one of the high or low traces, or perhaps two high

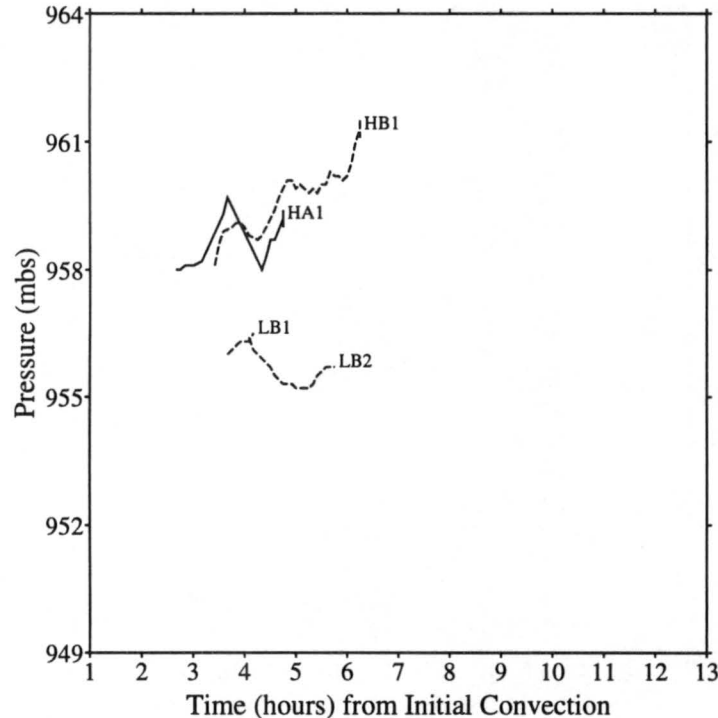


Figure 5.16: Central pressure of the 3 June transients.

traces, would not hide the divergence. HD1's trace soars. It is a pity that it was lost from sight so soon. The quasi-Lagrangian plot shows no low that corresponded to HD1. However, the low labeled LB1 may have become physically linked to HD1 late in the low's life even though at the start of its life it was clearly partnered with HB1. The atmosphere resists discretization and, as I wrote earlier in this chapter, readers should not place complete faith in family divisions. Elsewhere in the figure, LA1 lagged HA1 but slightly preceded HA2, and HC1 lived alone in Family C.

#### 5.5.8 4 June

The 4 June traces also diverge (Figure 5.18), but without the drama of the MCS that crossed the PRE-STORM array just hours earlier. A steady large-scale signal appears. The first four transients entered the array in some advanced stage of their lives, then HA1 left, having given us only a boring, slightly ascendent trace. Its low, LA1, varied in strength a little more before dying, apparently not because of data voids. The second B low, LB2, appeared only at the very end of the life of the lone B high, HB1—a pattern we have seen

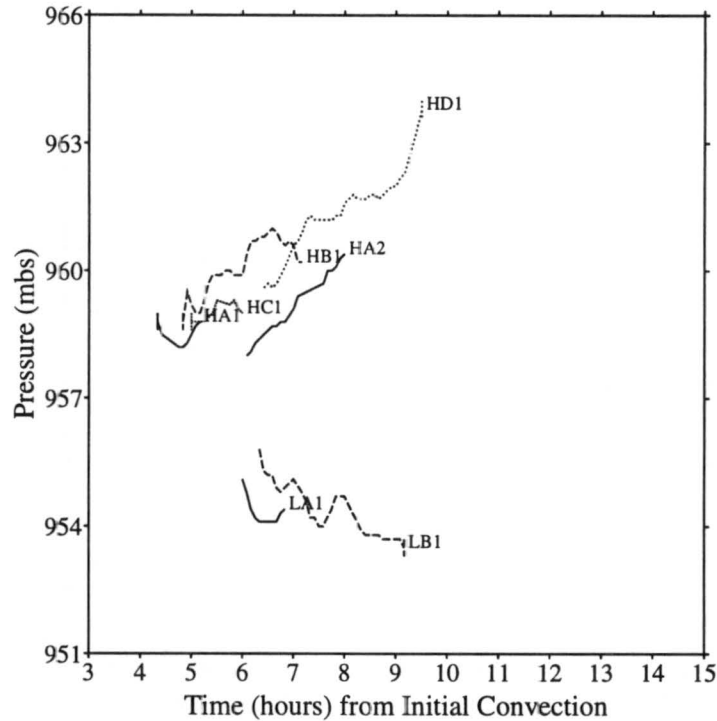


Figure 5.17: Central pressure of the 3–4 June transients.

before. Late in the observed life of the 4 June MCS, an expansive stratiform region covered the northeast part of the array and about 200 km separated HC1 from LB2; it is impossible to tell whether HC1 and LB2 were somehow linked. If they were, the connection was weak.

#### 5.5.9 11 June

The 11 June MCS generated 16 transients (Figure 5.19), the most by the 12 complexes. The high and low traces both rise as groups, indicating a rise in large-scale pressure. Then the E lows confuse the picture. Because HB2, the last of the highs, died before it had a chance to adopt the Es' pattern it is difficult to tell whether the dip in the traces is a sign that the synoptic pressure began falling. The E lows may just reveal a sudden divergence in the traces. Before the E lows appeared, the pattern was certainly not divergent.

Every family, except D (which had no low), at least hints at a lag in extrema. Family A shouts it. About 1 h passed between HA1's strongest moments and those of LA1. Family B is large and messy, but depending on how a viewer chooses to mentally align the upper ridges with the lower troughs, three lags may appear. In the third family, pressure within

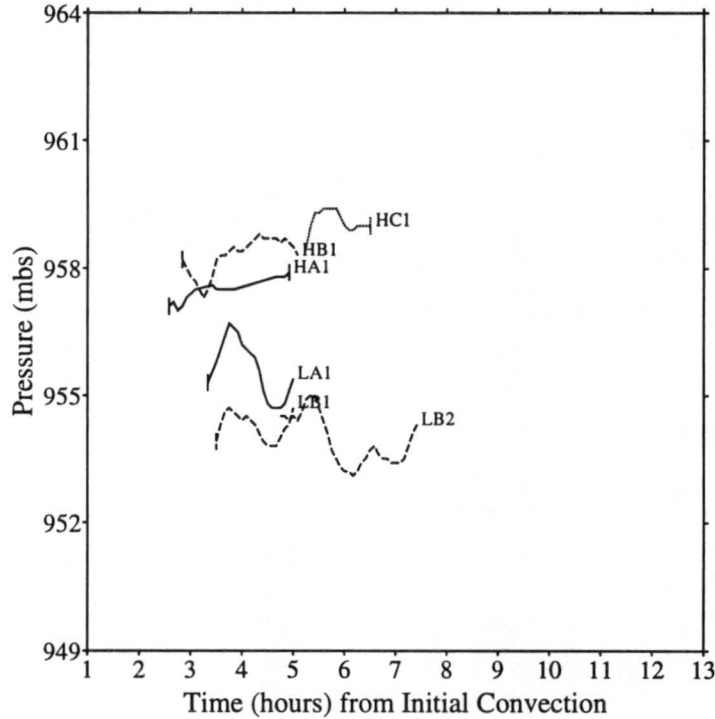


Figure 5.18: Central pressure of the 4 June transients.

LC1 dropped after HC1 and HC2 died. Note that we miss the early stages of LC1. Then there is the altogether strange Family E wherein one weak high formed and four lows formed, three of which were quite strong. The tight gradient at the extreme northeastern edge of the array at the time implies that a potent high grew just out of sight, which would explain resurgent E lows.

#### 5.5.10 15 June

Large-scale pressure on 15 June rose through the life of the MCS (Figure 5.20). Both the highs and lows show it. The two respective groups were separated by only a small pressure difference. Indeed, by the time the instruments detected the complex's first low, its pressure was higher than the initial highs' pressure. Highs lived for more than 3 h within the MCS before the first low, LF1, crossed the array threshold. Probably some, maybe all, of highs A through E had corresponding lows; they simply were too far southeast to be seen. This figure shows many incomplete traces of the transients within detection range. Even though traces of Families A, B, and G appear to be intact, the absence of detected

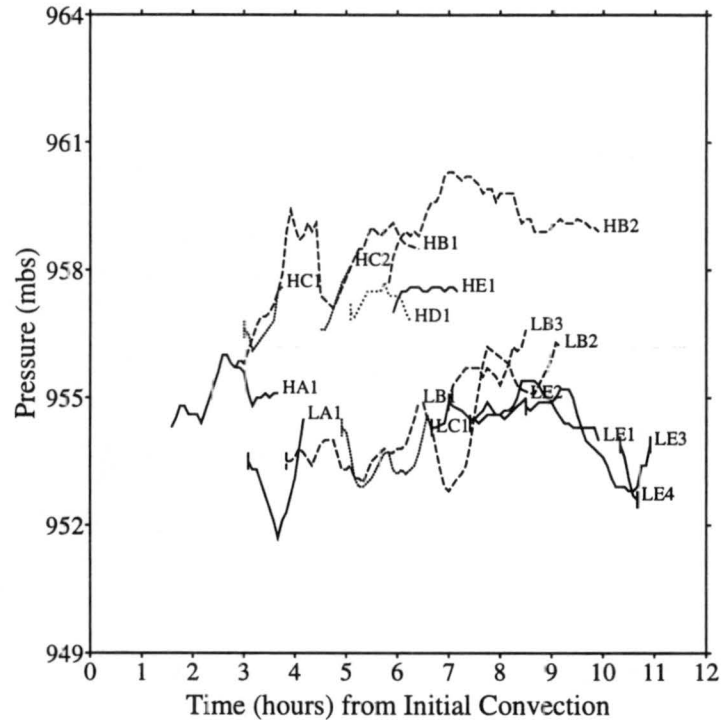


Figure 5.19: Central pressure of the 10–11 June transients.

lows in the first two and detected highs in the third are probably a result of the limited sampling. The traces are too confusing for us to decipher any divergence signature.

#### 5.5.11 24 June

As in the 13 May (S) and 28 May complexes, the pressure difference between the 24 June highs and lows was extreme (Figure 5.21). Large-scale pressure rose. The traces are non-divergent, and it appears that if the latter stages of LA1's life were visible, the traces might converge. The only transitory lows were LA1 and LA2, and LA2 was barely a low, with failing strength from the outset.

Only the middle of the lives of HA1 and LA1 were captured so we must be cautious of concluding too much, but the low's apparent climax lags the high's apparent climax by a little less than 1 h.

The movies and radar do not explain the apparent grouping of highs—HA1, HA2, and HC3 in the first bunch and HB1, HB2, HC1, and HC2 in the second. The pattern may be coincidental.

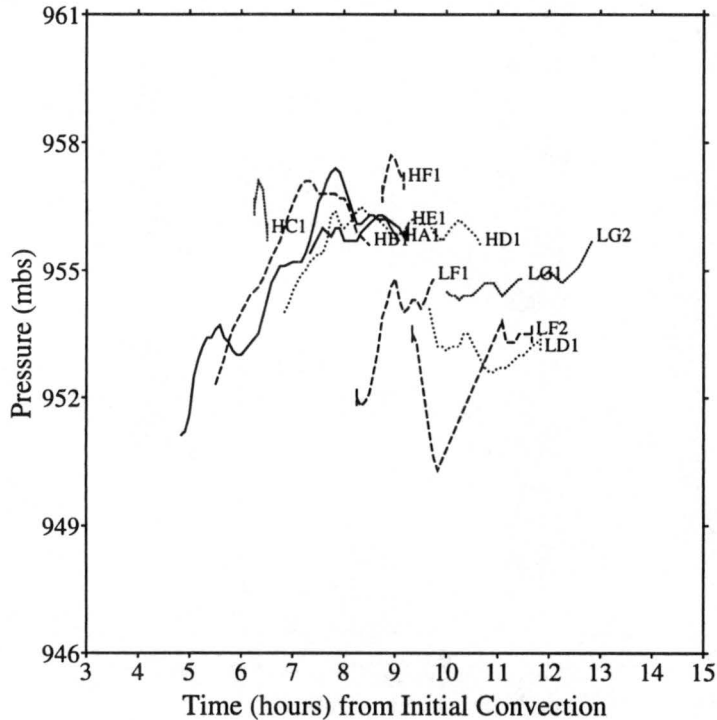


Figure 5.20: Central pressure of the 15 June transients.

#### 5.5.12 26–27 June

The 27 June MCS was unique among the 12 (Figure 5.22). The complex was slow and ragged despite its archetypal squall line eccentricity (the line was long and narrow, although its meager stratiform region was *not* archetypal). Two stages composed the line, the latter of which was stronger and more persistent (Stumpf and Gallus 1989). I address only the latter, because the line in its first guise did not force any significant surface pressure perturbations (Loehrer 1992); my research reveals that the mesohighs and wake lows Stumpf and Gallus found in the MCS's first stage are more likely station errors and synoptic perturbations from the sharp cold front in the area.

Even in the MCS's second stage, perturbations were small and weak. The 27 June complex is the only MCS of the 12 to live for even a minute without a transient once the first one developed or was detected. First for 40 min, then again for 2 h, and last for another 0.5 h, the complex had no transients. Six of the eight transients that did form were very weak and brief. Only the final two lows, LG1 and LH1, resemble the transients typical of the other complexes. Both lows left the array before they died.

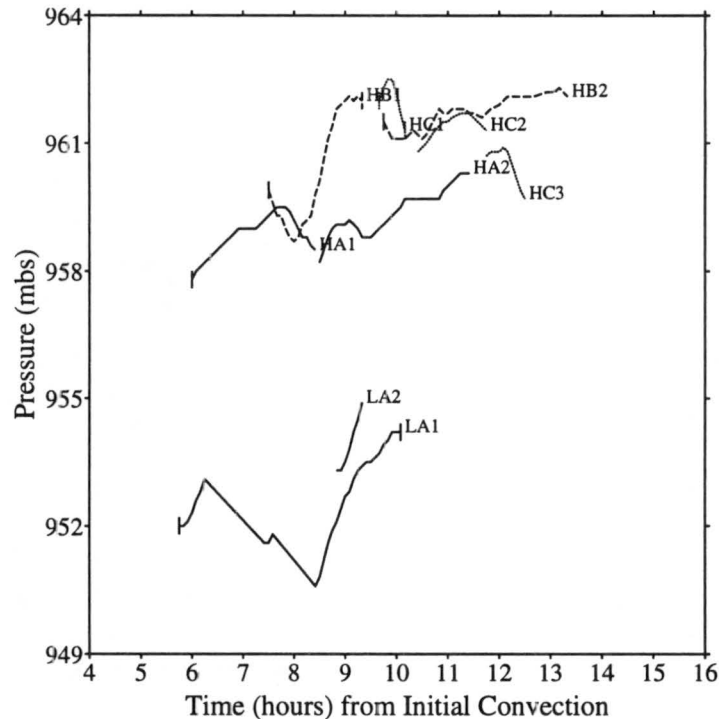


Figure 5.21: Central pressure of the 24 June transients.

Discussing lags is meaningless because each family contained only one member, nor can we conclude anything about divergence, although when the transient lows formed, their pressure did drop. The large-scale pressure appears to have risen, but the last lows again confuse the issue slightly.

## 5.6 Summary of Quasi-Lagrangian Traces

Large-scale pressure rose in 5 (42%) cases, fell in 1 (8%) case, did not change significantly in 3 (25%) cases, and in 3 (25%) cases plots were inconclusive. Pressures of transitory highs and lows collectively diverged in 7 of 12 MCSs, and they appear on the plots of: 7 May, 13 May (S), 28 May, 3 June, 3–4 June, 4 June, and 10–11 June. Plots of three MCSs are inconclusive: 13 May (N), 27 May, and 26–27 June. The only two non-divergent plots are of the 15 June and 24 June storms. As I mentioned in Section 5.5, collectively diverging pressure is not synonymous with an increase in the pressure gradient, but the two are loosely comparable because none of the MCSs exhibited a convective line that raced far ahead of its stratiform region and attendant meso- $\beta$ -scale lows. Thus, the distance between

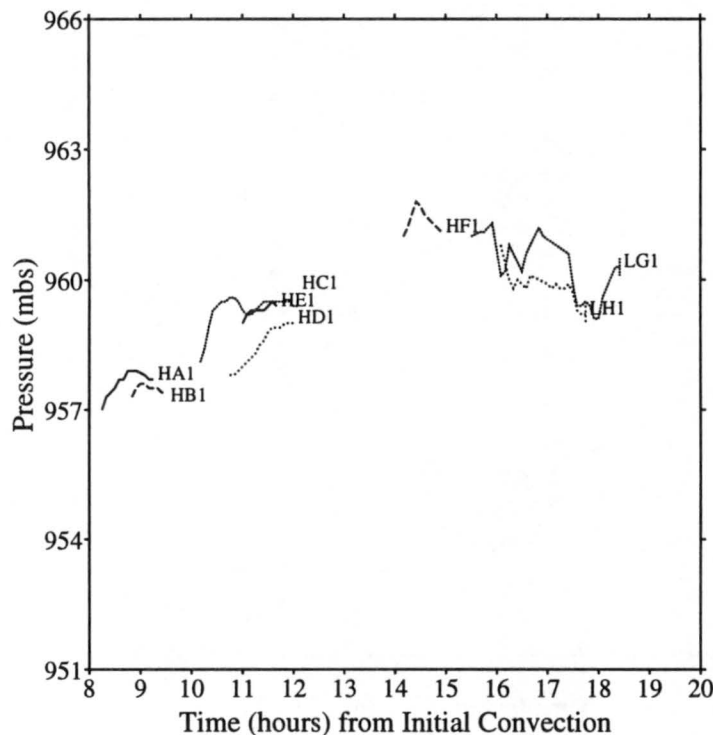


Figure 5.22: Central pressure of the 26–27 June transients.

the overall high and low pressure envelopes varied only within limits. Viewed in this light, it appears that one of MCSs' typical (but not mandatory) roles is to transform locally a weak synoptic pressure gradient into a stronger gradient, which then presumably slowly disappears through fluxes and mixing after an MCS has moved on or spent itself.

Some transitory lows clearly lagged their partner highs both in initiation and strength (e.g., Family C of 28 May and Family A of 10–11 June), but such obvious signatures were too infrequent to support strong conclusions about whether, as a rule, meso- $\beta$ -scale lows lag meso- $\beta$ -scale highs within MCSs, or whether such lags have a preferred duration. Ubiquitous, obvious lags would indirectly support theories that the most vigorous sections of the convective line produce the most abundant stratiform hydrometeors; the most intense towers presumably would generate the most potent cold pools, then the towers' remnants would become pockets of locally high ice and liquid water mixing ratios within the anvil, which would then cool the middle-tropospheric RTF flow, drive it groundward beyond its level of neutral buoyancy, and create wake lows. This delay from cold pool production to the positively buoyant RTF flow's descent might correspond to the transients' lag. We

do not see enough evidence to conclude any of this. However, the absence of consistent lags may not mean much. Without 5-min cross-sections extending from the convective cells through the RTF flow, I cannot be sure the loose family associations I determined always linked lows with their partner highs, if such things as “partner highs” even exist.

In addition to disclosing the evolving strengths of the 92 transients, the quasi-Lagrangian analysis upon which I founded this chapter allowed me to track transients' movements. I discuss their paths in Chapter 6.

## Chapter 6

### TRANSIENT PATHS AND MCS SYMMETRY

*... Look at every path closely and deliberately ... Then ask yourself, and yourself alone, one question ... Does this path have a heart? If it does, the path is good; if it doesn't it is of no use.*

—Carlos Castaneda,  
The Teachings of Don Juan

As MCSs grow beyond their first stages of organization, they do more than just expand to influence larger and larger volumes of the troposphere. The three fundamental precipitation regions within most complexes—the convective line, the stratiform region, and the separating transition zone—often change position with respect to one another. The paths of the examined 92 surface pressure transients reflect this structural shift in the 12 subject complexes.

#### 6.1 Observations and Modeling of Horizontal MCS Structure

During meteorologists' most recent six decades of documenting storm complexes, the leading-line/trailing-stratiform combination has emerged as the common (but not requisite) elemental precipitation motif among organized MCSs (Houze et al. 1990). In addition, observers of these storms have noticed that the relative location of the convective line and its attendant stratiform region often displays two patterns of its own. At times the stratiform region trails directly behind the line so the two are symmetric about their mutual motion vector (Figure 6.1.a). Other times, the stratiform region asymmetrically favors the left or right side of the convective line—usually the left in the Northern Hemisphere (Figure 6.1.b).

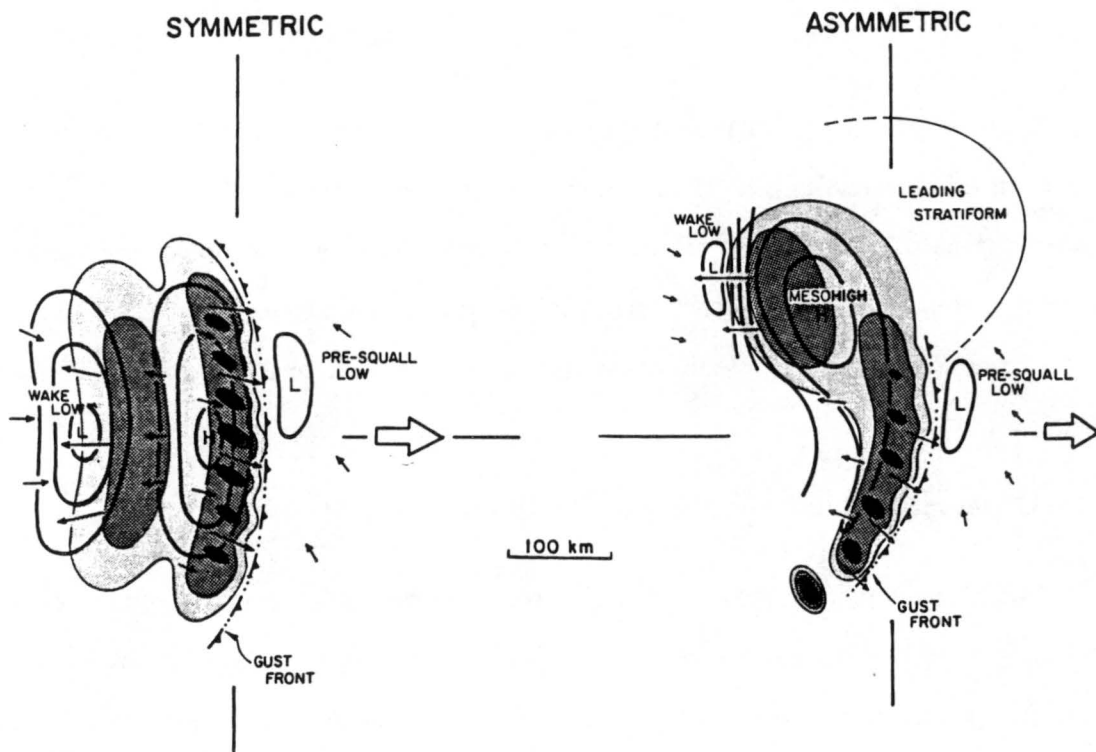


Figure 6.1: Schemata of a Symmetric and an Asymmetric MCS (from Loehrer and Johnson 1995).

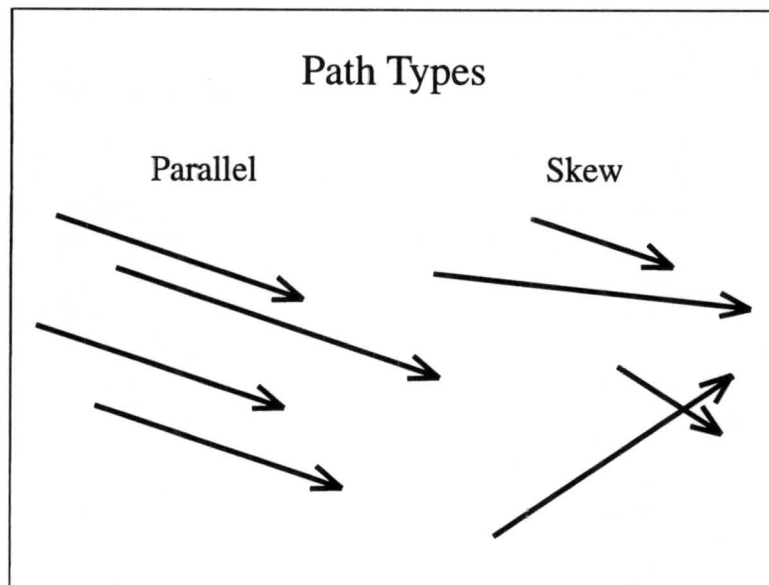


Figure 6.2: Schema of Parallel and Skew Path Types.

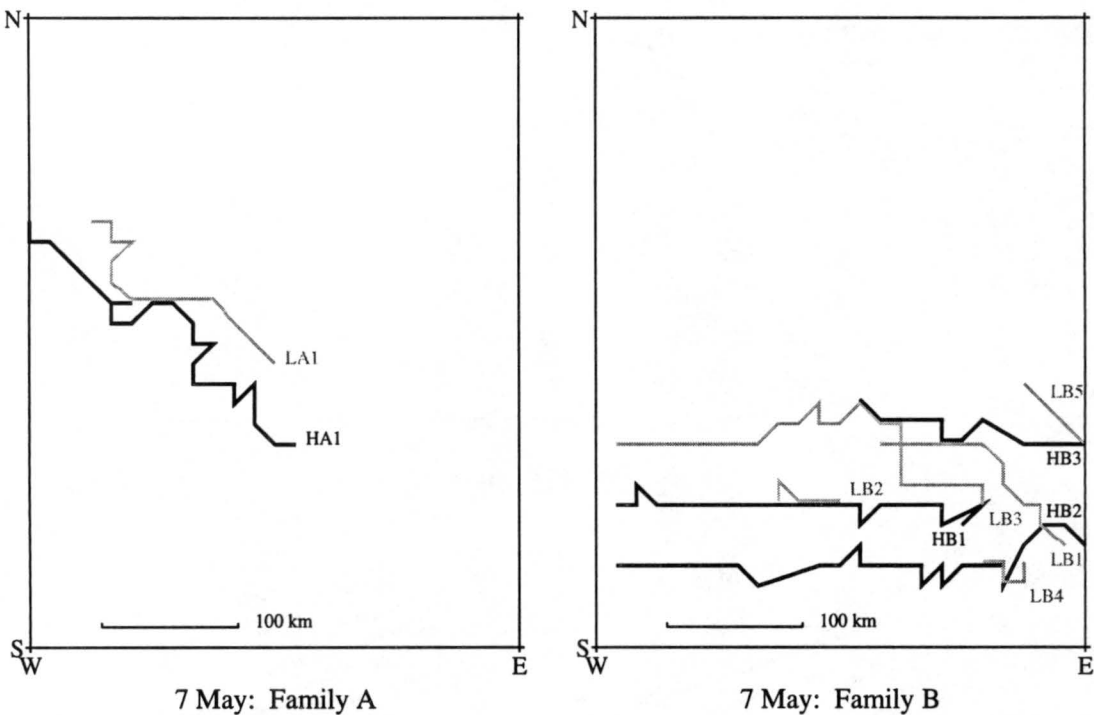


Figure 6.3: Transient Paths for 7 May.

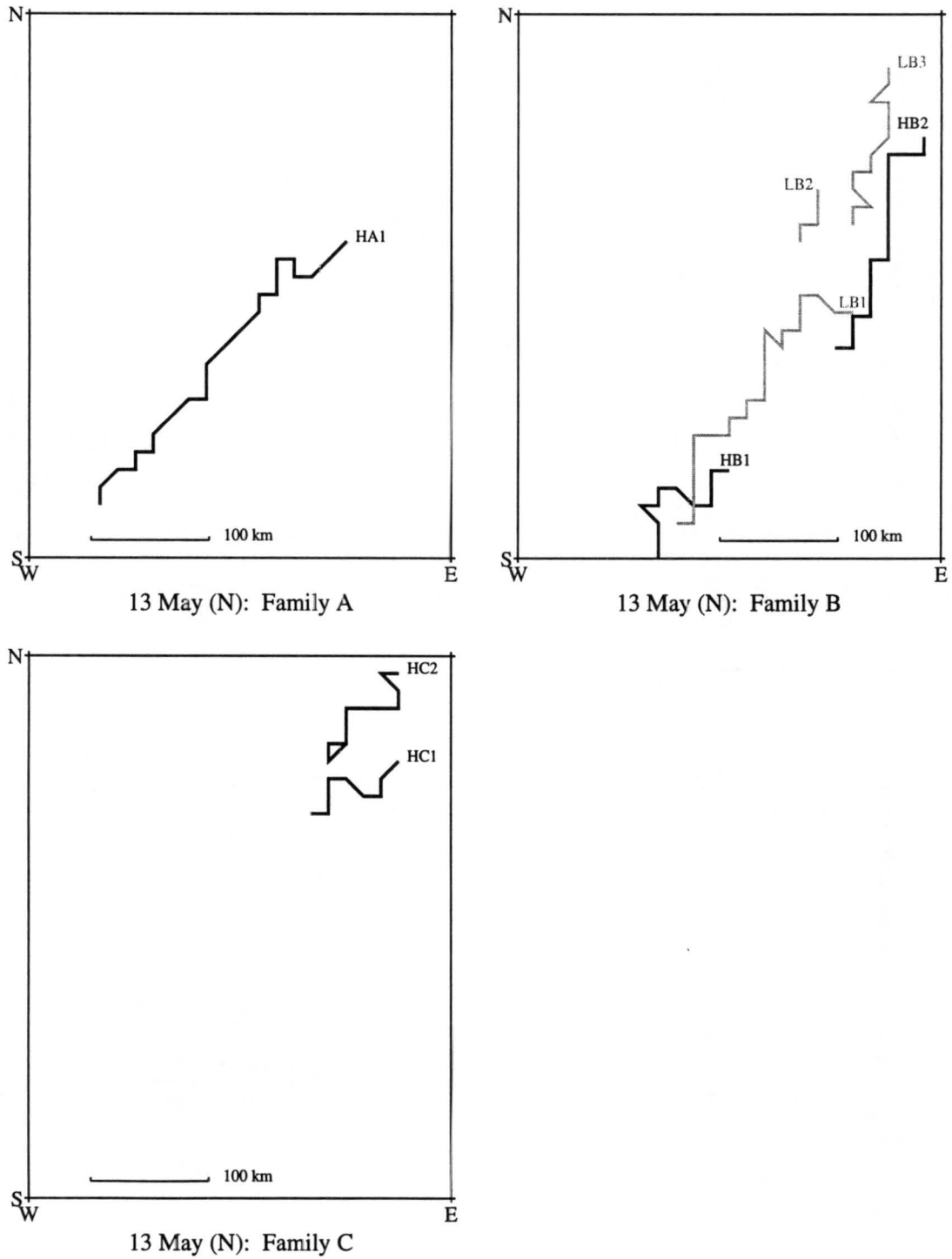


Figure 6.4: Transient Paths for 13 May (N).

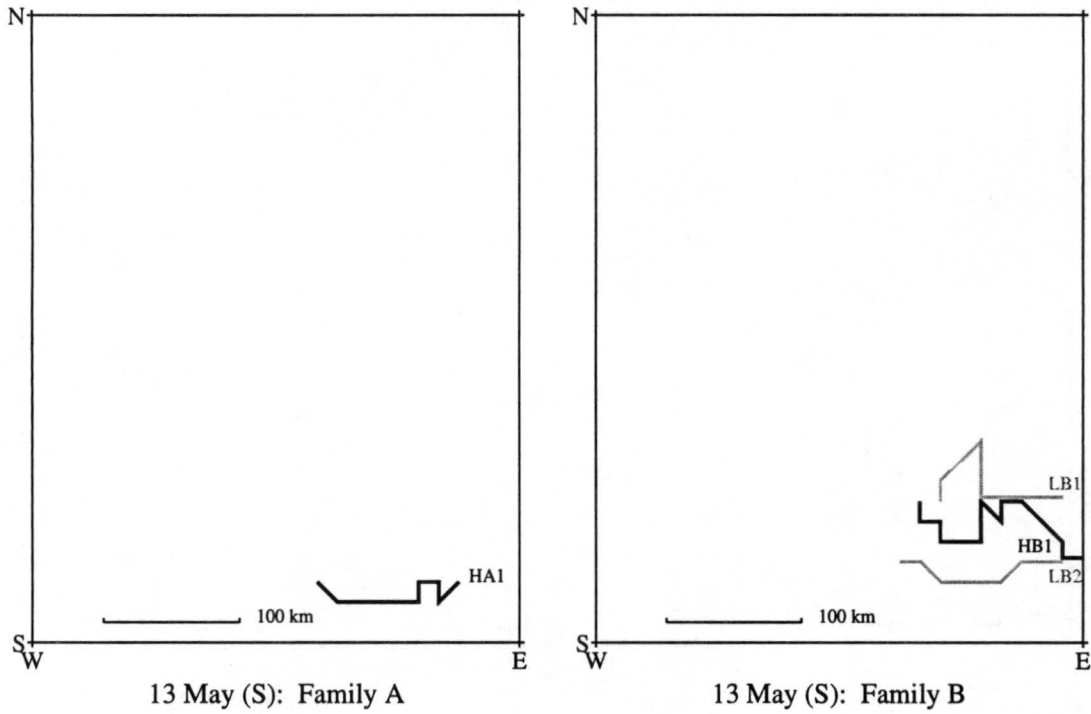


Figure 6.5: Transient Paths for 13 May (S).

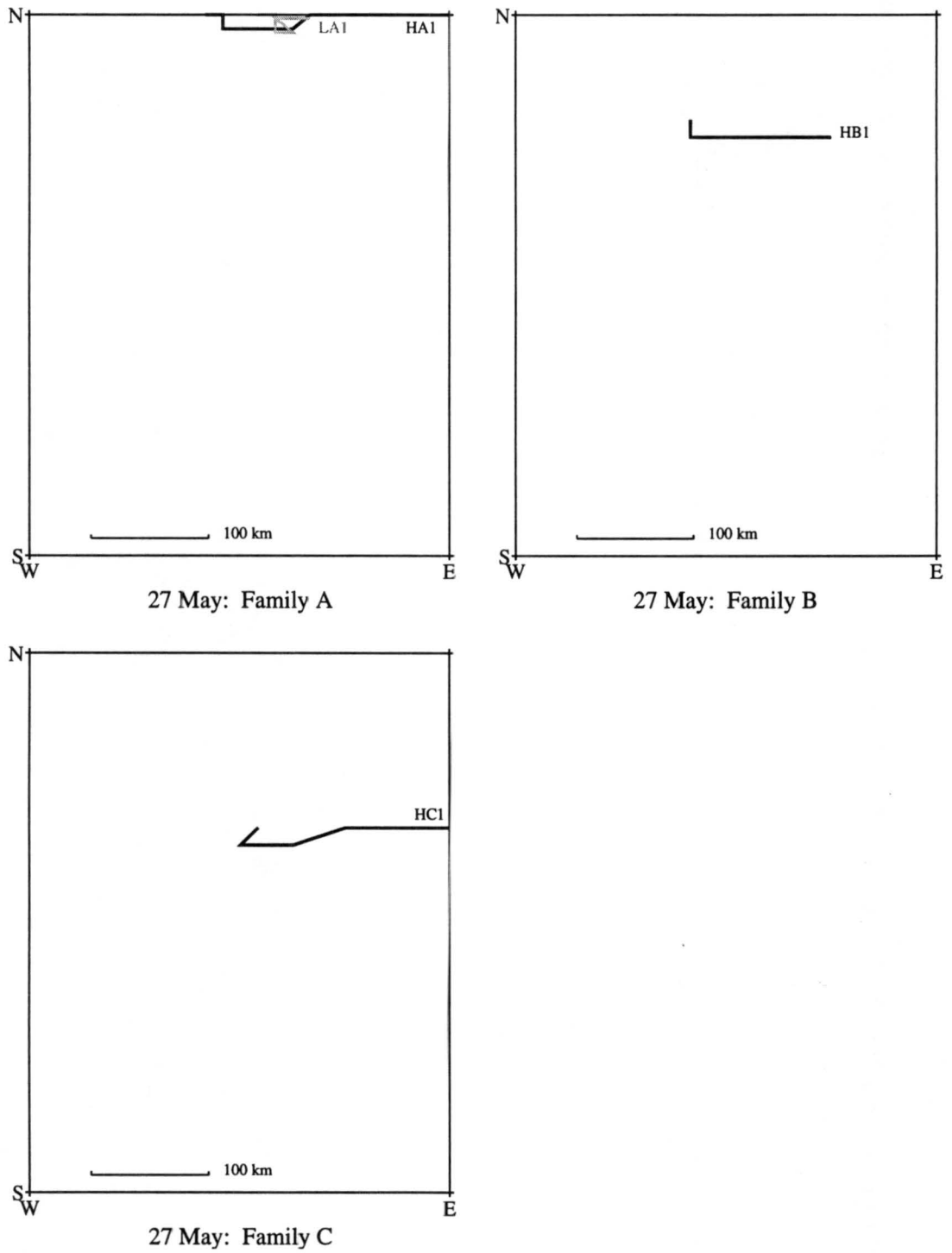


Figure 6.6: Transient Paths for 27 May.

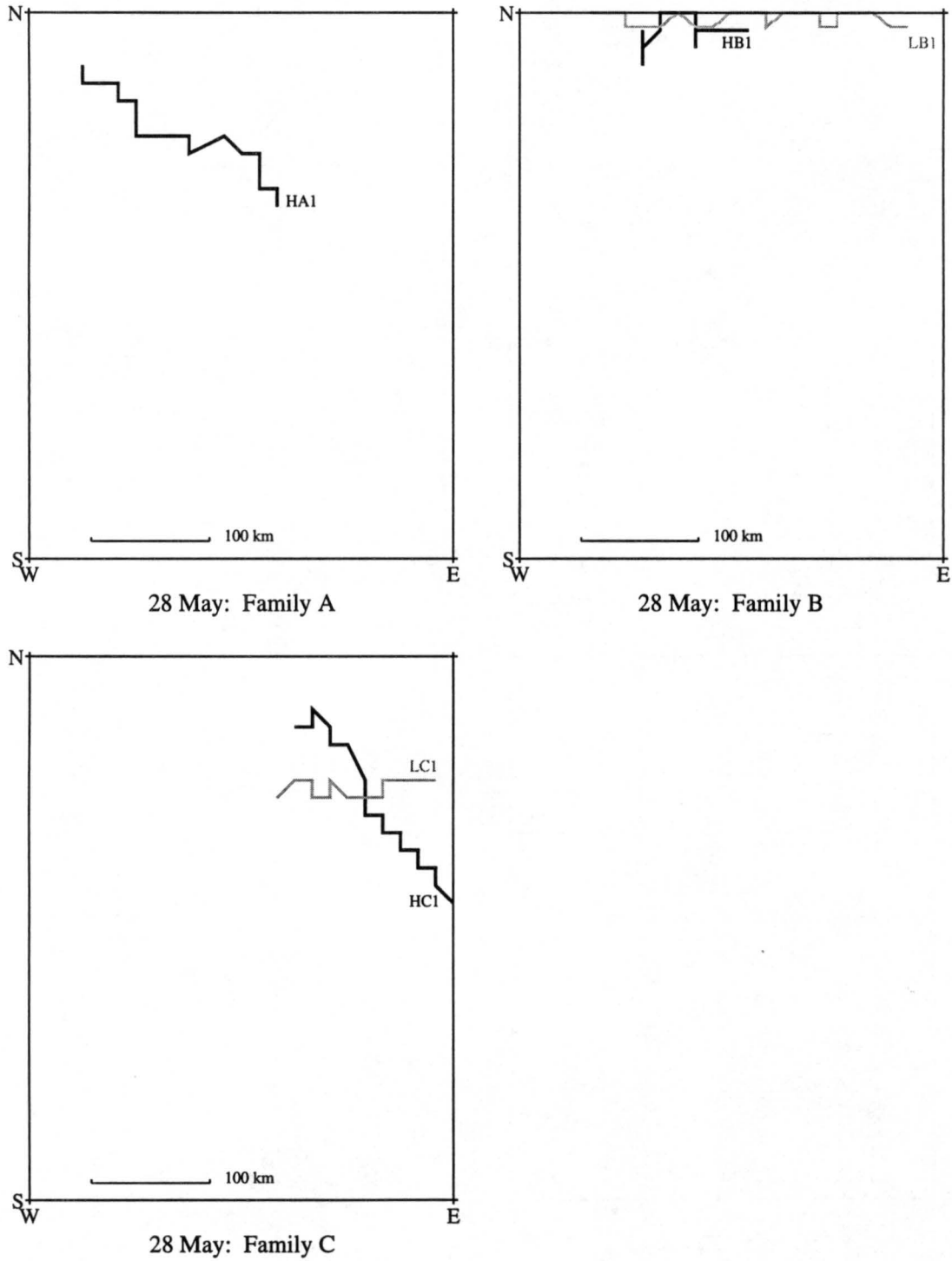


Figure 6.7: Transient Paths for 28 May.

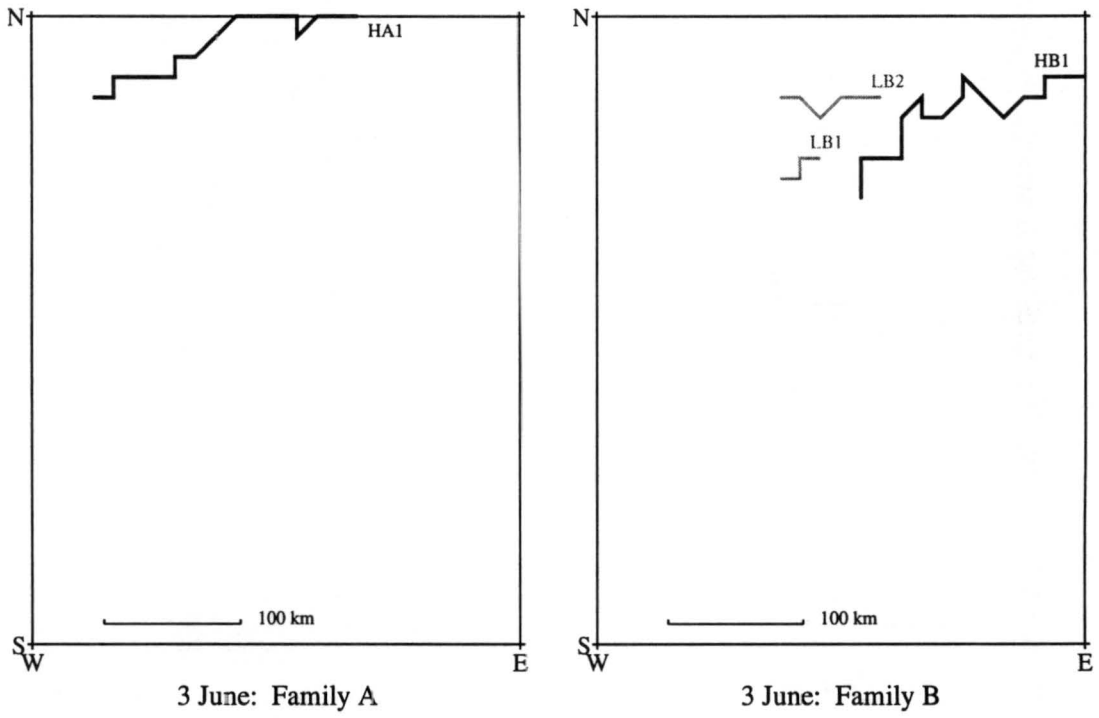
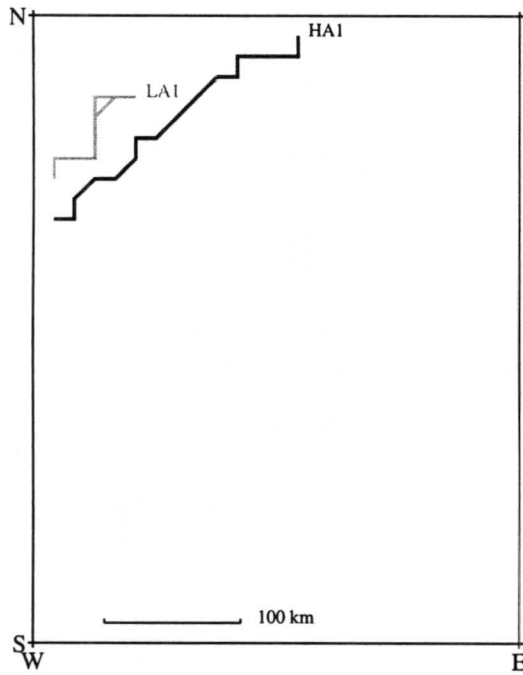
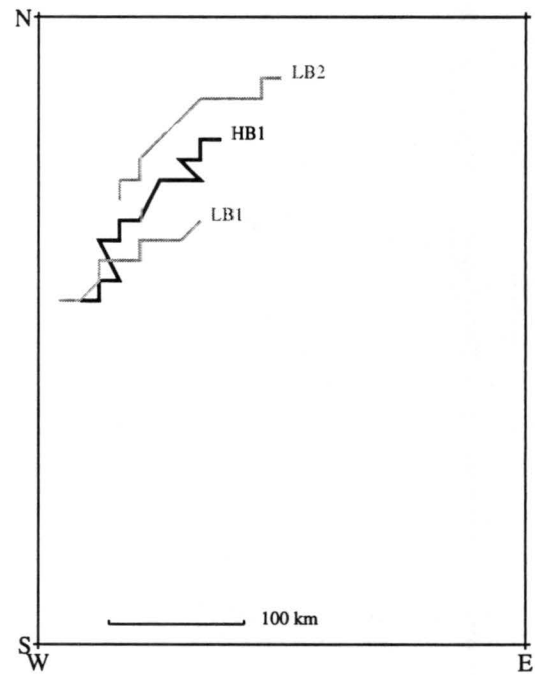


Figure 6.8: Transient Paths for 3 June.

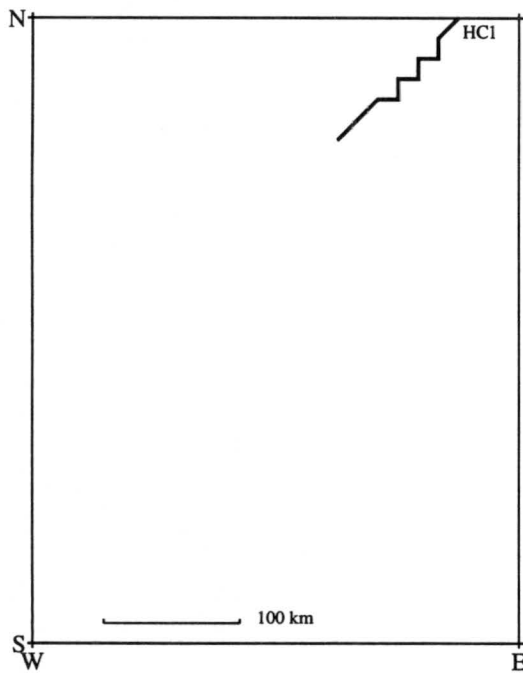




4 June: Family A

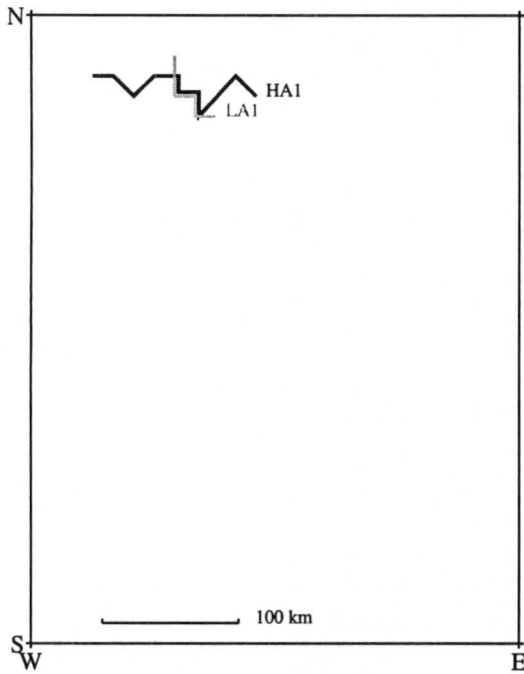


4 June: Family B

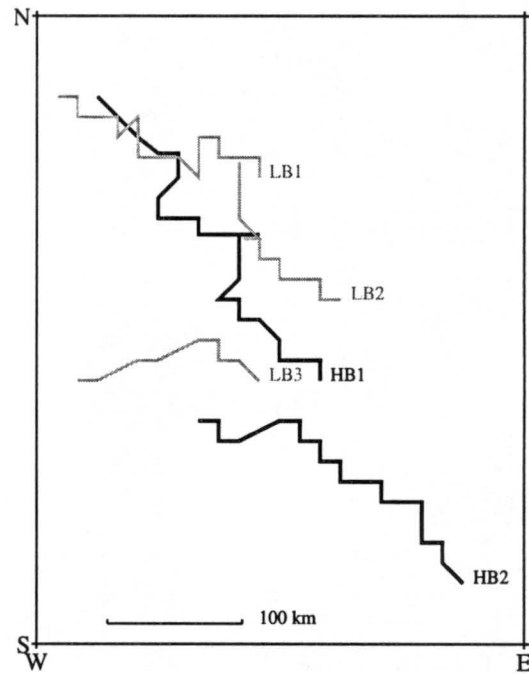


4 June: Family C

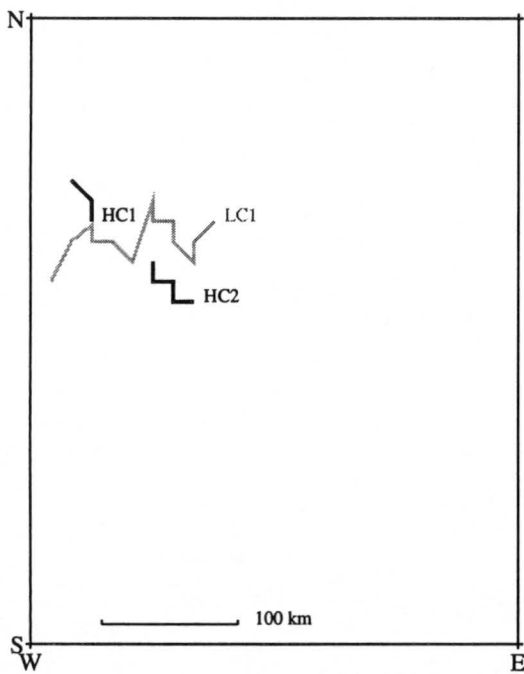
Figure 6.10: Transient Paths for 4 June.



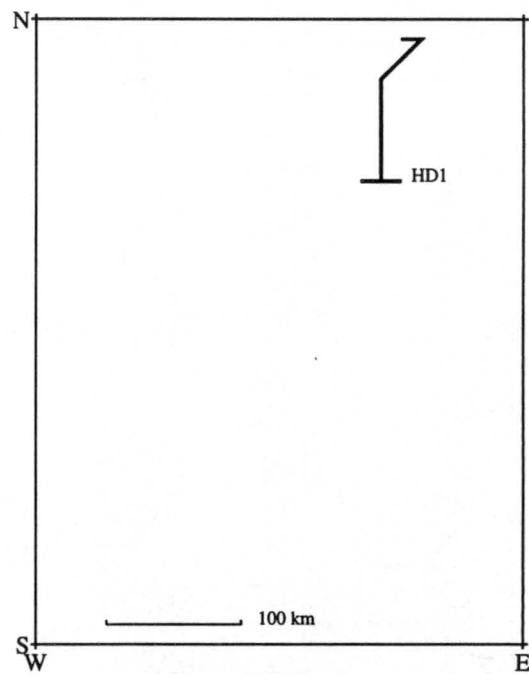
10-11 June: Family A



10-11 June: Family B

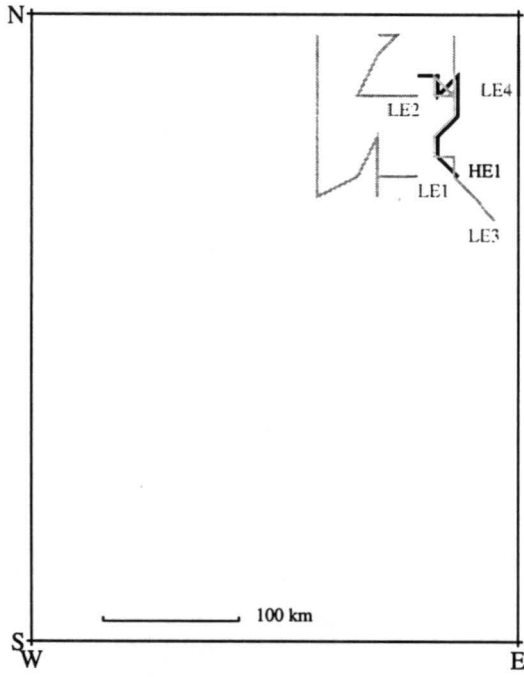


10-11 June: Family C



10-11 June: Family D

Figure 6.11: Transient Paths for 10–11 June (continued on the next page).



10-11 June: Family E

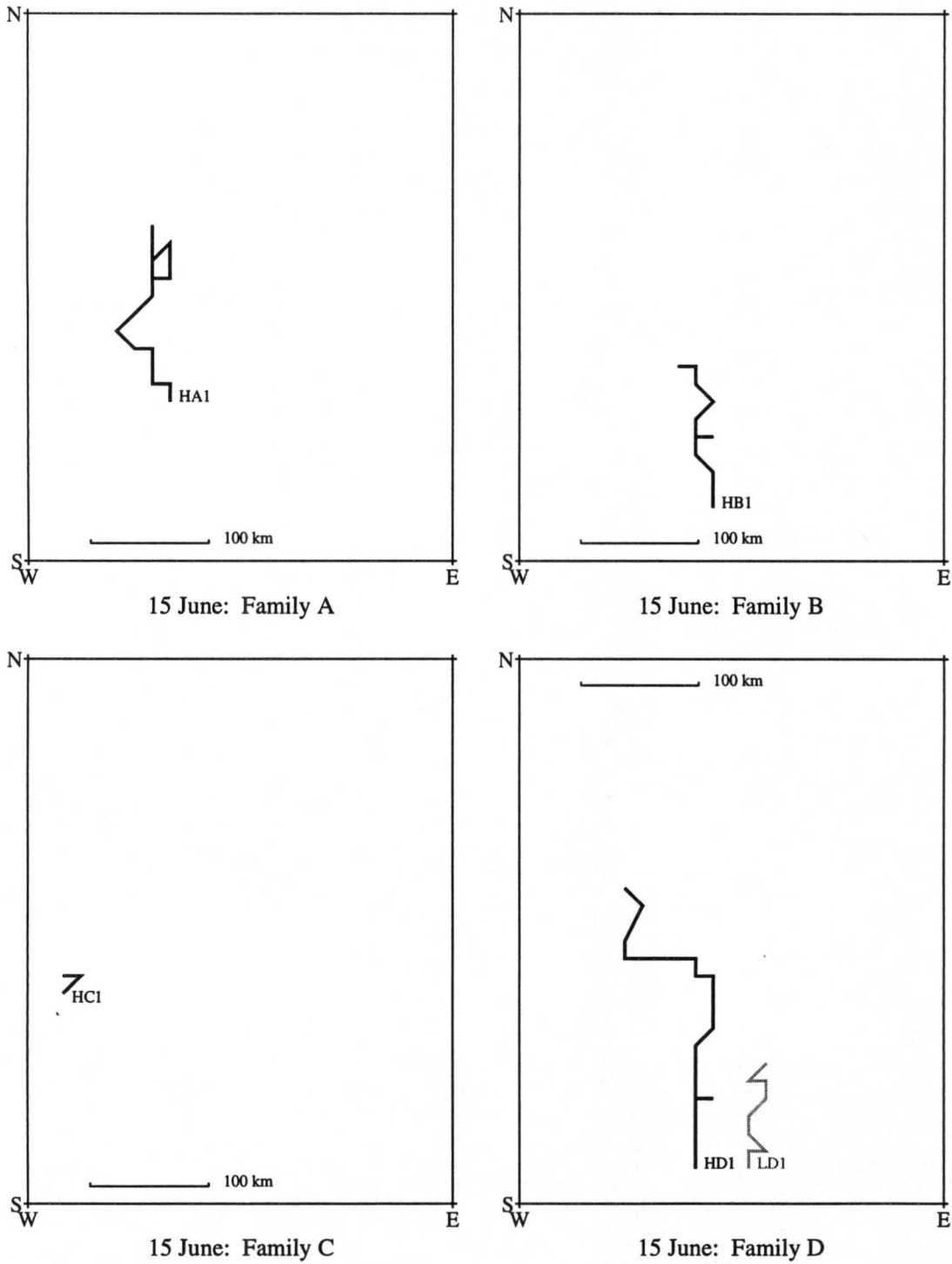
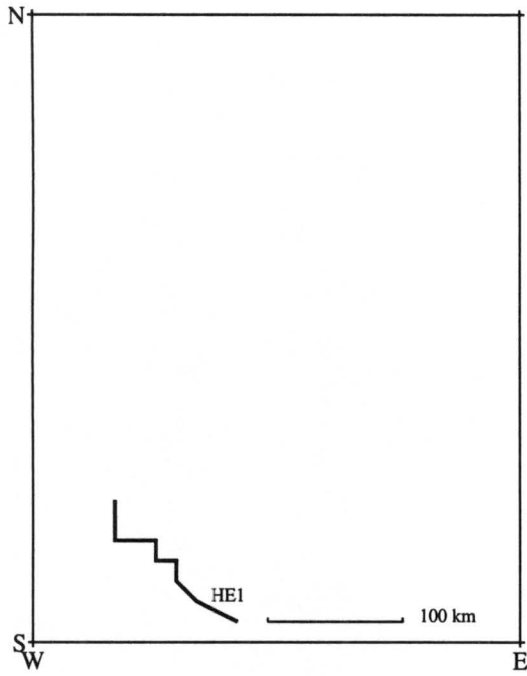
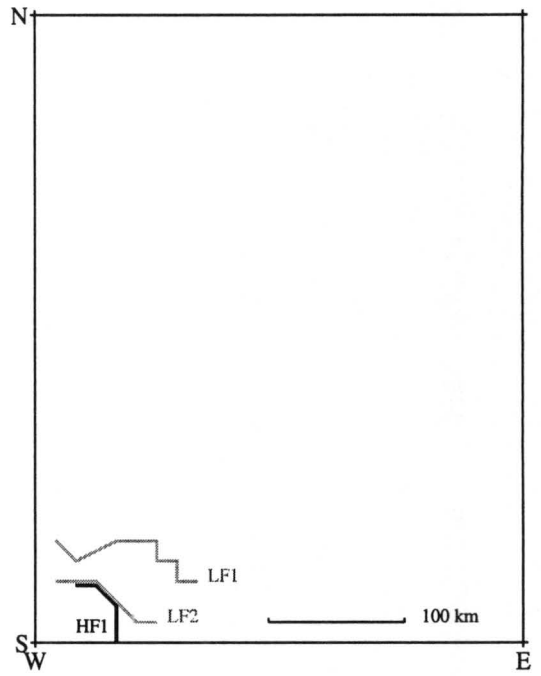


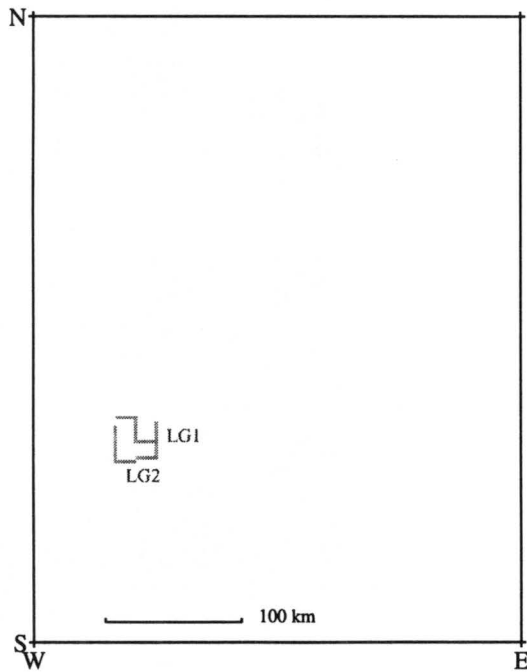
Figure 6.12: Transient Paths for 15 June (continued on the next page).



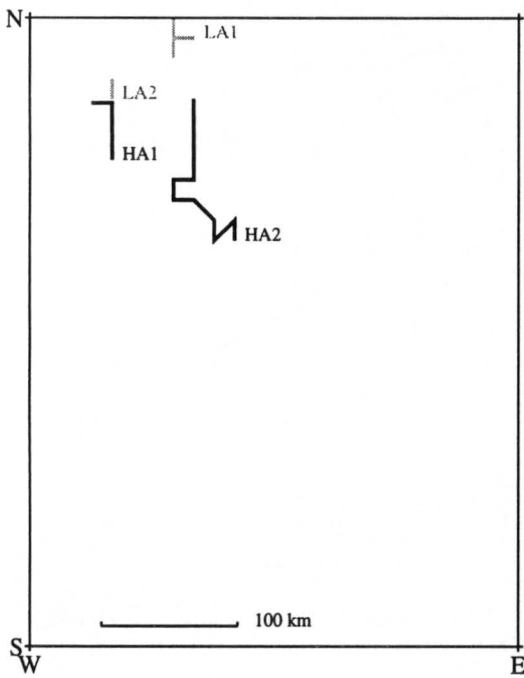
15 June: Family E



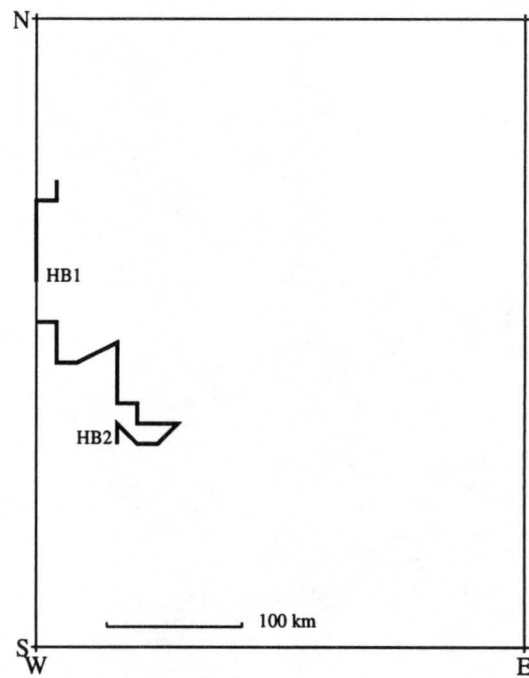
15 June: Family F



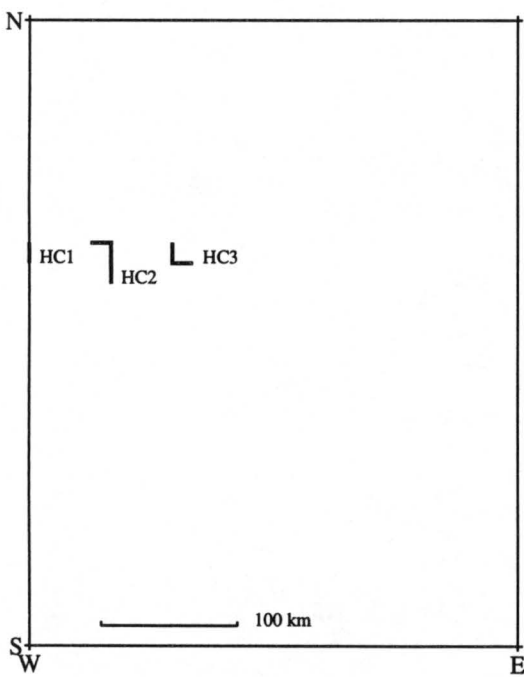
15 June: Family G



24 June: Family A



24 June: Family B



24 June: Family C

Figure 6.13: Transient Paths for 24 June.

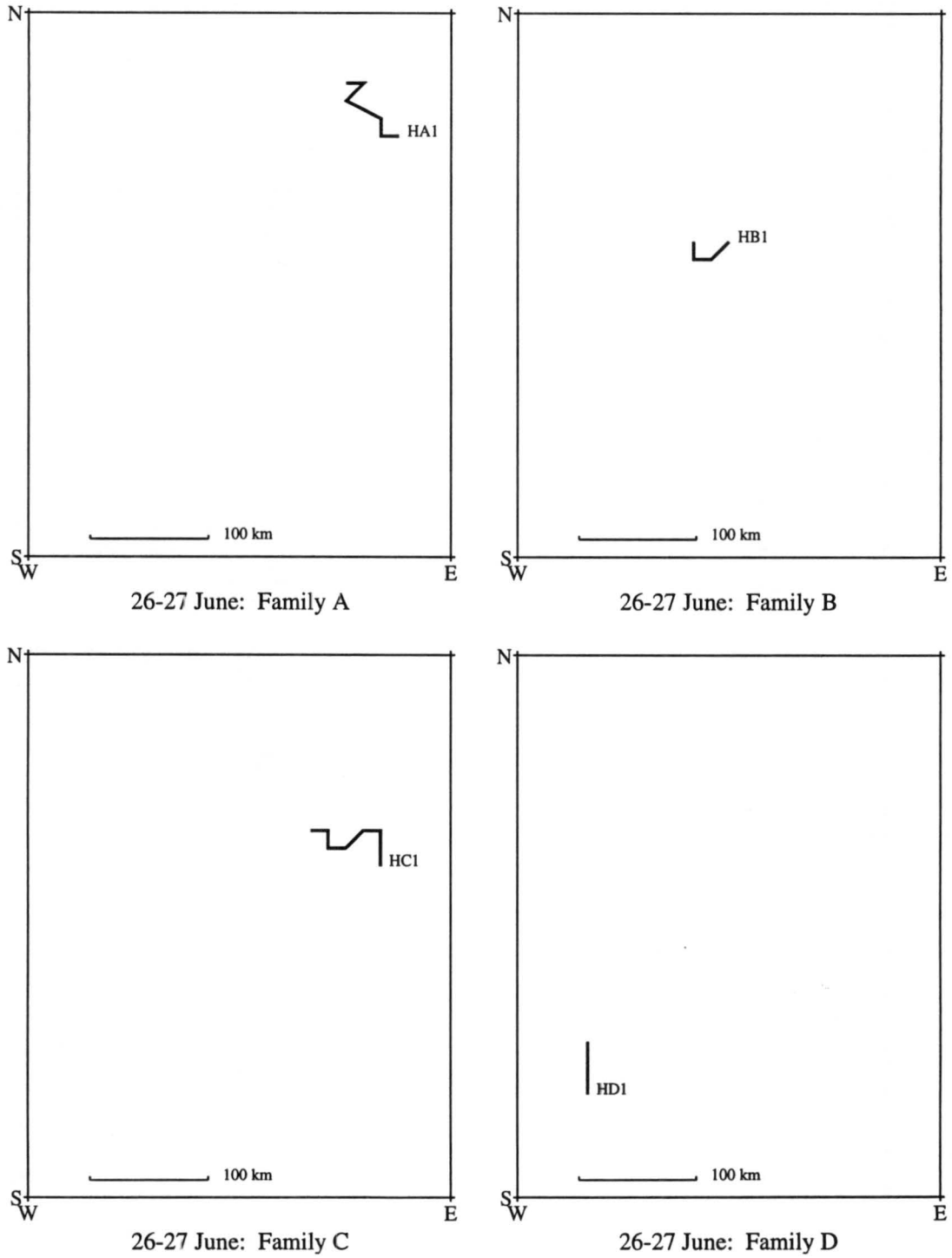
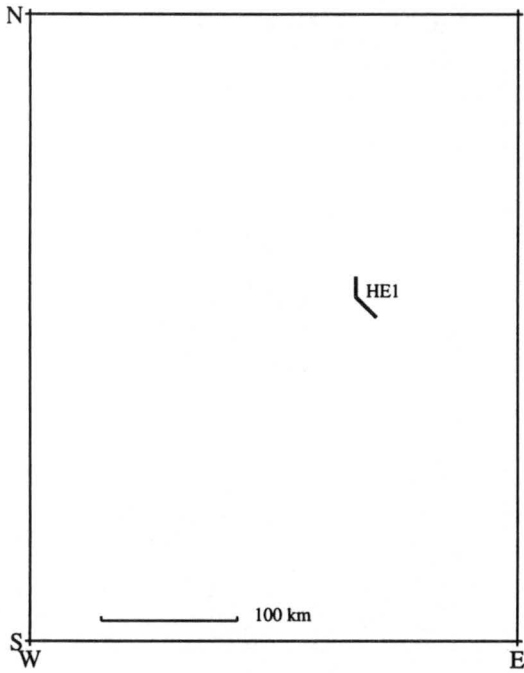
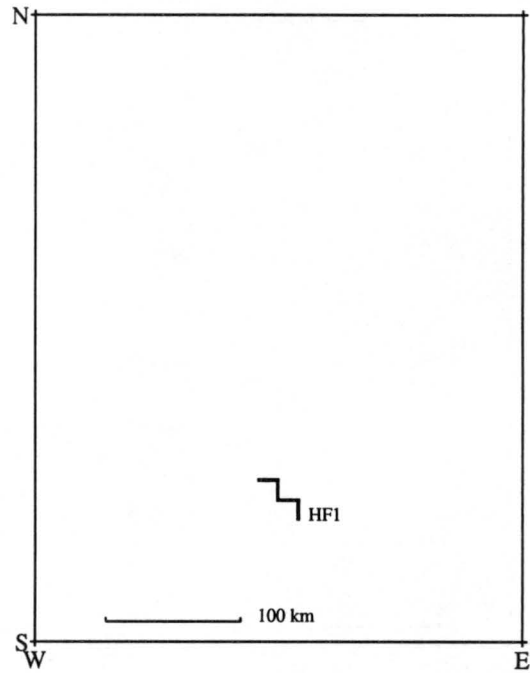


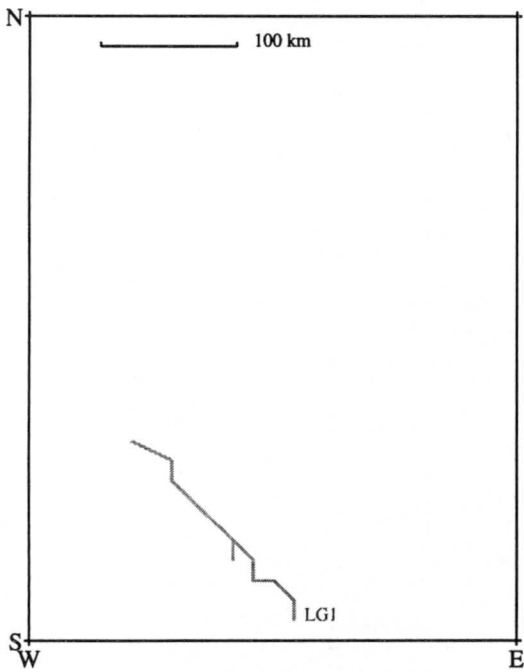
Figure 6.14: Transient Paths for 26–27 June (continued on the next page).



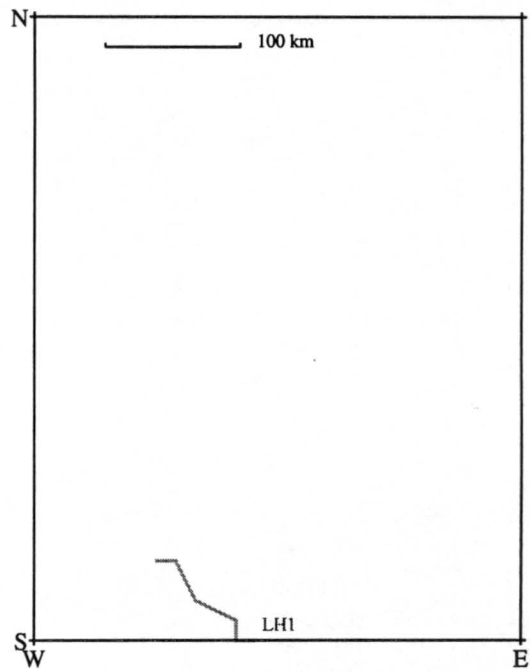
26-27 June: Family E



26-27 June: Family F



26-27 June: Family G



26-27 June: Family H

Until recently, most studies were one snapshot, or a small group of snapshots, of an MCS. Meteorologists documented a small part of the life of some midlatitude complex, and in their glimpse they would find a symmetric MCS (Ogura and Liou 1980; Srivastava et al. 1986; Smull and Houze 1987a,b) or an asymmetric MCS (Brunk 1948; Newton 1950; Pedgley 1962; Schmidt and Cotton 1985), or maybe an MCS that was not, or could not be, put into either category (Kessinger et al. 1987; Houze et al. 1990). Not until field research programs such as PRE-STORM made more comprehensive, continual MCS observations possible did meteorologists discover that the symmetric and asymmetric patterns that sometimes appear are not two *types* of MCSs, but two *stages* of some MCSs (Loehrer 1992; Skamarock et al. 1994).

Loehrer (1992) documented 16 PRE-STORM MCSs. In addition to the 12 cases herein, he studied MCSs from 21 May, 29 May, 9 June, and 22 June. Of the 16 complexes, 12 (75%) became asymmetric late in life, and of these 12, 4 (33%) spent a significant early part of their lives symmetric. (See Section 3.1 for a description of the radar reflectivity patterns for the 12 cases studied in these pages.) Based on his findings, Loehrer modified Houze et al.'s (1990) categories of symmetric, asymmetric, and unclassifiable by adding to the three a time dependency.

Skamarock et al. (1994) provided the first modeling corroboration of Loehrer's modification to Houze et al.'s taxonomy. In their three-dimensional nonhydrostatic simulation of an MCS, the Coriolis force amplified the mid-tropospheric cyclonic circulation in the northern part of the complex and suppressed it to the south, while at the surface it strengthened the forward surge at the southern end of the convective line, enhancing newly-initiated convection. After about 4 simulated hours the initially symmetric MCS was slowly forced into asymmetry by these Coriolis effects. Meanwhile, a modeled Coriolis-free MCS remained symmetric.

Scott and Rutledge (1995) explained that Coriolis forcing in MCSs that live long in only weakly disturbed synoptic environments reshapes a symmetric complex in part by redirecting FTR flow. Lower-tropospheric storm-relative easterly flow from the pre-squall environment captures hydrometeors from dying convective towers and instead of transport-

ing them directly westward into the stratiform area the inflow veers and carries the ice and water into the the anvil's left (north) side.

When an evolving organized MCS moves eastward, then, sometimes its most vigorous convection slides right (south) of the complex's path while the anvil and its associated rainfall broadens left (north) of the path. Surface pressure transients associated with the convective line and the stratiform region reflect this metamorphosis.

## 6.2 Transient Paths

For ease of understanding, consider all the transient paths (Figures 6.3–6.14) to be variations on two fundamental patterns: parallel and skew (Figure 6.2). Most families did not exhibit purely one pattern or the other, but if we overlook the ragged tracks produced by the coarse  $25 \times 32$  Barnes grid (see Chapter 3) most routes taken by the highs and lows are predominately parallel or predominately skew. Figures 6.3–6.14 are family-specific only for viewing clarity; definitions of parallel and skew indeed may be considered from an intra-family perspective (when more than one transient composes a family), but the two categories may be considered from an *inter-family/intra-MCS* perspective as well. The latter is probably more relevant because MCS leading-line/trailing-stratiform arrangements are storm scale, and the latter perspective is also probably safer because it obviates questions of whether or not I correctly placed the 92 transients into their respective families. Be mindful that each figure shows an *accumulation* of transient paths. Not all the transitory highs and lows depicted in Figures 6.3–6.14 existed at the same time.

### 6.2.1 Intra-Family Paths

The first family of the first case produced a good example of a pair of parallel transient paths (Figure 6.3.a). (Disregard the grid-level raggedness; it is an artifact with no merit and does not bear on any issues in this chapter.) HA1 and LA1 moved to the southeast steadily, apart from a mutual eastward jog midway in their travels. (Consider jogs of more than one grid point to be legitimate, although we cannot completely rule out the possibility that data omissions generated them.) Not all parallel paths are as straightforward. HC1

and HC2 of 13 May (N) traveled quasi-parallel to one another, although their paths appear drunken and aimless (Figure 6.4.c). The key is: The angle between their mean direction vectors—even if it is hard to decide on a mean vector—is negligibly small.

Family C of 28 May is an archetypal skew family (Figure 6.7.c). HC1 formed in the north-central part of the array and moved southeastward. Its partner low, LC1, formed south of HA1's origin and moved straight eastward. Their two motion vectors form an included angle of roughly  $45^\circ$ .

In many cases transients traveled in a manner that combined characteristics of parallel *and* skew paths. Sometimes initially skew paths turned parallel, as in the case of Family B of 3 June (Figure 6.8.b) and 15 June's Family D (Figure 6.12.d), while other times parallel paths became skew, as in the case of Family B of 13 May (S) (Figure 6.5.b) and Family A of 24 June (Figure 6.13.a). 10–11 June's Family B exhibits both changes (Figure 6.11.b).

Other families' transients maintained consistent courses, but both parallel and skew sets of paths occurred. The northern of the 13 May MCSs produced five Family B transients (Figure 6.4.b). They fell within two path groups; HB1 and LB1 traveled to the northeast, while HB2, LB2, and LB3 followed a more north-northeasterly route. Paths among transients within their own groups are parallel (i. e., HB2 and LB2 had parallel paths)—that is precisely why I consider them grouped—but the paths within the first group are not parallel to the paths of the second group (i. e., the paths of LB1 and LB3 are skew).

The larger transient families were likely to travel via most or all the above path types. In Family B of 7 May the overwhelming pattern among the highs and lows is one of eastward motion (Figure 6.3.b). However, notice that LB5 traveled southeastward and HB2, toward the end of its life, deviated from its steady eastward path and cut northeastward before veering southeastward at the very edge of the array. For a time LB3 moved eastward with almost every other transient until it broke southward then southeastward. LB1 followed a shorter path, but one similar to that of LB3. Overall, the paths of four transients are parallel: HB1, HB3, LB2, and LB4. LB5 traveled skew to these four. At first LB1 traveled parallel to the group of four and skew to LB5, then it switched and paralleled LB5. HB2

spent most of its life parallel to the first four, then its path became skew to every other path.

### 6.2.2 Inter-Family Paths

Combining all transient families of a single MCS and examining that one large group of paths provides insight into how transients repositioned themselves relative to each other as a few group's parent storms turned asymmetric late in life. Studies have shown that the symmetry of arrangements of radar reflectivity regions are imitated in surface pressure perturbations' arrangements (Figure 6.1). The meso- $\beta$ -scale highs and lows can become arranged in the asymmetric pattern of Figure 6.1's right MCS schema even if they begin symmetric as in the left MCS schema.

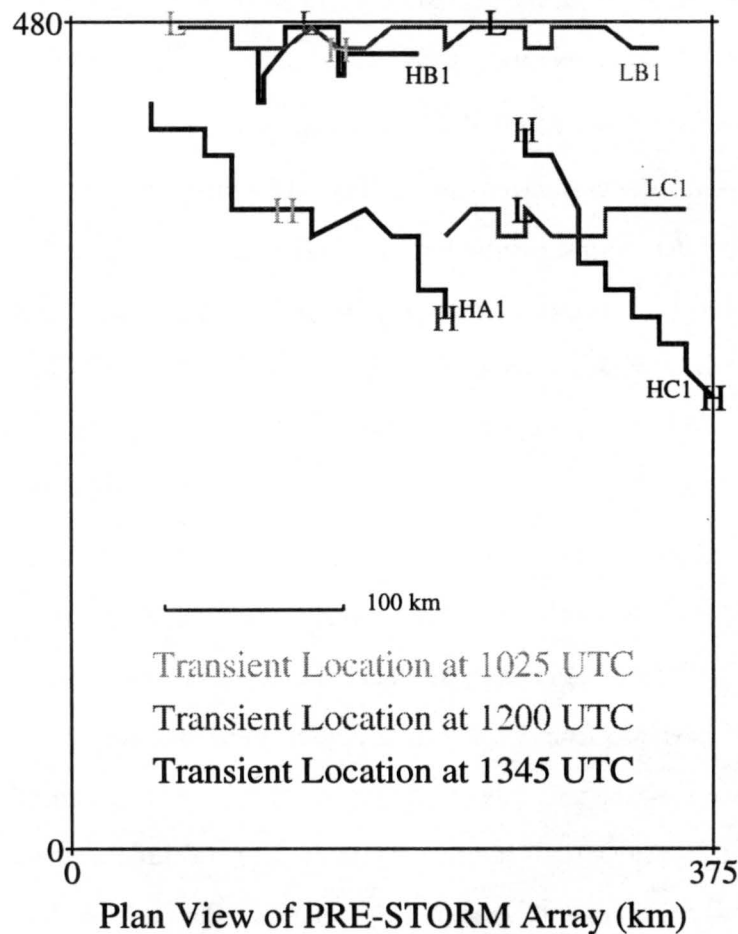


Figure 6.15: Skew Paths to Asymmetry on 28 May 1985. Transients' crossing or diverging paths moved them toward increasingly asymmetric locations relative to one another.

Both parallel and skew paths are possible vehicles for this rearrangement. Skew paths' role is obvious: a high-low pair originally aligned one behind the other will change its orientation if the low travels at some angle to the left of the high's direction of travel. That is generally what happened on 28 May. At 1025 UTC, HA1, HB1, and LB1 were arranged only slightly asymmetrically (Figure 6.15). As highs went to the southeast and lows went to the east, asymmetry became exaggerated during the nearly 3.5 h that followed. At 1200 UTC, HA1 had moved far southeast and was joined by HC1, while in the north HB1 had died. LB1 continued steadily to the east. At 1345 UTC the persistent northern transitory low, LB1, had been joined by LC1, while much farther southeast HC1 was the lone transitory high. HA1 was gone. The skew-path pattern does not imply that every transient that exists early in a complex's life will still exist at the end of its life. New transitory highs and lows form to replace those that die, and these newly-generated transients may form right or left of the old ones, which itself contributes to a complex's symmetry or asymmetry, supplementing the skew paths' role.

Indeed this very substitution of asymmetrically located transients for symmetrically located transients is how MCSs are able to produce an increasingly asymmetric pressure field *even when transients travel parallel to one another*. The initial symmetrically-arranged transitory highs and lows spend themselves, and when subsequent perturbations develop, new highs form to the right of old highs and/or new lows form to the left of old lows. For an example, observe the 4 June MCS, which spawned six transients. All paths were parallel (Figure 6.16). The complex was rooted in disorganization so it is not classified as a symmetric MCS in its early stages, yet its early transient arrangement was quasi-symmetric. At 0830 UTC, HA1 and HB1 were staggered north-northeast/south-southwest, and behind them to the west were LA1 and LB1. By 1000 UTC, HA1 had traveled ahead of the other transients and died, leaving HB1, LA1, LB1, and a new low, LB2, which formed to the left of HB1, the lone high at the time. The 1000 UTC pattern was almost exactly symmetric, yet only 1 h later the final two transients, HC1 and LB2, were positioned asymmetrically. During that intervening hour, LB1 and LA1 died and, more importantly, HB1 died and was replaced far to the right (east) by HC1. LB2 maintained its path. The loss of the right-most

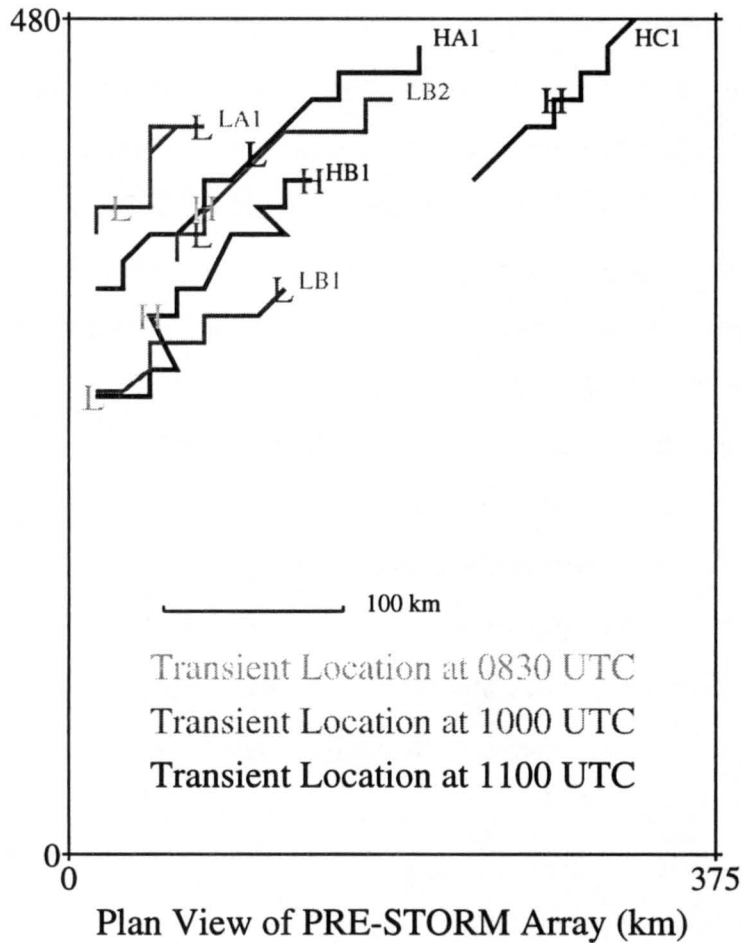


Figure 6.16: Parallel Paths to Asymmetry on 4 June 1985. Initial transients were replaced by subsequent transients that formed in increasingly asymmetrically-arranged locations.

low, LB1, the loss of the left-most high, HA1, and the gain of the right-most high, HC1, were paramount to the eventual asymmetric last stages of transient arrangement in the 4 June MCS.

The 28 May and 4 June storms detailed above are archetypes of the two path classes. Every other complex falls somewhere between these two. Not only are the other 10 groups of transients' first and last arrangements more confused, the patterns of the paths between the two arrangements are complex hybrids of parallel and skew. To force the 10 other MCSs into either the skew or the parallel category would be an unjust oversimplification. Merely regard the two path patterns as conceptual tools for visualizing what may happen to transients in the life of an increasingly asymmetric MCS; in the skew pattern, transients'

crossing or diverging paths move them toward increasingly asymmetric positions relative to one another, while in the parallel pattern initial transients are replaced by subsequent transients that form in increasingly asymmetrically-arranged locations. The patterns may also be clues to the restructuring of the kinematics and latent energy exchanges within evolving MCSs, for transients' formation, travel, and dissipation are a reflection of the storms' internal structure.

The next and final body chapter is one such attempt to read in the 92 transients clues to the mysterious restructuring within MCSs during their evolution from birth to maturity to death.

## Chapter 7

### THE QUESTION OF UPSCALE EVOLUTION

*... When we shall know the truth of things, we shall realize how absurd it is for us to worship isolated products of the incessant series of transformations as though they were eternal and real. Life is no thing or state of a thing, but a continuous movement or change.*

—S. Radhakrishnan,  
Indian Philosophy

MCS circulation scales are not constant. The first cumulus surges skyward well prior to any meso- $\beta$ -scale circulation, and an MCS's death is marked by meso- $\beta$ - and meso- $\alpha$ -scale circulation breakdowns that give way to synoptic weather (Braun and Houze 1995). The challenging question is: How do these circulations evolve between an MCS's birth and death? Do circulation scales shift steadily or explode upscale?

#### 7.1 Existing Theories and Evidence

Just what different scientists mean by upscale varies from person to person and from data set to data set. Generally researchers invoke the term whenever they attempt to explain the complex and elusive dynamics that transform initially scattered, vigorous convection into organized MCSs.

In one recent attempt to document exactly what does happen during the main growth spurt that characterizes some MCSs' early organizational stages, Nachamkin (1992) analyzed the 3 June storm. He argued that the circulation scale of the MCS over Kansas early that summer day suddenly increased as the complex matured. According to him, the MCS began as three clusters of cumulonimbi, one of which intensified as the others weakened. The dominant cluster rapidly increased upper-tropospheric mass flux, fostering a pronounced upper-tropospheric cold pool and high pressure perturbation. In a bore-like

fashion (Schmidt and Cotton 1990; Nachamkin, personal communication), the high expanded beyond the constituent cumulonimbi, obstructed horizontal flow, and forced one branch of westerlies to descend, which produced a wake low at the rear of the anvil. Meanwhile, convective-scale surface highs merged to form one central mesohigh, which then expanded to encompass both the convective and stratiform precipitation zones.

Some early MCS researchers theorized the same direct relationship between an MCS's age and its circulation scales. Pedgley (1962) characterized the growth stage of MCSs as a time when "storms are isolated or in small groups, [then] local pressure rises develop, eventually merging into a thunderstorm high, which then grows in areal extent..." He added, "The growth stage is typified by the weather systems becoming progressively more organized."

## 7.2 Evolution of the Number of Transients

Presumably, during the maturing of these 12 PRE-STORM MCSs, their meso- $\beta$ -scale highs and lows should have reflected this proposed upscale organization in two ways: by becoming fewer and by becoming larger. They did not—at least not entirely. But there is still room for interpretations of upscale evolution in what *did* happen.

Figure 7.1 depicts a composite of the 12 MCSs. Although the average number of total transients varied greatly over the observed life of the composite MCS, the variation was nearly symmetric about the observed midway point in the complex's life. This symmetry arises from adding the two curves of the transitory highs and lows, which are individually asymmetric but nearly exact mirror images of each other reflected about scaled time  $1/2$ .

### 7.2.1 Creating the Figure

The longest interval during which MCS-induced transients from any single complex were observed within the PRE-STORM array is 10 h 10 min for the 26–27 June storm. To prepare all the complexes' data for a composite, I matched the observed beginning, midpoint, and end of all 12 events by (1) separating by 10 h 10 min the beginning and end of every one of the other 11 storms, then (2) interpolating the raw data to the expanded interval.

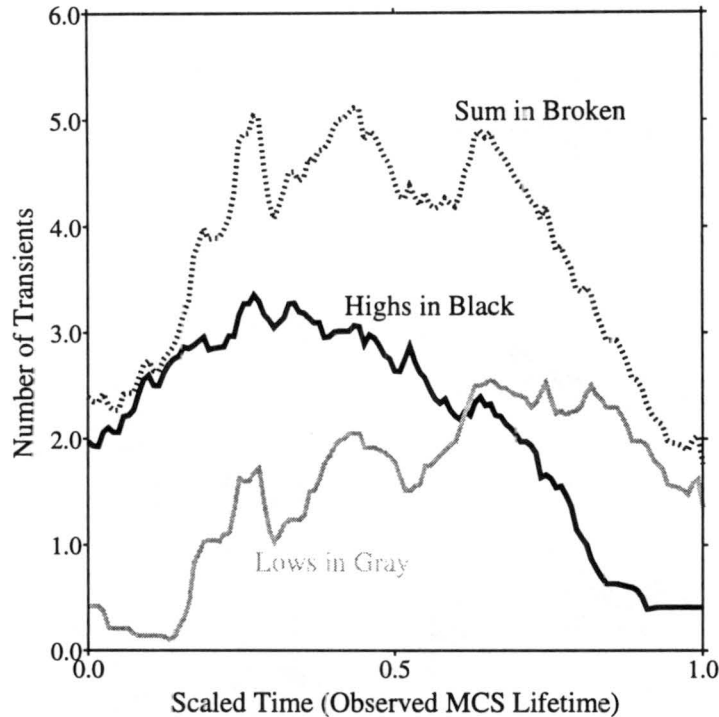


Figure 7.1: Composite Number of Transients vs. Time.

Even during what I call their observation intervals, most of the 12 MCSs were not *completely* observed. Their corners and edges skirted the PRE-STORM array, and at the beginning and end of the intervals the western and eastern edges of the MCSs usually were lost.

I area-weighted the data to compensate for this incomplete areal sampling. Because MCSs are not amorphous blobs wherein transients are as likely to develop in one place as another—mesohighs form almost exclusively along the major axis or along the back edge of the convective line, and wake lows form at the back of the stratiform region—I treated the convective line and back edge of the stratiform region individually.

Area-weighting involved dividing the number of recorded transients by the observed fraction of pertinent MCS region, anvil for lows and convective line for highs. If radar reflectivity indicated 80% of the convective line fell within the PRE-STORM perimeter, I divided the number of observed transitory highs by 0.80. If only 60% of the stratiform regions' back edge was detected, I divided the number of recorded transitory lows by 0.60. To simplify matters and keep myself from pointlessly debating whether 78% or 79% of an

MCS fell within the array, I determined the sampled fractions of the MCSs only to the nearest 20%, beginning at 20% (in order to avoid an infinite correction factor). Each 5-min plot received its own two correction factors. Because radar composites were only available at roughly 20- to 30-min intervals, I linearly interpolated fractional coverages for the periods between images.

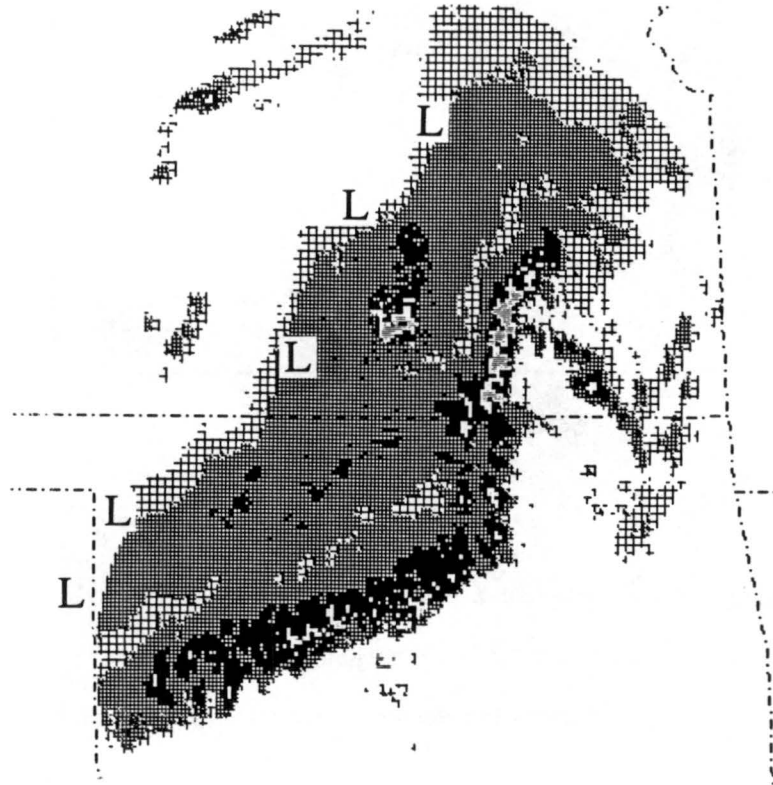


Figure 7.2: 0423 UTC 11 June 1985: Surface Transitory Lows and Radar Composite. Transitory lows are positioned regularly along the rear of the stratiform rain.

The area-weighting's validity rests on the assumption that transients are distributed uniformly within their spawning zones. For any one MCS at any one time, the assumption is questionable. For every example of an even distribution (Figures 7.2 and 7.3) there is a counter example of an uneven distribution (Figures 7.4 and 7.5). But the composite encompasses 12 MCSs and 855 total observations; some of the complexes skirted the array in the north and some of them skirted the array in the south; some of the MCSs were more developed on their northern ends, some on their southern. The large sample averaged the unsystematic inaccuracies in the assumption, which reduced their effect, and produced a reasonable composite representation. Note, too, that the characteristics of the composite



Figure 7.3: 1400 UTC 28 May 1985: Surface Transitory Lows and Radar Composite. Transitory lows are positioned regularly along the rear of the stratiform rain.

MCS to which I refer below are not subtle minutiae but larger-scale dominant signals. Even generous changes in the area-weighting factors would not fundamentally alter the figures' shapes.

Area-weighting reduced all but one potential data bias produced by the finite coverage of the PRE-STORM instruments—a bias that would be impossible to eliminate if it existed. If most of the MCSs crossed the array during similar early or late stages in their lives, the composite plot would be biased toward adolescent or elderly MCSs. This does not appear to have happened. Look at the beginning of the transitory low curve and at the end of the transitory high curve in Figure 7.1. Less than one half transitory low and one half transitory high exist at the start and end of the respective curves. The composite MCS's observed life apparently began just as its stratiform region and associated inflow had sufficiently developed to support transitory lows, and its observed life ended when its convective line no longer supported outflow-produced transitory highs. Roughly, then, the halfway point in the composite's observed life appears to correspond to the actual halfway point in a real

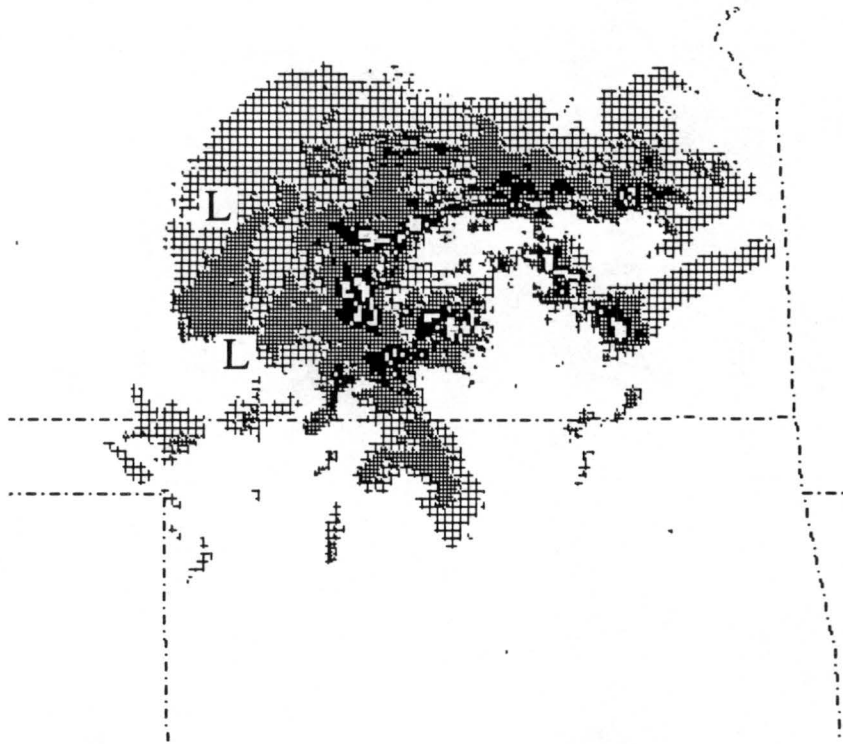


Figure 7.4: 0935 UTC 4 June 1985: Surface Transitory Lows and Radar Composite. Transitory lows are positioned irregularly along the rear of the stratiform rain.

MCS's organized life, if we measure an organized life from the beginning of the first low at the back of the anvil to the end of the last high beneath the convective line. An MCS's actual life begins a little earlier and ends a little later, of course, but it is less important that the composite capture the entire life of the 12 MCSs than it is that, on average, the midpoints in their 12 lives coincide with the midpoint in the composite's life. The average MCS lived within the PRE-STORM array for 6 h 20 min, so the abscissa may be interpreted in terms of hours instead of a unit observed lifetime.

### 7.2.2 *Interpreting the Figure*

It may be a mistake to assume that upscale circulation changes affect all transients similarly. Concepts of upscale dynamic evolution probably apply more to transitory highs than to lows, unless, in the case of the latter, RTF flow develops suddenly and a wake low forms and blossoms dramatically. A lone thunderhead is capable of producing a distinct convective-scale surface high. A group of thunderheads, all producing their individual little

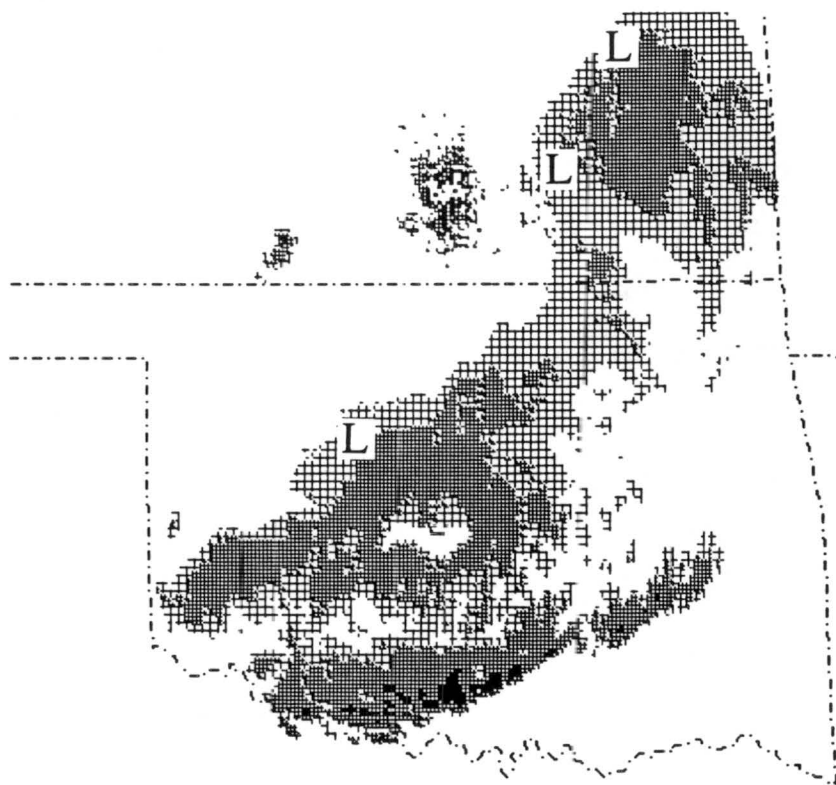


Figure 7.5: 0723 UTC 11 June 1985: Surface Transitory Lows and Radar Composite. Transitory lows are positioned irregularly along the rear of the stratiform rain.

highs, may generate a larger high as their cool, dense outflows merge. We do not have to look hard, then, for a mechanism by which transitory highs may evolve upscale.

Viewed in this light, the curve of the number of transitory highs in Figure 7.1 *does* display a signature consistent with upscale theories. It displays it quite clearly, in fact. The average number of highs peaked about one third of the way through the composite MCS's observed life, then steadily decreased to nearly zero at its life's end. Picture an MCS. From scaled time 0 through scaled time  $1/3$  the number of cumulonimbi increases, so the number of small high perturbations increases. Then at scaled time  $1/3$  consolidation begins. Outflows merge. The edges of the individual outflows are lost, and many highs become few highs. In the end, as the MCS nears the end of its life, and the downdrafts are shut off, the high or highs weaken as surface fluxes and mixing erode the gradients. The synoptic pressure field takes over.

Transitory lows are more complicated. Individual supercells sometimes produce them, but it is not common, and the cumulonimbi of incipient MCSs are not usually supercells

(Rotunno et al. 1988; Houze 1993). It seems a group of more modest cells must obtain a certain critical mass, as it were, before it can noticeably reduce surface pressure rearward of the main convection—a theory that is suggested by Fujita's (1963) diagram of mesosystem pressure cycles (his Figure 42). Convective clusters have this critical mass (Nachamkin 1992), so we need not wait for a fully-developed MCS to go wake-low hunting, but while a complex may produce mesohighs in its infancy, wake lows come later, if at all.

Very few lows (ignoring pre-squall lows) appeared early in the composite MCS's observed life, then they increased in number, if a little unsteadily, and reached a maximum at about scaled time  $2/3$ . They then became fewer, but did not quite reach zero, through the end of the observed life.

Perhaps the upscale metamorphosis occurred just before the first wake lows appeared, in which case their numbers would not reflect the scale change. Indeed, Nachamkin (1992) explains that during the rapid shift in circulation scales of the 3 June storm, the already-existing mesohigh *intensified* while the wake low *developed* as rear inflow consolidated, strengthened, and descended. The gradual increase in average transitory lows' number through most of the remaining observed life may thus have been simply a result of the expansion of the MCS, because complexes do grow for a time after their circulations reach maturity.

A more likely explanation is the point mentioned in Section 4.4.1. Even if many smaller circulations consolidated into a few large meso- $\alpha$ -scale conveyor belts, if these few belts impinged on consistently small pockets of high rain or snow rates, the resultant wake lows might have remained at the low end of the meso- $\beta$  scale even while the MCS circulations were evolving upscale. In this case, increasing numbers of wake lows might also indicate upscale evolution.

### 7.3 Evolution of the Sizes of Transients

The same composite MCS mentioned above appears in Figure 7.6. This time the three curves document the sizes of the transients in terms of total perimeter. Figure 7.6 resembles Figure 7.1 remarkably, almost eerily, closely. It is smoother, which I explain

below, but apart from that the plots are elementally identical. Highs are largest first, then lows' sizes exceed highs' at about scaled time  $2/3$ . The sum of the sizes is greatest about halfway through the composite complex's observed life, and is roughly symmetrical due to the mirrored asymmetry of the high and low curves (see the beginning of Section 7.2).

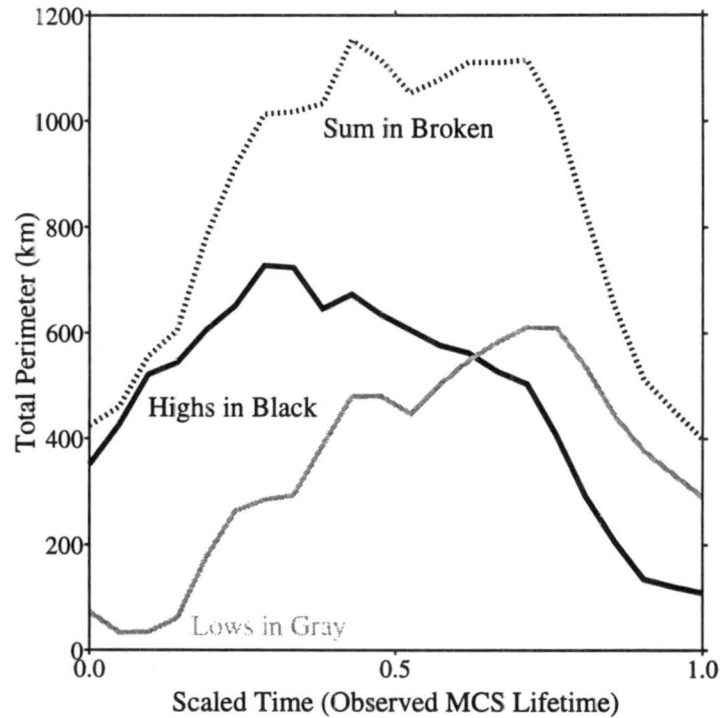


Figure 7.6: Composite Perimeter of Transients vs. Time.

### 7.3.1 Creating the Figure

I normalized data for lifetime and area-weighted them for sampling completeness the way in which I treated data for Figure 7.1 (see Section 7.2.1). I resolved the plot to 30 min instead of 5 min, however, which explains the apparent smoothing. The data themselves are not truly size data—that is, they are not values of area, they are values of perimeter. In undisturbed synoptic environments transients were quasi-circular so values of area roughly correspond to the square of perimeter values; little but the amplitude of the plot would change had I used the former. In environments with many transients and sharp gradients, the highs and lows deviated from circularity, but rarely into such amoeba-like contortions that perimeter was no longer a reasonable proxy for size.

When transients abutted one another to create one envelope of perturbed surface pressure, I traced only the perimeter of the envelope. Rarely could I tell where one transient ended and another began within such envelopes, so I chose determination of the total perimeter as the only reasonable option. As an unwanted side effect, multiple transients that were close but not touching one moment might barely merge in the next plot, so the total perimeter would artificially decrease sharply.

The outer edge of the highest local pressure gradient usually marked an envelope perimeter (Figure 7.7). When it did not I subjectively defined the edge based on an assumption of quasi-circularity or by interpolating between earlier and later plots that did display distinct edges. In Figure 7.6 the perimeters have units but I only have confidence in the relative values, not in the exact measurement of each perimeter. As I implied above, I often drew a perimeter where it *seemed* to fit and for no other reason. Because the subjectivity did not favor highs or lows, nor young or old MCSs, the plot of relative perimeters should be representative enough for loose interpretation.

### 7.3.2 *Interpreting the Figure*

The composite MCS perturbed the lowest level of the atmosphere greatest during the middle stages of its observed life. When the complex was young and its circulations were of modest strength and expanse, synoptic conditions retained control of the PRE-STORM environment. When it was old the complex grew increasingly impotent as FTR latent-energy rich flows dwindled, and cumulonimbi weakened, so their rearward supply of water, ice, and latent heat to the stratiform region became depleted. The dynamic mesoscale flows weakened in turn, and the ambient environment diluted convective and mesoscale drafts until only a few steadily waning transitory highs and lows remained. That is not to say that the pre-MCS synoptic conditions and the post-MCS synoptic conditions were the same. They were not. But in the end the distinction between meso- $\beta$ -scale surface features and meso- $\alpha$ -scale-to-synoptic surface features, altered or not, disappeared at the hands of the atmosphere's innumerable fluxes and stirring eddies.

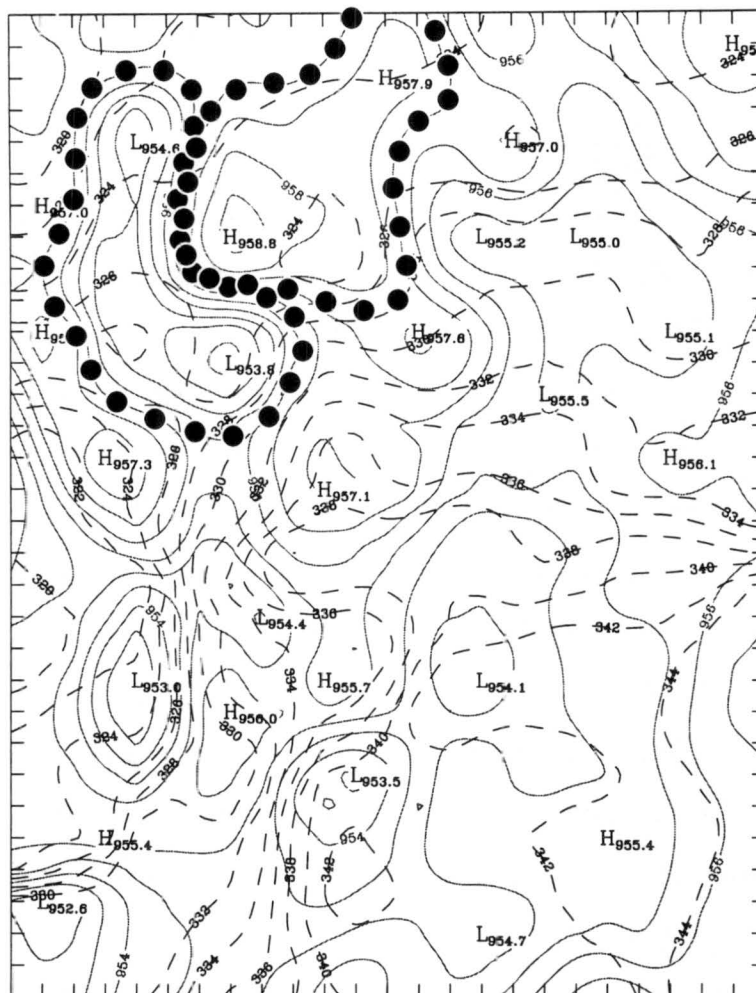


Figure 7.7: Perimeter of the Transitory High and Transitory Low Envelopes at 0940 UTC 4 June 1985. High gradients of pressure, and sometimes  $\theta_e$ , loosely mark the edge of the envelopes, but only after analysis of the movies excludes many local highs and lows from consideration as transients.

In the previous figure, the increase in transitory highs followed theories of upscale evolution; in this second figure the lows carry the upscale banner. Not until the final one fourth of the composite complex's observed life, presumably when the MCS's vitality was failing, did the lows' total perimeter begin shrinking. Almost from the beginning through scaled time 3/4 the lows' collective size increased.

The highs' total perimeter (that is, the perimeter of the envelope of perturbed high pressure at the surface) decreased steadily from scaled time 1/4. This trend is surprising. The density-current character of cumulonimbi cold pools (Wakimoto 1982; Rotunno et al.

1988; Carbone et al. 1990) should theoretically lead to increasingly expansive highs, even while an MCS is in its death throes. Why does this not appear to have happened here?

I mentioned above that transient edges were frustratingly elusive. This was especially true *for the largest transient envelopes*. At some point the cold pool of highs or the dry middle-tropospheric and surface air of lows expanded so much that the transients spread themselves too thin, literally, to maintain integrity against erosion by fluxes and mixing. Occasionally, during some MCSs,  $\theta_e$  fields guided me in locating perimeters, for the edges of surface meso- $\beta$ -scale airmasses can appear as  $\theta_e$  gradients. But such occasions were too infrequent to be valuable; often highs and lows were products of only the integrated atmosphere above the surface layer, not of the airmasses that existed at the level of PAM II and SAM sensors. Many times I was forced to abandon a vanishing expansive perimeter and redefine a new, smaller one (or a few new, smaller ones) that closely girded the transient centers. These centers were the youngest, most distinct parts of a meso- $\beta$ -scale perturbations; they were the sites of freshly introduced latently cooled or warmed air. The PAM II's and SAM's range and my simple technique limited how large I could resolve the transients, and how long I could track their expansion.

Three points can explain the extremely close similarity of Figures 7.1 and 7.6. First, the normalization and the area-weighting may have introduced into the data such a strong signal that two only vaguely similar data sets might have been transformed into near *doppelgängers* after they were manipulated. Unlikely. Most of the raw, single-MCS plots of both numbers and sizes (not shown) exhibit the same fundamental character of the two twice-processed composites.

The second possibility is that transients just did not vary greatly in size, either from one to another or from early in one's life to late in one's life. This would mean the most abundant transients would produce the greatest total perimeters, which is precisely what the two figures display. My close inspection of each frame of each movie compels me to side with this second explanation. There were notable exceptions (during the 10–11 June MCS for example) but on the whole, transients typically did not *appear* to blossom into vast perturbations late in their lives. In this context, the similarity between 7.1 and 7.6 is

further argument that transitory highs and lows are the basic building blocks of mesohigh and wake low envelopes.

I used *appear* two sentences earlier because the third possible explanation of the similarity between Figures 7.1 and 7.6 is that I was deceived by appearances. The faint, almost invisible gradient that often encompasses the largest transients may hide a few especially large transitory highs or lows that populated the PRE-STORM array at end of the MCSs' observed lives. Had they been counted as transients, the highs' and lows' curves in 7.6 would not descend toward the x-axis late in the composite's life.

#### 7.4 Comparison with Volumetric Rain Rate

If transitory highs and lows are products of convective and stratiform kinematics and thermodynamics within MCSs, as decades of circumstantial evidence intimates, convective and stratiform rain rates of MCSs should fluctuate in a manner that resembles the fluctuations of transient numbers and sizes. They do.

McAnelly and Cotton (1992) plotted a composite time-evolution of convective and stratiform rain rates from six MCSs—all of them MCCs—a few of which were from PRE-STORM (Figure 7.8). Showers produced increasingly high convective rain rates until just beyond the first third of the composites' life, then the showers tapered off. Steady anvil rain was nearly non-existent for about 3 h, at which time the rate increased, but more slowly than the convective showers increased. The stratiform rain reached peak intensity about 3 h later than the showers, then slowly weakened. In the last hours of the composites' life, stratiform rain under the anvil fell more heavily than showers at the MCS's leading edge. At their respective maxima, leading-line showers were more intense than the trailing rain.

Differences between McAnelly and Cotton's plot and Figures 7.1 and 7.6 are trivial. The former's  $\beta_{MX}$  and  $\beta_{MN}$  troughs and peaks do not appear in the latter two, but the noise in Figure 7.1 and the smoothing in Figure 7.6 could easily be masking them. McAnelly and Cotton's total rain rate peaks later than halfway through the composite's life, but only slightly. Last, the convective rain rate does not vanish to zero at the end of the composite's

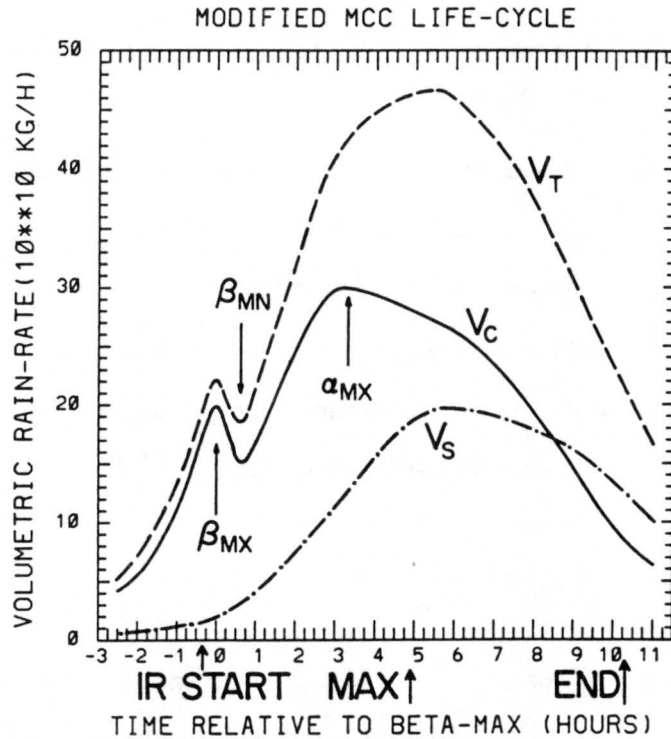


Figure 7.8: Composite MCC Stratiform and Convective Volumetric Rain Rates. Fluctuations in the convective rate,  $V_c$ , and the stratiform rate,  $V_s$ , closely resemble the fluctuations in transient number and size depicted in Figures 7.1 and 7.6.  $\beta_{MX}$  and  $\beta_{MN}$  mark the maximum and minimum in the meso- $\beta$ -scale cycle of  $V_c$ , and  $\alpha_{MX}$  marks the maximum in the meso- $\alpha$ -scale cycle of  $V_c$ .  $V_t$  is the total volumetric rain rate. Six MCCs compose the composite; only some are from PRE-STORM (from McAnelly and Cotton 1992).

life, but the transient numbers and sizes of Figures 7.1 and 7.6 nearly do.

The body of this thesis thus closes with further support for the wealth of existing circumstantial evidence associating post-squall MCS surface pressure perturbations with stratiform and convective precipitation. The following final chapter summarizes this research and points to where meteorologists concerned with these issues should turn their attention in the future.

## Chapter 8

### CONCLUDING REMARKS

*... try to love the questions themselves as if they were locked rooms or books written in a very foreign language. Don't search for the answers, which could not be given to you now.*

—Ranier Maria Rilke,  
Letters to a Young Poet

#### 8.1 Summary

Time-to-space enhanced surface pressure observations of 12 PRE-STORM MCSs exposed 53 transitory highs and 39 transitory lows living within larger mesohighs and wake lows. The transients are the more elemental MCS surface pressure perturbations; *mesohighs and wake lows are merely temporal and spatial envelopes of elemental transients*. Transitory highs are products of varied hydrometeor loads, varied downdraft strengths, and varied latent-cooling efficiencies among MCSs' leading cumulonimbi. Transitory lows are products of horizontal meso- $\beta$ -scale inhomogeneities in stratiform precipitation rate, in RTF flow speed, and in RTF flow humidity.

In the 12 subject MCSs most transitory highs lived less than 1.5 h, but some lived more than 4 h. Their average lifetime was 124 min. Most transitory lows also lived less than 1.5 h. The most persistent lows lived more than 3 h, and the average transitory low's lifetime was 91 min. Transitory high displacements ranged roughly from 0 to 350 km and averaged 115 km, but most highs traveled a net distance of less than 150 km. Even the most well-traveled transitory lows had displacements of 250 km or less. Low displacements averaged 84 km, and most lows traveled a net distance of roughly 50 km.

A quasi-Lagrangian analysis of strengths of the 92 transients produced traces that bore four primary signatures: from largest to smallest, (1) synoptic and storm-scale; (2) the

relative forcing by the convective lines and stratiform areas; (3) trends within dynamically-related families of highs and lows; and (4) fluctuations of each unique transient. At the first scale, the pressure rose in 5 (42%) of the cases, fell in 1 (8%) case, did not change significantly in 3 (25%) cases, and in 3 (25%) cases plots were inconclusive. On the second scale, 7 of 12 (58%) MCSs exhibited divergent high and low patterns, 2 (17%) MCSs were non-divergent, and 3 (25%) were inconclusive. On the third scale, there was no conclusive evidence that transitory highs consistently strengthened before their partner transitory lows, for although clear examples of this did appear, they were infrequent. Last, no systematic patterns appeared in the fourth and finest scale.

Transient paths reflected MCSs' occasional symmetric-to-asymmetric metamorphoses. Most paths were hybrids of two intra-MCS patterns: skew and parallel. Via both patterns, transients that were initially arranged symmetrically or quasi-symmetrically were able to become asymmetrically arranged. In the skew cases, transients' crossing or diverging paths moved them toward increasingly asymmetric relative positions, while in the parallel cases initial transients were replaced by subsequent transients that formed in increasingly asymmetrically-arranged locations.

Composites of the time-evolution of the numbers and sizes of the transients partially supports and partially refutes theories of upscale evolution, but the refutations are probably a product of problems within the compositing scheme and of the frequent difficulty of detecting aged transient perimeters. The number of transitory highs increased sharply through the first third of the composite's life, then slowly decreased, presumably as the outflows from various convective cells merged, which supports upscale evolution theories. The number of transitory lows began increasing later, and increased more slowly through two-thirds of the composite's life before decreasing late, which refutes upscale evolution theories. Examining transients' sizes was difficult and subjective because perimeters disappeared from the plots as transients' modified air expanded and surface fluxes and mixing eroded their perimeter gradients. I was biased toward excluding transients at their largest and oldest, when they were less discernible, so although the figure of transient sizes is very

similar to the figure of transient numbers, make only general, guarded conclusions about the former.

The composites of the time-evolution of the numbers and sizes of the transients closely resembles fluctuations in the composite-MCS volumetric rain rates of McAnelly and Cotton (1992). The similarity complements the already compelling reserve of circumstantial evidence associating post-squall MCS surface pressure perturbations with stratiform and convective precipitation.

The surface pressure plots upon which this thesis is based are reliable because I (1) adjusted data to compensate for elevation-induced pressure differences; (2) removed systematic instrument errors (3); filtered out the diurnal solar tide; (4) consulted radar composites to corroborate surface pressure fields; (5) excluded all transients observed by a single station; and (6) submitted to my processing procedures a controlled test that emerged fundamentally uncontaminated by the Barnes objective analysis and time-to-space enhancement.

## 8.2 Final Thoughts

Previous researchers may have overlooked transients because (1) data were spatially too coarse to resolve the divisions between one transient and its neighbor, leaving only their larger, collective influence to be measured; (2) data were temporally too coarse to mark the death of one transient and the birth of another, so successions of transients were interpreted as single, persistent perturbations; (3) on single, unanimated plots of station pressure, transients are often indistinguishable from noise and instrument errors—only the varying fluidity of animated pressure fields marks plotted extrema as the signatures of real meso- $\beta$ -scale transients.

Transients within mesohighs and wake lows should not surprise us. We should have expected them. Indeed, transients themselves likely harbor another set of yet smaller, more fleeting perturbations, and probably within those live more highs and lows, and so on. Such is the nature of a perturbed fluid with low viscosity.

Within the context of the perturbed-atmosphere continuum exist a few questions. To what degree are the sizes of the transients examined above a product of the observing array

resolution and the subsequent analysis methods? I think to a considerable degree. But I doubt the transients are *entirely* an artifact of the scientific system used to detect them. The atmosphere is non-discrete for all meteorologists' attempts at discretization, but large portions of the atmosphere's energy do reside at preferred temporal and spatial scales. In the case of MCS transients, *finding such preferred scales is a critical part of the search for the origins of post-squall MCS surface pressure perturbations*. Evidence for what produces mesohighs, wake lows, and the transients within them is primarily circumstantial; meteorologists note co-locations and associations, and they find phenomena that could theoretically increase or reduce the surface pressure the amount observed. But the proposed mechanisms must explain not only the magnitude of the perturbed pressure, but also the *temporal and spatial scope of the perturbations*.

A second question: Are individual transitory highs and transitory lows uniquely linked to one another, or do links exist only at the envelope scale and not at the finer end of the spectrum? For utilitarian reasons I inferred loose physical links in this thesis, but often on the most sketchy circumstantial evidence. I am not convinced the two classes of transients are dynamically linked, or even that the conclusions herein imply or require a link.

### 8.3 Future Research

This thesis has one glaring weakness. It pushes the limits of the data resolution almost too far. To truly test my argument that mesohighs and wake lows are envelopes of transients, meteorologists must sample MCSs with a resolution of perhaps 10 km, not the 50 km to which I have been relegated. We need an improvement of half an order of magnitude. Meteorology field projects are dauntingly expensive and complicated to organize, however, so it may be some time before a finer version of a PRE-STORM-like project is conducted.

Meanwhile, meteorologists can adopt the cheaper methods used at the dawn of meso-scale research. Barographs resolve MCS surface pressure patterns well enough to record transients' signatures. Methodical analysis of barographs in the path of MCSs should reveal transitory fluctuations within the ridge envelopes of mesohighs and the trough envelopes of wake lows.

Above the surface, MCS FTR and RTF flows must be sensed often and in many places if meteorologists are to expose possible physical links between transitory highs and transitory lows. Rawinsondes and multiple Doppler radars may be able to detect line-perpendicular flows that connect meso- $\beta$ -scale kinematic and thermodynamic inhomogeneities to specific transients.

The cost and logistical problems of observing the atmosphere will relegate some MCS studies to computer simulations. But models that do not contain three-dimensionally resolved cumulus convection will be limited in their portrayal of MCS surface pressure perturbations. Assuming advances in the near future will make such models possible, meteorologists will have to closely examine simulation results in small time steps to determine if the transients that appear in surface fields near the beginning of a run are the same transients that finish the run.

Early in my research I expected my quasi-Lagrangian traces and paths to provide useful information about possible relationships between transient intensities and their apparently fitful motions—perhaps they moved most slowly as they strengthened, or maybe as they weakened. But the  $25 \times 32$  Barnes grid was too coarse. I could not tell whether the spasmodic travels of the transients were natural or contrived. Perhaps other meteorologists can employ fine-grid mesoscale models and take up the search.

## REFERENCES

- Atlas, D., R. Tatehira, R. C. Srivastava, W. Marker, and R. E. Carbone, 1969: Precipitation-induced mesoscale wind perturbations in the melting layer. *Quart. J. Roy. Meteor. Soc.*, **95**, 544–560.
- Auden, W. H., 1991: *Collected Poems*. Vintage Books, New York, New York, 927 pages.
- Augustine, J. A. and F. Caracena, 1994: Lower-tropospheric precursors to nocturnal MCS development over the Central United States. *Wea. Forecasting*, **9**, 116–135.
- Augustine, J. A. and K. W. Howard, 1988: Mesoscale convective complexes over the United States during 1985. *Mon. Wea. Rev.*, **118**, 685–701.
- Barnes, S. L., 1964: A technique for maximizing details in numerical weather map analysis. *J. Appl. Meteor.*, **3**, 396–409.
- Bartlett, J., 1963: *The Shorter Bartlett's Familiar Quotations*. Pocket Books, New York, New York, 500 pages.
- Betts, A., 1976: The thermodynamic transformation of the tropical subcloud layer by precipitation downdrafts. *J. Atmos. Sci.*, **33**, 1008–1020.
- Betts, A. K., R. W. Grover, and M. W. Moncrieff, 1976: Structure and motion of tropical squall-lines over Venezuela. *Quart. J. Roy. Meteor. Soc.*, **102**, 395–404.
- Bedard, A. J., Jr. and T. J. LeFebvre, 1986: Surface measurements of gust fronts and microbursts during the JAWS Project: statistical results and implications for wind shear detection, prediction, and modeling. NOAA Tech. Memo. ERL WPL-135, Department of Commerce, Wave Propagation Laboratory, Boulder, Colorado, 112 pages.
- Bélair, S. and D.-L. Zhang, 1996: A numerical study of the along-line variability of a frontal squall line during PRE-STORM. *Mon. Wea. Rev.*, submitted.

- Bernstein, B. C. and R. H. Johnson, 1994: A dual-Doppler radar study of an OK PRE-STORM heat burst event. *Mon. Wea. Rev.*, **122**, 259–273.
- Biggerstaff, M. I. and R. A. Houze, Jr., 1991a: Kinematic and precipitation structure of the 10–11 June 1985 squall line. *Mon. Wea. Rev.*, **119**, 3034–3065.
- Biggerstaff, M. I. and R. A. Houze, Jr., 1991b: Midlevel vorticity of the 10–11 June 1985 squall line. *Mon. Wea. Rev.*, **119**, 3066–3079.
- Blanchard, D. O., 1990: Mesoscale convective patterns of the southern High Plains. *Bull. Amer. Meteor. Soc.*, **71**, 994–1005.
- Bleeker, W. and M. J. Andre, 1950: Convective phenomena in the atmosphere. *J. Meteor.*, **7**, 195–209.
- Bluestein, H. B., 1992: *Synoptic-Dynamic Meteorology in Midlatitudes. Volume 1: Principles of Kinematics and Dynamics*. Oxford University Press, New York, New York, 431 pages.
- Bluestein, H. B. and M. H. Jain, 1985: Formation of mesoscale lines of precipitation: severe squall lines in Oklahoma during the spring. *J. Atmos. Sci.*, **42**, 1711–1732.
- Bohren, C. F., 1987: *Clouds in a Glass of Beer: Simple Experiments in Atmospheric Physics*. John Wiley and Sons, New York, New York, 195 pages.
- Braham, R. R., 1952: The water and energy budgets of the thunderstorm and their relation to thunderstorm development. *J. Meteor.*, **9**, 227–242.
- Brandes, E. A., 1990: Evolution and structure of the 6–7 May 1985 mesoscale convective system and associated vortex. *Mon. Wea. Rev.*, **118**, 109–127.
- Brandes, E. A. and C. L. Ziegler, 1993: Mesoscale downdraft influences on vertical vorticity in a mature mesoscale convective system. *Mon. Wea. Rev.*, **121**, 1337–1353.
- Braun, S. A. and R. A. Houze, Jr., 1995: On the evolution of the 10–11 June PRE-STORM squall line: initiation, development of the rear inflow, and dissipation. *Mon. Wea. Rev.*, submitted.
- Bresch, J. F., 1994: Numerical simulation and analysis of a series mesoscale convective systems. Ph. D. Dissertation, Colorado State University, 286 pages.

- Brown, H. A., 1963: On the low-level structure of a squall line. Mesometeorology Research Paper No. 21, University of Chicago, 19 pages.
- Brown, J. M., 1979: Mesoscale unsaturated downdrafts driven by rainfall evaporation: a numerical study. *J. Atmos. Sci.*, **36**, 313–338.
- Brunk, I. W., 1949: The pressure pulsation of 11 April 1944. *J. Meteor.*, **6**, 181–187.
- Brunk, I. W., 1953: Squall lines. *Bull. Amer. Meteor. Soc.*, **34**, 1–9.
- Buell, C. E., 1943: The determination of vertical velocities in thunderstorms. *Bull. Amer. Meteor. Soc.*, **24**, 94–95.
- Byers, H. R. and R. R. Braham, 1949: *The Thunderstorm*. U. S. Department of Commerce, U. S. Weather Bureau, Washington, D. C., 287 pages.
- Carbone, R. E., J. W. Conway, N. A. Crook, and M. W. Moncrieff, 1990: The generation and propagation of a nocturnal squall line. Part I: Observations and implications for mesoscale predictability. *Mon. Wea. Rev.*, **118**, 26–49.
- Capra, F., 1984: *The Tao of Physics*. Bantam Books, New York, New York, 346 pages.
- Chapman, S. and R. S. Lindzen, 1970: *Atmospheric Tides*. Riedel, Dordrecht, Netherlands.
- Chong, M., P. Amayenc, G. Scialom, and J. Testud, 1987: A tropical line observed during the COPT 81 experiment in West Africa. Part 1: Kinematic structure inferred from dual-Doppler radar data. *Mon. Wea. Rev.*, **115**, 670–694.
- Cotton, W. R., M. S. Lin, R. L. McAnelly, and C. J. Tremback, 1989: A composite model of mesoscale convective complexes. *Mon. Wea. Rev.*, **117**, 765–783.
- Crook, N. A., R. E. Carbone, M. W. Moncrieff, and J. W. Conway, 1990: The generation and propagation of a nocturnal squall line. Part II: Numerical simulations. *Mon. Wea. Rev.*, **118**, 50–65.
- Cunning, J. B., 1986: The Oklahoma-Kansas Preliminary Regional Experiment for STORM Central. *Bull. Amer. Meteor. Soc.*, **67**, 1478–1486.
- Das, P., 1964: Role of condensed water in the life cycle of a convective cloud. *J. Atmos. Sci.*, **21**, 404–418.

- Doswell, C. A., III, 1991: Comments on mesoscale convective patterns of the southern High Plains. *Bull. Amer. Meteor. Soc.*, **72**, 389–390.
- Emanuel, K. A., 1986: Overview and definition of mesoscale meteorology. In *Mesoscale Meteorology and Forecasting*. P. S. Ray, ed., American Meteorological Society, Boston, Massachusetts, 1–17.
- Fortune, M. A., W. R. Cotton, and R. L. McAnelly, 1992: Frontal-wave-like evolution in some mesoscale convective complexes. *Mon. Wea. Rev.*, **120**, 1279–1300.
- Fortune, M. A., 1989: The evolution of vortical patterns and vortices in mesoscale convective complexes. Ph. D. Dissertation, Colorado State University, 183 pages.
- Foster D. S., 1958: Thunderstorm gust compared with computed downdraft speeds. *Mon. Wea. Rev.*, **89**, 91–94.
- Fovell, R. G. and Y. Ogura, 1988: Numerical simulation of a midlatitude squall line in two dimensions. *J. Atmos. Sci.*, **45**, 3846–3879.
- Fritsch, J. M., R. J. Kane, and C. R. Chelius, 1986: The contribution of mesoscale convective weather systems to the warm-season precipitation in the United States. *J. Clim. Appl. Meteor.*, **25**, 1333–1345.
- Fritsch, J. M. and R. A. Maddox, 1981a: Convectively-driven mesoscale weather systems aloft. Part I: Observations. *J. Appl. Meteor.*, **20**, 9–19.
- Fritsch, J. M., J. D. Murphy, and J. S. Kain, 1993: Warm-core vortex amplification over land. *J. Atmos. Sci.*, **51**, 1780–1807.
- Fujita, T. T., 1955: Results of detailed synoptic studies of squall lines. *Tellus*, **7**, 405–436.
- Fujita, T. T., 1959: Precipitation and cold air production in mesoscale thunderstorm systems. *J. Meteor.*, **16**, 454–466.
- Fujita, T. T., 1963: Analytical mesometeorology: a review. *Meteor. Monographs*, **5**, 77–125.
- Fujita, T. T., 1985: The downburst: microburst and macroburst. SMRP Research Paper No. 210, Dept. of Geophysical Sciences, University of Chicago, Chicago, Illinois, 122 pages. [NTIS-PB-148880].

- Gallus, W. A., Jr., 1993: The dynamics of circulations within the stratiform regions of squall lines. Ph. D. Dissertation, Colorado State University, 290 pages.
- Gallus, W. A., Jr., 1995: The influence of microphysics in the formation of intense wake lows: a numerical modeling study. *J. Atmos. Sci.*, submitted.
- Gallus, W. A., Jr. and R. H. Johnson, 1992: The momentum budget of an intense midlatitude squall line. *J. Atmos. Sci.*, **49**, 422–450.
- Gallus, W. A., Jr. and R. H. Johnson, 1995a: The dynamics of circulations within the trailing stratiform regions of squall lines. Part I: The 10–11 June PRE-STORM System. *J. Atmos. Sci.*, **52**, 2161–2187.
- Gallus, W. A., Jr. and R. H. Johnson, 1995b: The dynamics of circulations within the trailing stratiform regions of squall lines. Part II: Influence of the convective line and ambient environment. *J. Atmos. Sci.*, **52**, 2188–2211.
- Gamache, J. F. and R. A. Houze, Jr., 1982: Mesoscale air motions associated with a tropical squall line. *Mon. Wea. Rev.*, **110**, 118–135.
- Gao, K., D.-L. Zhang, M. W. Moncrieff, and H.-R. Cho, 1990: Mesoscale momentum budget in a midlatitude squall line: a numerical case study. *Mon. Wea. Rev.*, **118**, 1011–1028.
- Garstang, M. and A. K. Betts, 1974: A review of the tropical boundary layer and cumulus convection: structure, parameterization, and modeling. *Bull. Amer. Meteor. Soc.*, **55**, 1195–1205.
- Goff, R. C., 1976: Vertical structure of thunderstorm outflows. *Mon. Wea. Rev.*, **104**, 1429–1440.
- Gray, W. M., 1973: Cumulus convection and larger scale circulations: I. Broad-scale and mesoscale considerations. *Mon. Wea. Rev.*, **101**, 839–855.
- Green, J. L., 1989: Analysis of surface pressure features during an episode of mesoscale convective systems. M. S. Thesis, Texas Tech University, 75 pages.
- Hamilton, R. A. and J. W. Archibold, 1945: Meteorology of Nigeria and adjacent territories. *Quart. J. Roy. Meteor. Soc.*, **71**, 231–246.

- Hane, C. E. and D. P. Jorgensen, 1995: Dynamic aspects of a distinctly three-dimensional mesoscale convective system. *Mon. Wea. Rev.*, **121**, 3194–3214.
- Heymsfield, G. M. and S. Schotz, 1985: Structure and evolution of a severe squall line over Oklahoma. *Mon. Wea. Rev.*, **113**, 1563–1589.
- Hobbs, P. V. and J. D. Locatelli, 1978: Rainbands, precipitation cores, and generating cells in a cyclonic storm. *J. Atmos. Sci.*, **35**, 230–241.
- Holle, R. L., A. I. Watson, R. Ortiz, and R. E. Lopez, 1990: Spatial patterns of lightning, radar echoes, and severe weather in mesoscale convective systems. Preprints, *16th Conf. on Severe Local Storms*, Kananaskis, Alberta, Amer. Meteor. Soc., 721–726.
- Holle, R. L., A. I. Watson, R. E. Lopez, D. R. MacGorman, and R. Ortiz, 1994: The life cycle of lightning and severe weather in a 3–4 June 1985 PRE-STORM mesoscale convective system. *Mon. Wea. Rev.*, **121**, 1798–1808.
- Houze, R. A., Jr., 1977: Structure and dynamics of a tropical squall-line system observed during GATE. *Mon. Wea. Rev.*, **101**, 1540–1567.
- Houze, R. A., Jr., 1993: *Cloud Dynamics*. Academic Press, San Diego, California, 573 pages.
- Houze, R. A., Jr. and E. N. Rappaport, 1984: Air motions and precipitation structure of an early summer squall line over the eastern tropical Atlantic. *J. Atmos. Sci.*, **41**, 553–574.
- Houze, R. A., Jr., S. A. Rutledge, M. I. Biggerstaff, and B. F. Smull, 1989: Interpretation of Doppler weather radar displays of midlatitude mesoscale convective systems. *Bull. Amer. Meteor. Soc.*, **70**, 608–619.
- Houze, R. A., Jr., B. F. Smull, and P. Dodge, 1990: Mesoscale organization of springtime rainstorms in Oklahoma. *Mon. Wea. Rev.*, **118**, 613–654.
- Hoxit, L. R., C. F. Chappell, and J. M. Fritsch, 1976: Formation of mesolows or pressure troughs in advance of cumulonimbus [sic] clouds. *Mon. Wea. Rev.*, **104**, 1419–1066.
- Humphreys, W. J., 1929: *Physics of the Air*. McGraw-Hill, New York, New York, 654 pages.

- Johnson, R. H., 1976: The role of convective-scale precipitation downdrafts in cumulus and synoptic-scale interactions. *J. Atmos. Sci.*, **33**, 1890–1910.
- Johnson, R. H., 1993: Midlatitude convective systems. Notes for NCAR Colloquium on *Clouds and Climate*. 41 pages.
- Johnson, R. H., 1993: Dynamical effects of mesoscale convective systems. Notes for *International Workshop on Mesoscale Meteorology and TAMEX Program Review*, Taiwan, 8 pages.
- Johnson, R. H. and D. L. Bartels, 1992: Circulations associated with a mature-to-decaying midlatitude mesoscale convective system. Part II: Upper-level features. *Mon. Wea. Rev.*, **120**, 1201–1320.
- Johnson, R. H., S. Chen, and J. J. Toth, 1989: Circulations associated with a mature-to-decaying midlatitude mesoscale convective system. Part I: Surface features—heat bursts and mesolow development. *Mon. Wea. Rev.*, **117**, 942–959.
- Johnson, R. H. and P. J. Hamilton, 1988: The relationship of surface pressure features to the precipitation and airflow structure of an intense midlatitude squall line. *Mon. Wea. Rev.*, **116**, 1444–1472.
- Johnson, R. H. and B. D. Miner, 1994: Interacting flows between mesoscale convective systems along a cold front. *Mon. Wea. Rev.*, **123**, 585–599.
- Johnson, R. H. and M. E. Nicholls, 1983: A composite analysis of the boundary layer accompanying a tropical squall line. *Mon. Wea. Rev.*, **111**, 308–319.
- Johnson, R. H. and J. J. Toth, 1986: Preliminary data quality analysis for May-June 1985 Oklahoma-Kansas PRE-STORM PAM-II mesonet network. Atmospheric Science Paper No. 407, Colorado State University, 41 pages.
- Kessinger, C. J., P. S. Ray, and C. E. Hane, 1987: The 19 May 1977 Oklahoma squall line. Part I: A multiple Doppler analysis of convective and stratiform structure. *J. Atmos. Sci.*, **44**, 2840–2864.
- Klimowski, B. A., 1994: Initiation and development of rear inflow within the 28–29 June 1989 North Dakota mesoconvective system. *Mon. Wea. Rev.*, **122**, 765–779.

- Klemp, J. B. and R. B. Wilhelmson, 1978: The simulation of three-dimensional convective storm dynamics. *J. Atmos. Sci.*, **35**, 1070–1096.
- Knupp, K. R. and W. R. Cotton, 1987: Internal structure of a small mesoscale convective system. *Mon. Wea. Rev.*, **115**, 629–645.
- Koschmieder, H., 1934: Methods and results of definite rain measurements. *Mon. Wea. Rev.*, **62**, 5–7.
- Krumm, W. R., 1954: On the cause of downdrafts from dry thunderstorms over the plateau area of the United States. *Bull. Amer. Meteor. Soc.*, **35**, 122–125.
- Kuhn, T. S., 1970: *The Structure of Scientific Revolutions*, 2nd Edition. University of Chicago Press, Chicago, Illinois, 210 pages.
- Lafore, J.-P. and M. W. Moncrieff, 1989: A numerical investigation of the organization and interaction of the convective and stratiform regions of tropical squall lines. *J. Atmos. Sci.*, **46**, 521–544.
- Laing, A. G. and J. M. Fritsch, 1993: Mesoscale convective complexes in Africa. *Mon. Wea. Rev.*, **121**, 2254–2263.
- Leary, C. A. and T. M. Bals, 1989: Evolution of the 3–4 June PRE-STORM mesoscale convective system. Preprints, *24th Conf. on Radar Meteor.*, Tallahassee, Florida, Amer. Meteor. Soc., 471–474.
- Leary, C. A. and T. M. Bals, 1990: Physical processes associated with precipitation structure in the 3–4 June 1985 OK PRE-STORM mesoscale convective system. Preprints, *4th Conf. on Mesoscale Processes*, Boulder, Colorado, Amer. Meteor. Soc., 210–211.
- Leary, C. A. and R. A. Houze, Jr., 1979: Melting and evaporation of hydrometeors in precipitation from the anvil clouds of deep tropical convection. *J. Atmos. Sci.*, **36**, 669–679.
- Leary, C. A. and E. N. Rappaport, 1987: The life cycle and internal structure of a mesoscale convective complex. *Mon. Wea. Rev.*, **115**, 1503–1527.
- LeMone, M. A., 1983: Momentum transport by a line of cumulonimbus [sic]. *J. Atmos. Sci.*, **40**, 1815–1834.

- LeMone, M. A., G. M. Barnes, and E. J. Zipser, 1984: Momentum flux by lines of cumulonimbus [sic] over the tropical oceans. *J. Atmos. Sci.*, **41**, 1914–1932.
- Levine, J., 1942: The effect of vertical accelerations of pressure during thunderstorms. *Bull. Amer. Meteor. Soc.*, **23**, 52–61.
- Ligda, M. G. H., 1951: Radar storm observations. In *Compendium of Meteorology*. American Meteorological Society, Boston, Massachusetts, 1265–1282.
- Ligda, M. G. H., 1956: The radar observations of mature prefrontal squall lines in the midwestern United States. *VI Congress of Organisation Scientifique et Technique Internationale du Vol a Voile (OSTIV)*, Aeronautical International Federation, St-Yan, France, 1–3.
- Loehrer, S. M., 1992: The surface pressure features and precipitation structure of PRE-STORM mesoscale convective systems. M. S. Thesis, Colorado State University, 296 pages.
- Loehrer, S. M. and R. H. Johnson, 1995: Surface pressure and precipitation life cycle characteristics of PRE-STORM mesoscale convective systems. *Mon. Wea. Rev.*, **123**, 600–621.
- Maddox, R. A., 1983: Large-scale meteorological conditions associated with midlatitude, mesoscale convective complexes. *Mon. Wea. Rev.*, **111**, 1475–1493.
- Mal, S. and Y. P. Rao, 1945: Effect of vertical accelerations on pressure during thunderstorms. *Quart. J. Roy. Meteor. Soc.*, **71**, 419–421.
- Malkus, J. S. and R. S. Scorer, 1955: The erosion of cumulus towers. *J. Meteor.*, **12**, 43–57.
- McAnelly, R. L. and W. R. Cotton, 1986: Meso- $\beta$ -scale characteristics of an episode of meso- $\alpha$ -scale convective complexes. *Mon. Wea. Rev.*, **114**, 1740–1770.
- McAnelly, R. L. and W. R. Cotton, 1989: The precipitation life cycle of mesoscale convective complexes over the Central United States. *Mon. Wea. Rev.*, **117**, 784–808.
- McAnelly, R. L. and W. R. Cotton, 1992: Early growth of mesoscale convective complexes: a meso- $\beta$ -scale cycle of convective precipitation? *Mon. Wea. Rev.*, **120**, 1851–1877.

- Meitín, J. G. and J. B. Cunning, 1985: The Oklahoma-Kansas preliminary regional experiment for STORM-Central (OK PRE-STORM), Volume I. Daily operations summary. NOAA Tech. Memo. ERL ESG-20, Dept. of Commerce, Weather Research Program, Boulder, Colorado, 313 pages.
- Meitín, J. G. and A. I. Watson, 1989: Comparison of the kinematic structure and precipitation characteristics of squall and non-squall mesoscale convective systems. Preprints, *24th Conf. on Radar Meteor.*, Tallahassee, Florida, Amer. Meteor. Soc., 486–489.
- Middleton, W. E. K., 1964: *The History of the Barometer*. The Johns Hopkins Press, Baltimore, Maryland, 489 pages.
- Moncrieff, M. W. and M. J. Miller, 1976: The dynamics and simulation of tropical cumulonimbus [sic] and squall lines. *Quart. J. Roy. Meteor. Soc.*, **102**, 373–394.
- Morris, W. and M., eds., 1975: *Harper Dictionary of Contemporary Usage*. Harper & Row, New York, New York, 650 pages.
- Nachamkin, J. E., 1992: The upscale evolution of a midlatitude mesoscale convective complex. M. S. Thesis, Colorado State University, 122 pages.
- Newton, C. W., 1950: Structure and mechanism of the pre-frontal squall line. *J. Meteor.*, **7**, 210–222.
- Newton, C. W., 1966: Circulations in large sheared cumulonimbus [sic]. *Tellus*, **18**, 699–712.
- Newton, C. W. and J. C. Frankhauser, 1964: On the movements of convective storms, with emphasis on size distribution in relation to water-budget requirements. *J. Appl. Meteor.*, **3**, 651–668.
- Nicholls, M. E., 1987: A comparison of the results of a two-dimensional numerical simulation of a tropical squall line with observations. *Mon. Wea. Rev.*, **115**, 3055–3077.
- Nicholls, M. E., R. H. Johnson, and W. R. Cotton, 1988: The sensitivity of two-dimensional simulations of tropical squall lines to environmental profiles. *J. Atmos. Sci.*, **45**, 3625–3649.

- Ogura, Y. and M. T. Liou, 1980: The structure of the midlatitude squall line: a case study. *J. Atmos. Sci.*, **37**, 553–567.
- Ohsawa, K., 1958: Instability line with thunderstorm. *J. Meteor. Soc. Japan*, **36**, 227–237.
- Orlanski, I., 1975: A rational subdivision of scales for atmospheric processes. *Bull. Amer. Meteor. Soc.*, **56**, 527–530.
- Pedgley, D. E., 1962: A meso-synoptic analysis of the thunderstorms on 28 August 1958. Brit. Meteor. Off. Geophys. Mem. No. 106, 74 pages.
- Redelsperger, J.-L. and J.-P. Lafore, 1988: A three-dimensional simulations of a tropical squall line: convective organization and thermodynamic transport. *J. Atmos. Sci.*, **45**, 1334–1356.
- Riehl, H., 1968: Some aspects of cumulus-scale downdrafts. Atmospheric Science Paper No. 126, Part 1, Colorado State University, 32 pages.
- Riehl, H., 1969: Some aspects of cumulonimbus convection in relation to tropical weather disturbances. *Bull. Amer. Meteor. Soc.*, **50**, 587–595.
- Rotunno, R., J. B. Klemp, and M. L. Weisman, 1988: A theory for strong, long-lived squall lines. *J. Atmos. Sci.*, **45**, 463–485.
- Roux, F., 1988: The West African squall line observed on 23 June 1981 during COPT 81: kinematics and thermodynamics of the convective region. *J. Atmos. Sci.*, **44**, 406–426.
- Roux, F., J. Testud, M. Payen, and B. Pinty, 1984: West African squall line thermodynamic structure retrieved from dual-Doppler radar observations. *J. Atmos. Sci.*, **41**, 3104–3120.
- Rutledge, S. A. and R. A. Houze, Jr., 1987: A diagnostic modeling study of the trailing stratiform region of a midlatitude squall line. *J. Atmos. Sci.*, **44**, 2640–2656.
- Rutledge, S. A., R. A. Houze, Jr., M. I. Biggerstaff, and T. Matejka, 1988: The Oklahoma-Kansas mesoscale convective system of 10–11 June 1985: precipitation structure and single-Doppler radar analysis. *Mon. Wea. Rev.* **116**, 1409–1430.
- Sanders F. and K. A. Emanuel, 1977: The momentum budget and temporal evolution of a mesoscale convective system. *J. Atmos. Sci.*, **34**, 322–330.

- Sawyer, J. S., 1946: Cooling by rain as the cause of the pressure rise in convective squalls. *Quart. J. Roy. Meteor. Soc.*, **72**, 168.
- Sasaki, Y., 1962: Effects of condensation, evaporation, and rainfall on development of mesoscale disturbances: a numerical experiment. Proceedings, *Int. Symp. Numerical Weather Prediction*, Meteor. Soc., Tokyo, Japan, 477–500.
- Schmidt, J. M. and W. R. Cotton, 1985: Bow echo structure and evolution within a High Plains mesoscale squall line. Preprints, *14th Conf. on Severe Local Storms*, Indianapolis, Indiana, Amer. Meteor. Soc., 77–80.
- Schmidt, J. M. and W. R. Cotton, 1990: Interactions between upper and lower tropospheric gravity waves on squall line structure and maintenance. *J. Atmos. Sci.*, **47**, 1205–1222.
- Schaffer, W., 1947: The thunderstorm high. *Bull. Amer. Meteor. Soc.*, **28**, 351–355.
- Schubert, W. H., J. J. Hack, P. L. Silva Dias, and S. R. Fulton, 1980: Geostrophic adjustment in an axisymmetric vortex. *J. Atmos. Sci.*, **37**, 1464–1484.
- Scott, J. D., 1994: Doppler radar observations of an asymmetric MCS and associated vortex couplet. M.S. Thesis, Colorado State University, 103 pages.
- Scott, J. D. and S. A. Rutledge, 1995: Doppler radar observations of an asymmetric MCS and associated vortex couplet. *Mon. Wea. Rev.*, in press.
- Shaw, W. N. and W. H. Dines, 1904: The study of the minor fluctuations of atmospheric pressure. *Quart. J. Roy. Meteor. Soc.*, **31**, 39–52.
- Skamarock, W. C., M. L. Weisman, and J. B. Klemp, 1994: Three-dimensional evolution of simulated long-lived squall lines. *J. Atmos. Sci.*, **51**, 2563–2584.
- Smull, B. F. and J. A. Augustine, 1989: Structure and environment of a non-squall mesoscale convective complex observed during PRE-STORM. Preprints, *24th Conf. on Radar Meteor.*, Tallahassee, Florida, Amer. Meteor. Soc., 502–504.
- Smull, B. F. and J. A. Augustine, 1993: Multiscale analysis of a mature mesoscale convective complex. *Mon. Wea. Rev.*, **121**, 103–132.
- Smull, B. F. and R. A. Houze, Jr., 1985: A midlatitude squall line with a trailing region of stratiform rain: radar and satellite observations. *Mon. Wea. Rev.*, **113**, 117–133.

- Smull, B. F. and R. A. Houze, Jr., 1987a: Dual-Doppler radar analysis of a midlatitude squall line with a trailing region of stratiform rain. *J. Atmos. Sci.*, **44**, 2128–2148.
- Smull, B. F. and R. A. Houze, Jr., 1987b: Rear inflow in squall lines with trailing stratiform precipitation. *Mon. Wea. Rev.*, **115**, 2869–2889.
- Smull, B. F., D. P. Jorgensen, and C. E. Hane, 1991: Comparison of retrieved pressure and buoyancy perturbations with in situ observations of an intense wake low in a midlatitude mesoscale convective system. Preprints, *25th Conf. on Radar Meteor.*, Paris, France, Amer. Meteor. Soc., 135–138.
- Sommeria, G. and J. Testud, 1984: COPT 81: A field experiment designed for the study of dynamics and electrical activity of deep convection in continental tropical regions. *Bull. Amer. Meteor. Soc.*, **65**, 4–10.
- Srivastava, R. C., T. J. Matejka, and T. J. Lorello, 1985: Doppler radar study of the trailing anvil region associated with a squall line. *J. Atmos. Sci.*, **43**, 356–377.
- Stensrud, D. J. and R. A. Maddox, 1988: Opposing mesoscale circulations: a case study. *Wea. Forecasting*, **3**, 189–204.
- Stensrud, D. J., R. A. Maddox, and C. L. Ziegler, 1991: A sublimation-initiated mesoscale downdraft and its relation to the wind field below a precipitating anvil cloud. *Mon. Wea. Rev.*, **119**, 2124–2139.
- Stumpf, G. J., 1988: Surface pressure features associated with a mesoscale convective system in O. K. PRE-STORM. M. S. Thesis, Colorado State University, 148 pages.
- Stumpf, G. J. and W. A. Gallus, 1989: An examination of new convective development with a PRE-STORM squall line case. Preprints, *24th Conf. on Radar Meteor.*, Amer. Meteor. Soc., Tallahassee, Florida, 506–509.
- Stumpf, G. J. and R. H. Johnson, 1989: Lower tropospheric profiling needs in relation to the initiation of mesoscale convective systems. Preprints, *Conf. on Profiling Needs*, Boulder, Colorado, Amer. Meteor. Soc., 29–30.

- Stumpf, G. J., R. H. Johnson, and B. F. Smull, 1991: The wake low in a midlatitude mesoscale convective system having complex convective organization. *Mon. Wea. Rev.*, **119**, 134–158.
- Suckstorff, G. A., 1935: Die Strömungsvorgänge in Instabilitätsschauern. *Z. Meteor.*, **25**, 449–452.
- Suckstorff, G. A., 1939: Die Ergebnisse der Untersuchungen an tropischen Gewittern und einigen anderen Erscheinungen. *Gerlands Beitr. Geophysik*, **55**, 138.
- Szeto, K. K., R. E. Stewart., and C. A. Lin, 1988: Mesoscale circulations forced by melting snow. Part II: Application to meteorological features. *J. Atmos. Sci.*, **45**, 1642–1650.
- Tepper, M., 1950: A proposed mechanism for squall lines: the pressure jump line. *J. Meteor.*, **7**, 21–29.
- Toth, J. J. and R. H. Johnson, 1987: The portable automated mesonet in Oklahoma-Kansas PRE-STORM. Preprints, *Sixth Symposium on Meteorological Observations and Instrumentation*, Amer. Meteor. Soc., Boston, Massachusetts, 4 pages.
- Trier, S. B. and D. B. Parsons, 1993: Evolution of environmental conditions preceding the development of a nocturnal mesoscale convective complex. *Mon. Wea. Rev.*, **121**, 1078–1098.
- Tripoli, G. and W. R. Cotton, 1989a: A numerical study of an observed orogenic mesoscale convective system. Part I. Simulated genesis and comparison with observations. *Mon. Wea. Rev.*, **117**, 273–304.
- Tripoli, G. and W. R. Cotton, 1989b: A numerical study of an observed orogenic mesoscale convective system. Part II. Analysis and governing dynamics. *Mon. Wea. Rev.*, **117**, 305–328.
- Vescio, M. D. and R. H. Johnson, 1992: The surface-wind response to transient mesoscale pressure fields associated with squall lines. *Mon. Wea. Rev.*, **120**, 1837–1850.
- Wakimoto, R. M., 1982: The life cycle of thunderstorm gust fronts viewed with Doppler radar and rawinsonde data. *Mon. Wea. Rev.*, **110**, 1060–1082.

- Weisman, M. L., 1992: The role of convectively generated rear-inflow jets in the evolution of long-lived mesoconvective systems. *J. Atmos. Sci.*, **49**, 1826–1847.
- Weisman, M. L., J. B. Klemp., and R. Rotunno, 1988: Structure and evolution of numerically simulated squall lines. *J. Atmos. Sci.*, **45**, 1990–2012.
- Williams, D. T., 1948: A surface micro-study of squall-line thunderstorms. *Mon. Wea. Rev.*, **76**, 239–246.
- Williams, D. T., 1953: Pressure wave observations in the central Midwest, 1952. *Mon. Wea. Rev.*, **81**, 278–289.
- Williams, D. T., 1954: A surface study of a depression-type pressure wave. *Mon. Wea. Rev.*, **82**, 289–295.
- Williams, D. T., 1963: The thunderstorm wake of May 4, 1961. National Severe Storms Project Rep. No. 18, U. S. Dept. of Commerce, Washington, D. C., 23 pages. [NTIS-PB-168223].
- Yang, M.-J. and R. A. Houze, Jr., 1995b: Sensitivity of squall-line rear inflow to ice microphysics and environmental humidity. *Mon. Wea. Rev.*, **123**, 3175–3192.
- Zhang, D.-L. and K. Gao, 1989: Numerical simulation of an intense squall line during 10–11 June 1985 PRE-STORM. Part II: Rear inflow, surface pressure perturbations, and stratiform precipitation. *Mon. Wea. Rev.*, **117**, 2067–2094.
- Zhang, D.-L. and K. Gao, and D. B. Parsons, 1989: Numerical simulation of an intense squall line during 10–11 June 1985 PRE-STORM. Part I: Model verification. *Mon. Wea. Rev.*, **117**, 960–994.
- Zipser, E. J., 1969: The role of organized unsaturated convective downdrafts in the structure and rapid decay of an equatorial disturbance. *J. Appl. Meteor.*, **8**, 799–814.
- Zipser, E. J., 1977: Mesoscale and convective scale downdrafts as distinct components of squall-line structure. *Mon. Wea. Rev.*, **105**, 1568–1589.

## Appendix A

### MESOSCALE SIZE CLASSIFICATIONS

Ligda (1951) first applied the term *mesoscale* to describe weather too small to be detected by the national synoptic network but too large to be entirely depicted on radar scopes. He intended no specific numerical scale, and certainly the atmosphere is a continuum that defies strict, clean spatial or temporal divisions. But it is sometimes helpful to discretize weather anyway.

No mesoscale divisions are universally accepted, but one sees Orlanski's (1975) mesoscale divisions as often as any. His *mesoscale* encompasses phenomena from 2–2000 horizontal kilometers. Within this umbrella *meso- $\gamma$ -scale* covers 2–20 km, *meso- $\beta$ -scale* covers 20–200 km, and *meso- $\alpha$ -scale* covers 200–2000 km. I adopted Orlanski's classes because they are useful, not because the applicable kinematics and cloud physics vary distinctly from phenomena in one class to phenomena in another.